

POLITECNICO DI TORINO

Dipartimento di Energia

**Corso di Laurea Magistrale
in Ingegneria Energetica e Nucleare**

Tesi di Laurea Magistrale

**SIMULATION AND ANALYSIS OF A POLYGENERATION PLANT
WITH THE INTEGRATION OF A $\text{CeO}_2/\text{Ce}_2\text{O}_3$ CHEMICAL LOOPING**



Relatori

dott. Davide Papurello
dott. Domenico Ferrero
prof. Massimo Santarelli

Candidato

Greta Magnolia

Dicembre 2020

ABSTRACT

Climate changes, carbon depletion, greenhouse emissions and worldwide raising energy demand are becoming increasingly important problems. This opens the door to innovative and green pathways for electric/thermal power and fuels production. In the present study, a polygeneration plant integrated with a chemical looping fed by concentrated solar power for the production of electricity, heat, dimethyl-ether, methanol and syngas is analysed and discussed. The prime mover of the plant is the two-step chemical looping, operating at 1.2 bar and 900°C. The redox pair $\text{CeO}_2/\text{Ce}_2\text{O}_3$ coupled with biomethane partial oxidation is chosen for its manifested advantages compared to other materials. The reduction reaction is endothermic, heat is provided by concentrated solar energy. The prime mover produces the fuel for the secondary devices of the plant: a Solid Oxide Fuel Cell (supplied by the syngas obtained in the reduction reaction) and a DME synthesis and distillation unit (supplied by the syngas obtained in the oxidation reaction). This last section of the system is integrated with a solar aided biomethane reforming reactor for syngas production at 800°C. SOFCs can only operate properly at base-load conditions, the main problem in the coupling of the FC with the solar syngas is given by the yearly, seasonally and daily intermittence of solar energy, which produces a discontinuous operation of the chemical looping and, consequently, a discontinuous production of syngas. This issue is solved under-sizing the SOFC compared to the CL; the surplus of syngas obtained from the reduction reaction during the operation of the chemical looping is stored in an AISI316L tank to be used in those periods of unavailability of solar energy. Thus, the SOFC unit operates continuously throughout the year, while the CL and DME synthesis and distillation unit, whose products are DME, methanol and syngas, only operate when there is a sufficient high irradiance irradiating the reduction receiver-reactor. To have an idea of the possible yearly operating hours of the chemical looping, the seasonal daily average temperature curves of the receiver at the focus of the Dish system installed on the roof of the Energy Center are considered; when this receiver reaches a temperature higher/equal than 900°C, the CL is in on state. The obtained plant is sustainable, green and emission-free because Carbon Capture and Utilization is applied through the use of the separated CO_2 from the anodic exhausts of the SOFC and the exhausts of the DME synthesis and distillation unit in the oxidation reactor of the CL and the reforming reactor respectively. Another important output of the system is thermal power, which could be used for auto-consumption or the supply of different users. The plant performance both under the presence of sunlight and not is studied through the software Aspen Plus v8.8. The electric power production of this system reveals to be much lower than another similar plant available in the literature. Two attempts to increase the electricity production of the plant are made by decoupling the CL operation from the intermittence of solar energy and feeding the reduction reaction with the heat produced by the SOFC. However, these two other plants present the problem of sequestration of the CO_2 because the lack of solar energy should be compensated through the oxyfuel combustion of biomethane. An experimental analysis of the $\text{CeO}_2/\text{Ce}_2\text{O}_3$ chemical looping is also executed.

Keywords: Polygeneration, Ceria, Biomethane, Chemical looping, SOFC, DME, CCU, CSP

CONTENTS

ABSTRACT.....	1
CONTENTS.....	i
LIST OF FIGURES	iv
LIST OF TABLES	vii
INTRODUCTION	2
1. SOLAR CONCENTRATING SYSTEMS	7
1.1. Energy from the Sun.....	8
1.1.1. The Sun.....	8
1.1.2. Solar radiation	9
1.1.3. Earth-Sun Interaction	11
1.2. Operation of a solar concentration panel	15
1.3. Concentration ratio: definition and limits	16
1.4. Maximum receiver temperature	18
1.5. Geolocation of CSP systems	20
1.6. Classification of concentrators	21
1.6.1. Linear concentrators	22
1.6.1.1. Parabolic Trough (PT) collectors.....	22
1.6.1.2. Linear Fresnel Reflector (LF).....	24
1.6.2. Point concentrators.....	25
1.6.2.1. Central tower collectors	25
1.6.2.2. Parabolic dish collectors.....	25
2. SYNTHESIS GAS (SYNGAS).....	28
2.1. Syngas composition and applications.....	28
2.1.1. Power generation through combustion or electrochemical oxidation.....	29
2.1.2. Synthesis of chemicals and fuels	29
2.2. Production of syngas with thermochemical processes powered by solar energy.....	30
2.2.1. Photochemical or photobiological conversion	30
2.2.2. Electrochemical conversion.....	31
2.2.3. Thermochemical conversion	31
2.2.3.1. Reforming.....	32
2.2.3.2. Gasification.....	33
2.2.3.3. Splitting cycles.....	33
3. THERMOCHEMICAL SPLITTING CYCLES	35
3.1. History of thermochemical cycles	35
3.2. Carbon capture and utilization (CCU).....	36

3.3.	Classification of two-step solar thermochemical cycles (STC)	39
3.3.1.	Volatile cycles	40
3.3.1.1.	ZnO/Zn cycle	40
3.3.1.2.	SnO ₂ /SnO cycle	41
3.3.2.	Non-volatile cycles	42
3.3.2.1.	Iron Oxide Cycles	42
3.3.2.2.	Cerium-based cycles	43
3.3.2.2.1.	Stoichiometric cerium cycle	44
3.3.2.2.2.	Non- stoichiometric cerium cycle	47
3.3.2.2.3.	Doped-cerium cycle	50
3.3.2.2.4.	Cerium cycle coupled with methane partial oxidation	51
4.	SOLAR RECEIVER-REACTORS	56
4.1.	Directly and indirectly irradiated receivers	56
4.2.	Structured and non-structured receiver-reactors	56
4.3.	Temperature swing between the two steps of the thermochemical cycle	57
4.4.	Solar receiver-reactors for volatile and non-volatile cycles	57
4.5.	Solar reactors chosen in the present study	57
5.	Fuel cells	60
5.1.	Focus on the SOFC	61
5.1.1.	SOFC voltage and polarization curve	63
5.1.2.	Thermal balance in a SOFC	65
6.	CASE STUDY: POLYGENERATION PLANT	67
6.1.	Plant scheme and components	70
6.1.1.	Modelling and simulation of the plant in Aspen Plus	71
6.1.2.	Plant operating components in a high irradiance and clear sky day	72
6.1.2.1.	Chemical looping	72
6.1.2.1.1.	Simulation of the chemical looping in Aspen Plus	73
6.1.2.2.	Storage system	76
6.1.2.2.1.	Simulation of the storage system in Aspen Plus	77
6.1.2.3.	Solid oxide fuel cell (secondary device)	78
6.1.2.3.1.	Simulation of the SOFC in Aspen Plus	78
6.1.2.4.	DME production (secondary device)	81
6.1.2.4.1.	DME synthesis	81
6.1.2.4.2.	Simulation of the DME synthesis reactor in Aspen Plus	82
6.1.2.4.3.	Distillation unit	84
6.1.2.4.4.	Simulation of the distillation unit in Aspen Plus	86
6.1.2.5.	Steam production	88
6.1.2.6.	Solar Tower and heliostats	90

6.1.3.	Plant operating components in the absence of a sufficient irradiance	93
6.2.	Thermal balance of the plant	93
6.2.1.	Thermal analysis of the chemical looping	93
6.2.2.	Thermal analysis of the SOFC	95
6.2.3.	Thermal analysis of the reforming unit	96
6.2.4.	Thermal analysis of the distillation unit.....	97
6.3.	Inputs and outputs of the plant.....	99
6.4.	Plant efficiencies	101
6.4.1.	Electric efficiency of the system	102
6.4.2.	Thermal efficiency of the system	102
6.4.3.	Solar/biomethane-to-fuel efficiency of the system.....	103
6.4.4.	Global efficiencies of the system.....	103
6.5.	Evaluation of the plant results.....	104
6.5.1.	Results discussion.....	104
6.5.2.	Improvement in the electricity production of the plant.....	106
6.6.	Applications of the useful outputs of the plant.....	111
6.6.1.	Steam applications	112
6.6.2.	Methanol: properties and applications	112
6.6.3.	Dimethyl ether: properties and applications.....	113
7.	FOCUS ON THE CHEMICAL LOOPING MODEL	116
7.1.	Thermodynamic vs kinetics	116
7.2.	Comparison between the model of this study and other models in the literature	117
7.2.1.	Reduction reaction	117
7.2.2.	Oxidation reaction.....	118
8.	EXPERIMENTS AT THE ENVIRONMENT PARK.....	120
8.1.	Description of the test bench	120
8.2.	Experiments parameters and results.....	125
9.	CONCLUSIONS	129
	REFERENCES.....	131

LIST OF FIGURES

Figure 1: Countries that joined the Paris climate agreement up to now	2
Figure 2: Duck curve [5]	3
Figure 3: Scheme of a generic two-step thermochemical cycle fed by CSP [7]	4
Figure 4: Schematic representation of the chosen chemical looping in the present study	5
Figure 5: Solar layers [12]	8
Figure 6: Electromagnetic spectrum; tones as a function of wavelengths (values on the axis are not in scale)	10
Figure 7: Extra-terrestrial spectral irradiance vs black body spectral emission at 5800 K [15]	11
Figure 8: Representation of the ideal Sun-Earth interaction [16]	12
Figure 9: Sun-Earth geometry [17]	12
Figure 10: Attenuation of the solar spectrum in the atmosphere [19]	13
Figure 11: Definition of "Air Mass"	14
Figure 12: Spectral distributions of solar radiation $g(\lambda)$ for different values of Air Mass [18]	14
Figure 13: Concentrator-receiver scheme of a CSP panel	15
Figure 14: Aperture area and receiver area of a CSP panel [20]	16
Figure 15: Example of distribution of local radiation intensity over the receiver in an imaging collector [20]	17
Figure 16: Receiver area as a black body [17]	18
Figure 17: Global efficiency of a CSP system coupled with a Carnot cycle [17]	20
Figure 18: Geolocation of CSP systems	20
Figure 19: CSP plant technologies	21
Figure 20: Scheme of Parabolic Trough collectors	22
Figure 21: Parabola of the PT	23
Figure 22: Tracking system of a PT	23
Figure 23: Linear Fresnel collector	24
Figure 24: Structure of a Solar Tower system	25
Figure 25: Structure of a parabolic dish collector	26
Figure 26: The Solar Card Plant in Peoria, Arizona (USA)	26
Figure 27: Syngas applications	28
Figure 28: IGFC plant [22]	29
Figure 29: Syngas production technologies [7]	30
Figure 30: Thermochemical processes for syngas production [7]	32
Figure 31: Different pathways for Carbon Capture [28]	37
Figure 32: Post-combustion Carbon Capture [28]	37
Figure 33: Pre-combustion Carbon Capture [28]	38
Figure 34: Example of an Oxy-combustion combined cycle [28]	38
Figure 35: Scheme of the ZnO/Zn cycle for syngas production [30]	40
Figure 36: Scheme of the WS through the $\text{CeO}_2/\text{Ce}_2\text{O}_3$ thermochemical cycle	44
Figure 37: Scheme of the solar reactor used to reduce CeO_2 in a controlled atmosphere	45
Figure 38: Scheme of the reactor used for the reduction of H_2O	46
Figure 39: Experimental reactor for the production of H_2 from H_2O and CeO_{2-x}	46
Figure 40: Solar reactor for the non-stoichiometric reduction of ceria	48
Figure 41: Conceptual scheme of the chemical looping syngas production through (a) solar thermal reduction and (b) methane reduction and corresponding splitting of water and carbon dioxide, usually present in waste gas from industrial applications [47]	52
Figure 42: Conceptual scheme of the chemical looping for syngas production through methane reduction and corresponding splitting of water and carbon dioxide [48]	52

Figure 43: Receiver-reactor at the focus of the Dish system of the Energy Center	58
Figure 44: <i>Generic scheme of a fuel cell</i>	60
Figure 45: Comparison between a thermal machine and an electrochemical machine	61
Figure 46: SOFC structure	62
Figure 47: SOFC at open circuit.....	63
Figure 48: SOFC operation at a close circuit	64
Figure 49: SOFC polarization curve at different temperatures and fixing a $FU = 0.85$, an $AU = 0.25$ and a pressure $P=1$ bar [53].....	65
Figure 50: Inputs and outputs of the polygeneration plant	67
Figure 51: Prime mover and secondary devices of the polygeneration plant during a clear sky day ..	68
Figure 52: Operating components of the plant in the absence of solar irradiance.....	69
Figure 53: Seasonal daily average temperature curves of the solar reactor for the different meteorological seasons. Values were obtained from a 2D modelling on Comsol [51].....	69
Figure 54: Chemical looping in Aspen Plus	74
Figure 55: Storage system in Aspen Plus	78
Figure 56: SOFC scheme in Aspen Plus when the CL is in ON-STATE.....	79
Figure 57: SOFC scheme in Aspen Plus when the CL is in OFF-STATE.....	79
Figure 58: Post-combustion unit in Aspen Plus	81
Figure 59: Pre-treatment of the syngas sent to the DME reactor in Aspen Plus.....	82
Figure 60: Simulation of the DME reactor in Aspen Plus.....	83
Figure 61: Treatment of the gaseous output of the DME reactor and reforming unit in Aspen Plus ..	87
Figure 62: Distillation unit in Aspen Plus	87
Figure 63: Solar field of the Spanish Gemasolar system.....	92
Figure 64: Central receiver tower of the Spanish Gemasolar system	92
Figure 65: Thermal balance of HEA-CDS1 and HEA-CDS2 in Aspen Plus	94
Figure 66: Thermal balance of HEAT-CO2 in Aspen Plus	95
Figure 67: Thermal balance of HEAT-H2O in Aspen Plus	95
Figure 68: Thermal balance of HEAT-RE in Aspen Plus	96
Figure 69: Thermal balance of HEAT-ST in Aspen Plus	97
Figure 70: Thermal balance HEAT-D2 in Aspen Plus.....	98
Figure 71: Thermal balance of HEAT-D3 in Aspen Plus.....	98
Figure 72: Mixer of the steam and hot water streams of the plant and simulation of the cooling of the output stream (STE-TOT) to obtain useful thermal power (THE-REQ) when CL is in ON-state ...	100
Figure 73: Simulation of the thermal recovery from steam when CL is in OFF-state.....	101
Figure 74: ASU specific energy consumption [76]	108
Figure 75: Rankine cycle	112
Figure 76: Comparison of dimethyl ether's physical and thermo-physical properties to commonly used fuels [79].....	113
Figure 77: Schematic of the solar particle-transport reactor of the study of Welte, Warren and Scheffe [84]. Material flows are indicated by the coloured arrows for either co-current (dashed) or counter-current (solid) flow configuration.....	116
Figure 78: Carbolite Gero microreactor	120
Figure 79: Microchannels in alumina.....	120
Figure 80: Location of the Alumina microchannels	121
Figure 81: Scheme of the microreactor	121
Figure 82: Weight scale of the ceria particles.....	121
Figure 83: Case for the fulfilling of the tubes	122
Figure 84: Emerson Gas Analyzer	122
Figure 85: Power supply of the microreactor	123
Figure 86: Pipeline of the streams entering/exiting the microreactor	124
Figure 87: Pressure reducers, cylinders and demineralized water tank.....	124

LIST OF FIGURES

Figure 88: Scheme of the test bench	125
Figure 89: Example of one cycle of the experiment	127
Figure 90: Peak of H ₂ in the reduction	127
Figure 91: Peak of H ₂ in the oxidation reaction	128

LIST OF TABLES

Table 1: Maximum value of the concentration ratio for different technologies	17
Table 2: Concentration factors and solar efficiencies characteristic for CSP technologies	22
Table 3: Characteristic temperatures and efficiencies for CSP technologies	22
Table 4: Properties of cerium oxides	44
Table 5: Main assumptions and hypothesis used in the process simulation.....	72
Table 6: Particle size distribution of the ceria as a function of the frequency obtained from ELPI measurements [61].....	74
Table 7: Inlet streams of the reduction reactor.....	74
Table 8: Outlet streams of the cyclone after reduction reactor.....	75
Table 9: Inlet streams in the oxidation reactor.....	75
Table 10: Outlet streams of the cyclone after the oxidation reactor	76
Table 11: Re-integration of ceria at each cycle.....	76
Table 12: Cyclones' characteristics [62].....	76
Table 13: Syngas stream entering the DME reactor	83
Table 14: Parameters of the DME reactor	83
Table 15: Kinetic parameters used in DME synthesis.....	84
Table 16: Stream PROD-3 exiting from the DME synthesis reactor.....	84
Table 17: Input and output flows of the reforming reactor	87
Table 18: Recirculated syngas stream and syngas stream sent to the duct.....	87
Table 19: Distillation columns of operation parameters	88
Table 20: Outlet streams from the distillation columns	88
Table 21: Hot side of the heat recovery steam generators	89
Table 22: Water requirements in SRG1 and SRG2.....	89
Table 23: Additional water requirement from the external environment	90
Table 24: Average DNI on the receiver-reactors in the different seasons when $T \geq 900^{\circ}\text{C}$	91
Table 25: Thermal balance of the chemical looping.....	94
Table 26: Inlet and outlet streams of HEA-CDS1 and HEA-CDS2	94
Table 27: Inlet and outlet streams of HEAT-CO2	95
Table 28: Inlet and outlet streams of HEAT-H2O in Aspen Plus	95
Table 29: Outlet and inlet streams of HEAT-RE	96
Table 30: Outlet and inlet streams of HEATST	97
Table 31: Thermal balance of the reforming unit.....	97
Table 32: Inlet and outlet streams of HEAT-D2 and HEAT-D3	98
Table 33: Input and output material streams.....	100
Table 34: Input and output work streams	101
Table 35: Data inserted in the formula (104) and (105)	102
Table 36: Data inserted in equations (108) and (109).....	103
Table 37: Comparison between the present study and the Farooqui et al. one [4] considering the two different operations of the present polygeneration plant	104
Table 38: Comparison between the yearly average outputs of the plants	105
Table 39: Comparison between the present study and the Farooqui et al. one [4] considering the operation of the present polygeneration plant with the CL in ON state.....	105
Table 40: Comparison between the yearly average syngas produced by the chemical loopings of the plants.....	105
Table 41: Comparison between the electricity output of the present plant and the GemaSolar system	106
Table 42: Effect of the biomethane/CeO2 molar ratio on the completion of the reduction of ceria	107
Table 43: Input and output streams of the chemical looping in the new plant	107

Table 44: Results of the simulation of the new plant 109

Table 45: Comparison between the solar fed plant, the new plant and the pant of Farooqui et al. [4] at steady state conditions..... 109

Table 46: Comparison of the yearly average outputs of the three plants..... 110

Table 47: New plant without reforming unit at steady-state 111

Table 48: Global Warming Potentials 113

Table 49: Comparison of the thermodynamic results of the model of this study with the results reported by Farooqui et al. [48] for the reduction of ceria with methane at the chosen operating conditions of the solar aided CL 118

Table 50: Comparison of the thermodynamic results of the model of this study with the results reported by Warren et al. [85] and by Farooqui et al. [48] for the reduction of ceria with methane at different operating conditions..... 118

Table 51: Comparison of the thermodynamic results of the model of this study with the results reported by Farooqui et al. [48] for the oxidation of ceria with H₂O and CO₂ at the chosen operating conditions of the solar aided CL..... 119

Table 52: Main parameters of the experiments in Environment Park 126

Table 53: Hydrogen in the reduction reaction..... 127

Table 54: Hydrogen in the oxidation reaction 128

INTRODUCTION

One of the sentences that could resume the present global and Italian situation in terms of electricity and fuels production can be: *"Ulteriora mirari, presentia sequi"* (Cornelio Tacito). It means that we have to "Stay in our time having a look at the future". The glance towards the future is, without any doubt, in the energy transition, decarbonisation and renewable energy sources, but we also have to stay in our time being aware of the fact that innovation, change and evolution cannot be further procrastinated and they have to start now. Climate changes, greenhouse emissions and carbon depletion are problems that have to be faced as soon as possible. In November 2014, the Intergovernmental Panel on Climate Change (IPCC) released the Fifth Assessment Report updating the studies on climate changes highlighting the important role played by humans concerning this issue: "Human influence on the climate system is clear and growing, with impacts observed on all continents. If left unchecked, climate change will increase the likelihood of severe, pervasive and irreversible impacts for people and ecosystems" [1]. This human influence is strongly related to greenhouse emissions into the atmosphere through industrial activities, which produce the rising of the earth surface temperature. The main anthropogenic greenhouse gases are: CH₄, N₂O, O₃ and, in an indirect way, H₂O [2]. In the perspective of reducing this impact on the environment, in 2015, the historic Paris Agreement (COP21), held by 195 countries, was fundamental because it was the first universal and legally binding agreement on climate changes. It established to hold the global average temperature increase well below 2°C above pre-industrial levels and, in particular, to limit it at 1.5°C above pre-industrial levels since this would reduce a lot the risks and impacts on climate [3]. After this COP21, every five years the member countries have to fix new objectives for their efforts in climate matter, so the current year 2020 is crucial.



Figure 1: Countries that joined the Paris climate agreement up to now

A key role in the reduction of greenhouse emissions is played by the energy production sector: CO₂ emissions from the energy sector (mainly from the combustion of fossil fuels) constitute the highest amount of the global anthropogenic GHG emissions, equal to the 58% of the total emissions [4]. Solar energy exploitation is a fundamental weapon to face the problem of high fossil fuel consumption and to substitute conventional fuels with renewable and abundant energy sources. Solar irradiation is highly available, widely distributed worldwide and clean; it can be both converted into heat or electricity. However, the main problems concerning solar energy are:

- its intermittence and discontinuity;

- the recurrent mismatch between the times of higher energy production from this energy source and the times of the highest demand from consumers e.g. the peaks of generation do not commonly correspond to those of demand, as it can be seen looking at the Duck Curve in *Figure 2*. Most of us wake up in between 7 and 8 AM and uses electric energy for different purposes, this produces the first spike in demand, forming the tail of the duck. Then the energy consumption stabilizes and even slightly decreases as people go to the office/school/occupation, meanwhile, solar power production sharply increases. During lunch hours and early in the afternoon, the peak of solar energy production is reached, but we use less electric energy. Finally, in the evening, we return home and the electricity consumptions increase, while the solar generation rapidly decreases as the sunsets.

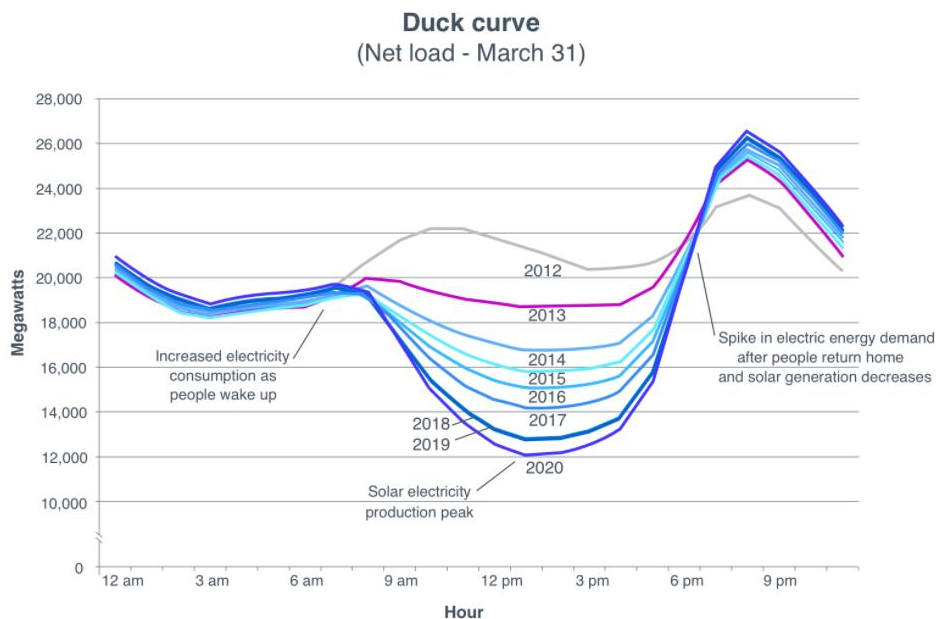


Figure 2: Duck curve [5]

These issues can be overcome through the use of solar concentrating systems to convert and store solar energy itself in the form of synthetic chemical fuels (H_2 and CO), such as syngas, via thermochemical reactions. Therefore, syngas can be used as an energy carrier for the storage of solar energy and this energy vector can be easily transported and exploited according to the energy demand. In this perspective, the present study focuses on the exploitation of concentrated solar energy to produce syngas in a chemical looping process. Single-step solar thermal dissociation of water and CO_2 (thermolysis) for the production of syngas is impractical for the extremely high-temperature requirement, that exceeds $2200\text{ }^\circ\text{C}$, thereby facing the limitations imposed by the reactor materials as well as thermal radiation losses, possible recombination of the products or the problem of their separation to avoid the realization of an explosive mixture. A way to lower the reduction temperature of both H_2O and CO_2 is the use of metal oxide redox cycles and, in particular, the realization of a chemical looping [6]. In a chemical looping, products and reactants are continuously reproduced in a cycle. The most efficient chemical looping processes are those composed of two different steps, as shown in *Figure 3*:

- 1) reduction reaction. It is endothermic, the metal oxide MO_{OX} is subjected to a thermal reduction and releases oxygen (MO_{RED} is obtained). In this study, this reaction is made to occur in a receiver-reactor placed at the focus of a solar irradiated CSP system;
- 2) oxidation reaction. It is exothermic, the reduced metal oxide is made react with water and carbon dioxide to obtain both the re-oxidation of the metal oxide itself (MO_{OX} is obtained), that is recirculated to the first step and the reduction of H_2O and CO_2 with the subsequent production of syngas. In this work, the oxidation reaction takes place simultaneously with the

reduction reaction, but in a non-solar reactor. The simultaneity of the two reactions is possible applying the following “trick”:

- when the plant is switched on for the first time, in the reduction reactor, ceria particles are reduced;
- when the ceria particles are completely reduced, they are sent to the oxidation reactor to be oxidized and, meanwhile, other ceria particles CeO_2 from the external environment are introduced in the reduction reactor;
- when the oxidation completely occurs, the oxidized ceria particles are sent to the reduction reactor and the just reduced particles in the reduction reactor are recirculated to the oxidation reactor.

After this first cycle, the steady-state in the chemical looping operation could be reached (after the stabilization of the fluxes, of the temperatures...) with the two reactors operating simultaneously. This kind of design is implemented to guarantee a continuous operation of the reduction reactor when high values of concentrated solar power are present and, consequently, to exploit the largest amount possible of solar energy. For the realization of the reactors of the chemical looping, continuous flow reactors could be used; in the present study, these reactors are simulated through Gibbs reactors, so the steady-state condition at the equilibrium is analysed and the kinetics of the reactions is neglected.

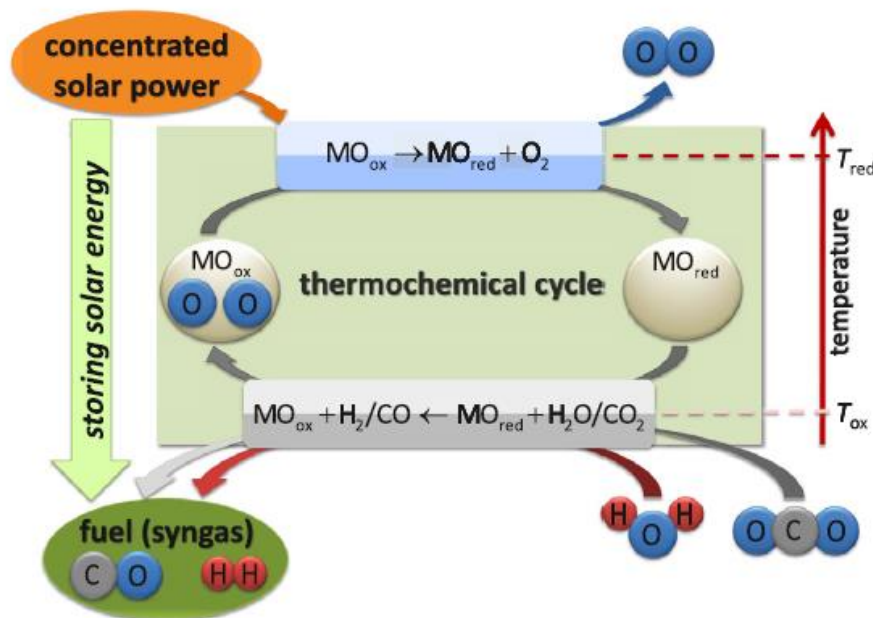


Figure 3: Scheme of a generic two-step thermochemical cycle fed by CSP [7]

Different metal redox pairs have been studied for the chemical looping processes and ceria is currently considered the most attractive for different reasons (as written in [Chapter 3](#)):

- high crystallographic stability through extensive thermal cycling;
- high oxygen release and storage capacities;
- fast oxygen exchange rates;
- reversible shift between Ce^{4+} and Ce^{3+} oxidation states;
- fast kinetics during thermochemical cycles as compared to other non-volatile metal oxides.

As a result, in this study, the redox pair $\text{CeO}_2/\text{Ce}_2\text{O}_3$ is chosen as metal oxides in the chemical looping process. Since the reduction reaction of pure ceria only takes place at very high temperatures (above 2000°C), it is chosen to introduce biomethane. The partial oxidation of biomethane simultaneously with ceria reduction allows the realization of an iso-thermal and iso-pressure CL at 900°C and 1.2 bar:

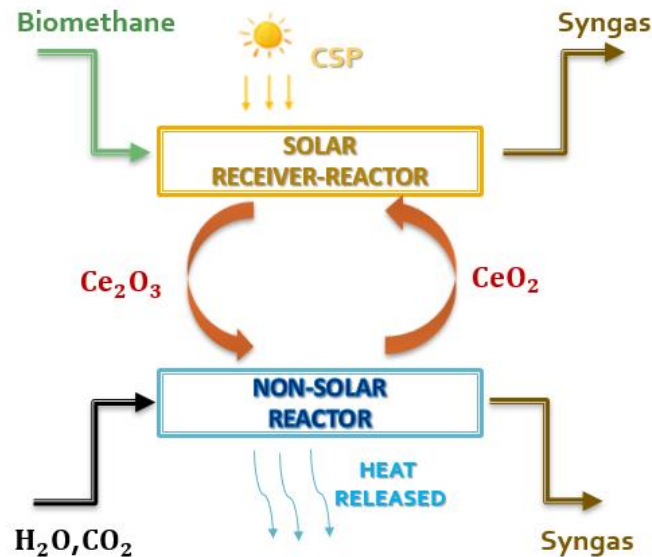
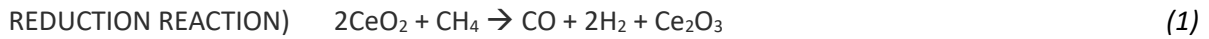


Figure 4: Schematic representation of the chosen chemical looping in the present study

In the present work, the above-mentioned chemical looping, analysed at the thermodynamic equilibrium, is integrated into a polygeneration plant for the production of:

- 1) electricity;
- 2) dimethyl-ether;
- 3) syngas;
- 4) methanol;
- 5) thermal power.

The plant is constituted of four main units:

- 1) chemical-looping unit. It is the prime mover of the plant and produces the fuel of the other secondary devices;
- 2) Solid Oxide Fuel Cell unit. It is a secondary device and it is supplied by the syngas produced in the reduction reaction of the CL. This unit produces electricity;
- 3) DME synthesis and distillation unit, integrated with a reforming reactor to apply CCU and produce syngas. It is another secondary device and it is fed by the syngas produced in the oxidation reaction of the CL. From this unit, DME, methanol and syngas are obtained;
- 4) steam production unit. In the plant, there are five heat recovery steam generators to produce steam exploiting the hot streams of the system, this steam is used in the plant to heat other cold streams and for producing thermal power, used for auto-consumption or for the supply of other users.

It is important to highlight that the chemical looping is able to work properly only under the presence of a sufficient irradiance heating the solar receiver-reactor of the reduction reaction to 900°C; for low values of the irradiance, the chemical looping shuts down. Therefore, the plant analysis is split into two different studies according to the two different operating conditions of the plant itself:

- 1) in the first operating conditions, it is evaluated the presence of a high amount of irradiance. In this case, all the components of the system properly operate;

- 2) in the second operating conditions, it is considered the presence of a low value of irradiance. In this case, only the SOFC can work. The SOFC is under-sized compared to the solar receiver-reactor of the CL so that it is fed by an amount of syngas that is lower than the value of the syngas stream produced in the reduction reaction. The surplus of the produced syngas is stored in an AISI316L tank to be then used in those periods in which the CL does not operate. This escamotage is applied to couple a high-temperature fuel cell, that has to work at constant operating conditions to have high efficiency (base-load operation), with the discontinuous and intermittent solar energy source.

Additionally, in the present system, a Carbon Capture and Utilization is executed in two different ways:

- 1) the CO₂ injected in the oxidation reactor of the chemical looping comes from the anodic exhausts of the SOFC after being separated in a flash unit at 15°C and 1 bar;
- 2) the CO₂ obtained from the exhausts of the DME synthesis and distillation unit, after being separated from water, is inserted in the biomethane reforming reactor to obtain a useful syngas stream.

Thus, the studied system is sustainable, green and emission-free. As shown in [Chapter 6](#), the polygeneration plant analysis and simulation are executed through the software Aspen v8.8. Global efficiencies of around 62.56% and 59.08%, thermal productions of 111.97 MWt and 35.82 MWt and electricity productions of 6.17 MWe and 28.96 MWe are respectively obtained when the CL is in ON-state and in OFF-state. The fuel production, which only occurs when the CL is in ON-state, is of $6.18 \frac{kg}{s}$ of DME, $0.71 \frac{kg}{s}$ of methanol and $19.67 \frac{kg}{s}$ of syngas. Two attempts to increase the electricity production of the system are made through the decoupling of the chemical looping operation from the intermittence of solar energy, which is executed feeding the reduction reactor with the heat produced by the SOFC. However, these two other plants present the problem of sequestration of the CO₂ produced in the system because the lack of solar energy should be compensated through the oxyfuel combustion of biomethane. The Aspen Plus chemical looping model is further investigated through comparisons with literature data of similar models and experimental studies. Additionally, preliminary experimental studies on the CeO₂/Ce₂O₃ chemical looping, coupled with methane reforming, are executed in the test bench at Environment Park.

1. SOLAR CONCENTRATING SYSTEMS

Solar energy is the main source of renewable energy on our planet. It is strongly distributed all over the world and it is in much larger quantities than the consumption related to human activities: the total amount of radiant energy that arrives on Earth from the Sun per unit of time and surface area is equal to 1.4 kW/m², therefore it could largely satisfy the world's energy needs. Solar energy is inexhaustible, available to all and clean: during its exploitation, it does not involve CO₂ and fine dust emissions. This energy source can be used for the production of electricity and heat. During the last years, the development of systems based on the use of solar energy has become increasingly important due to the focusing on the environment and, in particular, on the reduction of emissions and of the exploitation of non-renewable energy sources. In this regard, the Paris conference, held by 195 countries in December 2015, was crucial: an agreement (COP21) was reached to keep the average global temperature increase well below 2°C compared to pre-industrial levels and this increase was limited to 1.5°C [3]. It is also important to stress the economic benefits of solar energy. For example, even if the installation costs of a photovoltaic system are high, this investment is characterized by a sufficiently short payback time (around 8-10 years). However, the main disadvantage of solar energy is in its intermittence: solar radiation is not continuous due to the alternation day/night and climatic events. As a result, the continuity of production is not guaranteed. To overcome this problem, it is possible to opt for a system with storage, which allows to be able to dispose of thermal energy even when the system does not produce it. The main technologies that can be used to exploit solar energy are the solar thermal panel, the photovoltaic panel and the solar concentration panel. The solar thermal panel uses solar rays to heat domestic water or environments (e.g. houses and businesses). The main component of a solar thermal system is the thermal collector that heats a liquid, called heat transfer fluid, which will then move in the system to bring the heat to the desired areas. Solar thermal systems constitute a sustainable heating method as they do not involve the combustion of fossil fuels. The photovoltaic panel has as fundamental components the photovoltaic cells, which convert sunlight into electrical energy. Photovoltaic cells are made of silicon, which is a semiconductor material: when light radiates semiconductor materials, a flow of electrons is produced and it gives rise to an electric current. This study concerns concentrating solar systems used for rising the temperature of ceria particles involved in a chemical cycle and of gaseous streams involved in biomethane reforming downstream the DME unit respectively. When comparing photovoltaic systems and CSPs, the following advantages of CSPs should be taken into account:

- 1) there is no direct conversion of solar energy into electricity (as it happens in photovoltaic panels). The power cycle of these systems is very similar to those fed by fossil fuels, therefore, for the process of decarbonisation of electricity production, old systems (powered by fossil fuels) can be coupled with such CSP systems;
- 2) they could generate electricity 24 hours a day. Photovoltaic solar panels produce electricity intermittently, while some CSP systems can store heat in the form of molten salts and this thermal energy can produce electricity even in periods of low irradiance. This property makes CSP plants more predictable and reliable;
- 3) solar energy from CSP systems can also be used for other purposes than electricity generation, e.g. in chemical reactions for the production of solar fuels (the subject of this paper). This makes these systems more versatile.

A common disadvantage between CSP systems and photovoltaic panels is that they require large land areas that could otherwise be used for commercial, residential or agricultural development. M. Enjavi-Arsanji, K. Hibordi and M. Yaghoubi also found out that a CSP system is economical only for places with normal direct irradiation over $1800 \frac{kWh}{m^2 \cdot year}$ such as in wide-open spaces and desert areas; it is not economical in populated areas and regions that receive less sunlight during the year [8]. Another disadvantage of concentrated solar energy is that it uses a lot of water either to drive steam turbines

to generate electricity or to cool thermochemical reactors. Although the use of seawater may be a conventional solution, this would involve the construction of a CSP plant near the coast, which, in turn, may not be suitable for the possible low amount of solar radiation it receives.

1.1. Energy from the Sun

As previously written, solar radiation is at the basis of the operation of solar concentration panels (CSP).

1.1.1. The Sun

The Sun is the central star of the Solar System. With an age of about 4.5 billion years, the Sun has a radius of 0.696 km (about 109 times the radius of the Earth), a mass of 2×10^{30} kg and consists of 71% of hydrogen, about 27% of helium and the remaining 2% of all other elements [9]. Being mainly composed of rarefied gases, its average density is four times lower than that of the Earth and it is equal to 1.41 g/cm^3 [10]. As a result, the Sun is a sphere of gases at very high temperatures; these gases are concentrated around a central nucleus thanks to the gravitational force. As far as its structure is concerned, there are six concentric layers [11], as shown in *Figure 5*:

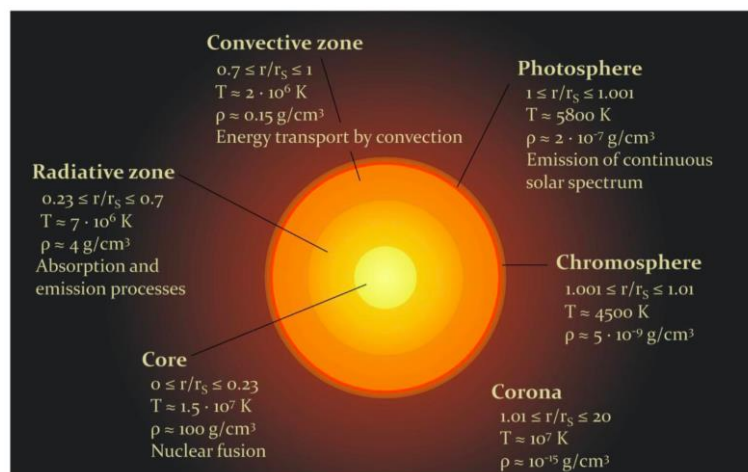


Figure 5: Solar layers [12]

The core is the innermost part of the Sun and it extends itself for about 20% of the solar radius. Inside the core, there are:

- a high concentration of hydrogen atoms;
- a high pressure (about 250 billion atm);
- a high density;
- a high temperature (estimated around 15 million °C).

In the core, heat and pressure are so high that nuclear fusion processes are maintained at full capacity. These reactions are based on the fusion of two hydrogen atoms (colliding with each other) into a helium atom, the helium atom (output) being less heavy than the two initial hydrogen atoms (input). The difference in a matter between the output and the input is transformed into energy:

$$E = \Delta m \times c^2 = 26,7 \text{ MeV for each reaction [13]} \quad (3)$$

with E =energy, Δm = difference between input mass and output mass, c =speed of light ~ 300000 km/s. This energy propagates outward from the star, while the helium atoms remain in the core (due to high pressure). The second layer is the radiative zone, which extends to about 70% of the Sun's radius beyond the core. This layer surrounds the core and it is characterized by much lower densities and pressures, as well as a temperature of about 7 million degrees. The energy produced in the nucleus, in the form of high-energy photons, moves towards the radiative zone through a process of radiation (there is no exchange of matter because the gas atoms in the nucleus are so packed that they cannot move). Photons move at the speed of light, but their frequent collisions with other particles make them not to follow a straight path outwards, so they are characterized by a very slow movement outside the radiative zone (energy takes more than 170,000 years to radiate through this layer of the sun [14]). Then, there is the convection zone. In this zone, energy is transferred very quickly by convection: the hotter gas, coming from the radiative zone, expands and rises through the convective zone because the latter is colder than the radiative zone and, therefore, less dense. When the gas rises, it cools and then it sinks back into the radiative zone. As the gas approaches the radiative zone, it heats again and rises; this process is repeated creating convection currents. The continuous movement of stellar matter produces very intense electric currents, which, in turn, generate important magnetic fields. The photosphere is a very thin layer in which light (visible electromagnetic radiation that propagates in space) is emitted. Therefore, this layer is the layer of the Sun that we see from the Earth and it is estimated to have an average temperature of 5800°C. As a result, energy is produced in the innermost regions of the Sun through nuclear reactions that release electromagnetic radiation (and particles), which is irradiated towards more external layers. However, the interior of the Sun is very dense and the radiation produced in the centre is continuously scattered by the collision with this dense matter: the radiation is absorbed by the matter and promptly re-emitted. As the radiation itself proceeds towards the outside, the density of the gas is reduced and the radiation undergoes fewer and fewer deviations; at a certain point, the radiation emitted by the gas no longer finds obstacles (in the photosphere) and can exit freely outside, so it crosses the increasingly less dense atmosphere and reaches the Earth. Strictly speaking, light from the Sun's yellow disk is emitted for the last time in the solar photosphere even though it is "generated" in the deepest interior of the star. Once a minimum temperature has been reached at the outer limit of the photosphere, the temperature itself begins to rise in the chromosphere (first layer of the solar atmosphere). The chromosphere is a layer of red-orange gas, generally, it cannot be seen with the naked eye because the light from the photosphere overhangs it. Finally, the corona is the outermost zone of the solar atmosphere and it has such a low luminosity that it can be seen with the naked eye only during a solar eclipse. Temperatures in the corona can approach two million degrees.

1.1.2. Solar radiation

A body at a temperature T , higher than the absolute zero, emits heat in the form of thermal radiation. Thermal radiation is strictly temperature-dependent and it is distributed over a continuous spectrum. From a radiation point of view, the Sun is a perfect emitter: it behaves like a body that absorbs all incident radiation without reflecting it (black body). The emission spectrum of a black body (distribution of the energy intensity of the radiation as a function of the wavelength) is defined by Planck's law and it is closely related to the temperature of the external surface (for the sun, this temperature is about 5800°C of the photosphere):

$$E_{\lambda}(T) = \frac{c_1}{\lambda^5 \left(e^{\frac{c_2}{\lambda T}} - 1 \right)} \left[\frac{W}{m^3} \right] \quad (4)$$

with:

- $c_1 = 2\pi hc^2$;
- $c_2 = \frac{hc_0}{k}$;
- $h = \text{Planck constant} = 6.62 \cdot 10^{-34} \text{ J}\cdot\text{s}$;
- $c = \text{speed of light} = 3 \cdot 10^8 \frac{m}{s}$
- $k = \text{Boltzmann constant} = 1.38 \cdot 10^{-23} \frac{J}{K}$

The wavelength, at which the maximum of the emission spectrum is obtained, can be expressed by the Wienn's law (or the law of displacement of maxima):

$$\lambda_{MAX} = \frac{2898}{T} [\mu\text{m}] \quad (5)$$

Therefore, the energy transported by the individual quanta that constitute the solar radiation is strictly dependent on the wavelength and this relationship can be expressed as follows:

$$e = h \cdot \frac{c}{\lambda} [\text{J}] \quad (6)$$

with $e =$ energy of the single quantum; thermal radiation carries a quantity of energy equal to an integer multiple of e . Considering the electromagnetic spectrum, at the two extremes of the wavelengths axis, there are: ultraviolet and gamma rays, very energetic and characterized by very small wavelengths and infrared rays and radio waves, low energetic and with high wavelengths. In the intermediate wavelengths (and energies), there is electromagnetic radiation visible to the human eye (light) which is characterized by shades ranging from 400 nm of violet to 700 nm of red. To sum up, rays with very small wavelengths (gamma, X, ultraviolet) are the most energetic, while the larger wavelengths are associated with infrared rays and radio waves, which are less energetic. At the centre, the range of lengths visible to the human eye is present and, mixing these wavelengths, they are perceived as white light.

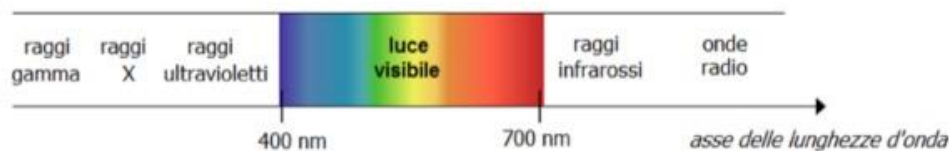


Figure 6: Electromagnetic spectrum; tones as a function of wavelengths (values on the axis are not in scale)

In the following *Figure 7*, a comparison between the real emission spectrum of the Sun outside the atmosphere (in the extraterrestrial zone) and the ideal emission spectrum of a black body at 5800 K (according to Planck's law indicated above (4)) is made:

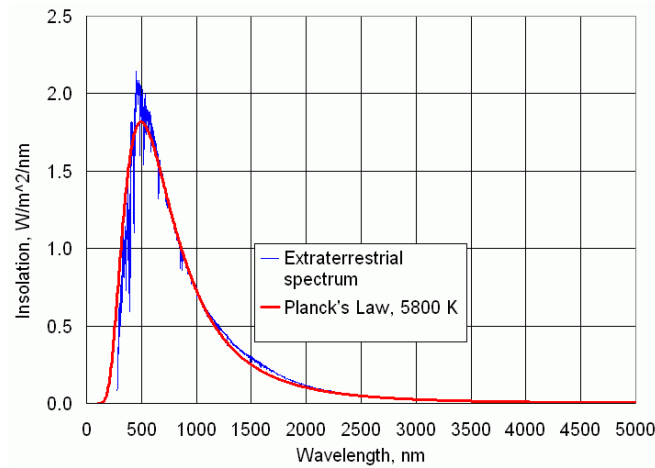


Figure 7: Extra-terrestrial spectral irradiance vs black body spectral emission at 5800 K [15]

As it could be expected, the two curves are almost superimposed (hence the approximation of the Sun to a black body), the area subtended by the curves is very similar and equal to 1367 W/m^2 . The maximum of the emission spectrum is around a wavelength of 480 nm (green colour of the visible spectrum). About the 6.4% of the total energy is in the ultraviolet ($\lambda < 380 \text{ nm}$), the 48% is in the visible spectrum and the remaining 45.6% is in infrared ($\lambda > 780 \text{ nm}$). By integrating the emission spectrum of the sun $g(\lambda)$ on the wavelengths of the solar radiation itself, the irradiance $G \text{ [W/m}^2\text{]}$ is obtained. The irradiance is the flow of solar energy incident on a surface per unit area of the surface and, by assimilating the sun to a black body, it can also be calculated through Stefan-Boltzmann's law:

$$\text{Total emissive power} = E(T) = G = \sigma \cdot T^4 \left[\frac{W}{m^2} \right] \quad (7)$$

with $\sigma = \text{Stefan- Boltzmann constant} = 5.67 \cdot 10^{-8} \frac{W}{m^2K^4}$. By integrating the irradiance over time, the irradiation $[\text{J/m}^2, \text{kWh/m}^2]$ is evaluated, i.e. solar energy incident on a surface per unit area of the surface.

1.1.3. Earth-Sun Interaction

The solar constant G_{sc} is defined as the solar energy per unit of time that is incident on a surface perpendicular to the Sun's rays and placed at the mean distance between the Earth and the Sun in absence of the atmosphere: $G_{sc} = 1367 \text{ W/m}^2$. This value is obtained by considering the total power of solar radiation W_s , evaluated through the Stefan Boltzmann's law (with $T = \text{photosphere temperature} = 5800 \text{ K}$) and the emission surface (equal to the external surface of the Sun):

$$W_s = \sigma \cdot T^4 \cdot 4\pi r_{sun}^2 = 5.67 \cdot 10^{-8} \cdot 5800^4 \cdot 4\pi \cdot (6.965 \cdot 10^8)^2 = 3.85 \cdot 10^{26} \text{ W} \quad (8)$$

and assuming that all the radiant energy leaving the Sun reaches the orbit on which the Earth is located with earth-sun distance = $d_{t-s} = 1.5 \cdot 10^{11} \text{ m}$:

$$G_{SC} = \frac{W_S}{4\pi d_{t-s}^2} = \frac{3.85 \cdot 10^{26}}{4 \cdot \pi \cdot (1.5 \cdot 10^{11})^2} = 1367 \frac{W}{m^2} \quad (9)$$

The solar radiation that, ideally, can be intercepted by the Earth can be evaluated from the radius of the Earth itself, equal to about 6367 km. In the ideal case, it is necessary to consider the absence of the atmosphere and a circular useful "section" for the interception of the solar radiation, the ray of the section is equal to the ray of the Earth itself and this circle is arranged perpendicularly concerning the direction of the solar rays (as shown in [Figure 8](#)).



Figure 8: Representation of the ideal Sun-Earth interaction [16]

In this case, the radiant power that the circular surface (and, therefore, the Earth) would receive would be 174 million gigawatts:

$$\text{Ideal radiant power} = G_{SC} \times \text{Area} = 174 \text{ milioni di GW} \quad (10)$$

with $\text{Area} = \pi \times R_{\text{earth}}^2$. However, the planets of the solar system, so also the Earth, can intercept only a fraction of the energy radiated by the Sun into space. This energy fraction mainly depends on the solid angle under which each of the planets is seen by the Sun and this angle depends on the size of the planet and its distance from the Sun. The Earth is about 150 million km (150 Gm) from the Sun and the solid angle between the Earth and the Sun is 4.65 mrad as shown in [Figure 9](#).

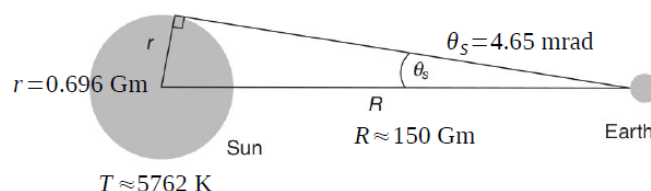


Figure 9: Sun-Earth geometry [17]

Other important factors that contribute to the actual solar radiation that is intercepted by the Earth are:

- the variation of the Earth-Sun distance throughout the year. Our planet reaches the closest point to the Sun in January (perihelion) and the furthest point in July (aphelion). To take this into account when calculating the irradiance, the solar constant must be corrected by $\pm 3.3\%$ [18]: $+3.3\%$ in January (maximum irradiance = 1412.1 W/m^2) and -3.3% in July (minimum irradiance = 1321.8 W/m^2);
- the presence of the atmosphere surrounding the planet. The various layers of the Earth's atmosphere attenuate sunlight through two phenomena: absorption and scattering. The attenuation of sunlight takes place at all wavelengths of the spectrum, but, depending on the specific wavelength, the effects vary, so the electromagnetic spectrum reaching the Earth has a completely irregular profile. At the Earth's surface, due to the absorption, spectral solar irradiance with a significant energy value occurs in wavelengths between 0.29 and $2.5 \mu\text{m}$. Considering the diffusion, instead, after having crossed the atmosphere, solar irradiance reaches the earth in the form of two components: direct solar irradiance (directly received from the Sun, without scattering from the atmosphere) and solar irradiance diffused from the sky (received from the Sun after its direction has been modified by scattering).

$$G_{\text{global earth}} = G_{\text{beam}} + G_{\text{diffuse}} . \quad (11)$$

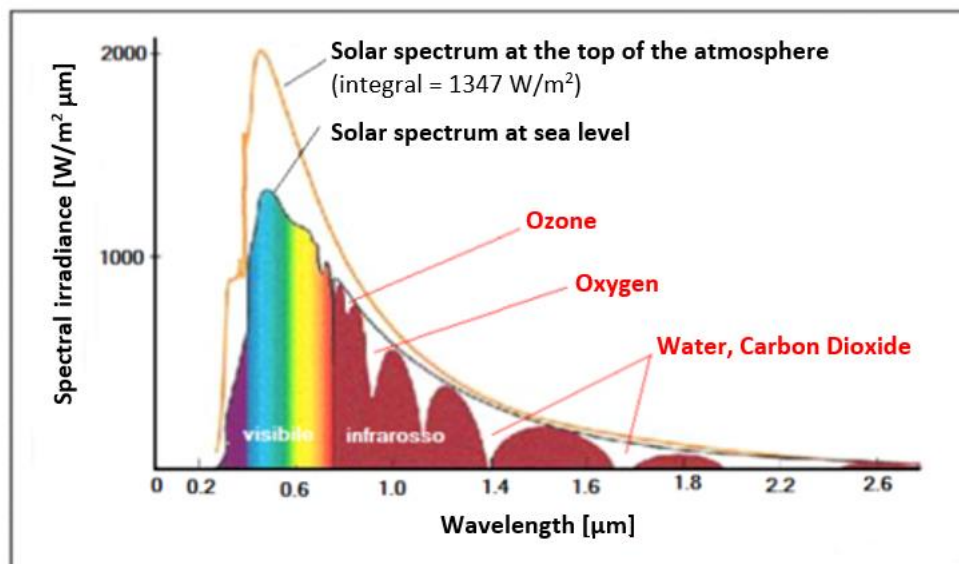


Figure 10: Attenuation of the solar spectrum in the atmosphere [19]

In *Figure 10*, the highest curve refers to the profile detectable at the top of the atmosphere: it is approximately that one of the emissions of a black body at a temperature equal to 5780K (the Sun's temperature); the slight deviations from the regular profile of the black body are due to the absorption by molecules and by atoms wandering in the interplanetary space (hydrogen etc.). On the other hand, the lowest curve refers to the profile found at ground level; irregularities and attenuation are more pronounced due to the numerous molecules of the atmospheric layer that absorb rays selectively. Aerosols absorb almost uniformly at all wavelengths, while particular molecules (oxygen, carbon dioxide, ozone, etc.) are responsible for downward peaks at particular lengths. To take into account the attenuation effects of solar radiation produced by the atmosphere, the definition of "Air Mass" (AM) is very important. Air Mass is a measure of how much of the atmosphere the sun's rays have to pass through on their way to the Earth's surface. Since the particles in the atmosphere absorb or disperse the

sun's rays, the longer the path of solar radiation in the atmosphere, the less solar energy can reach the Earth. At any given moment, the Air Mass can be expressed as the ratio between the length of the real path performed by the direct solar radiation in the atmosphere (\overline{AP} in *Figure 11*) and the length of the path that would be if the Sun were at Zenit (\overline{BP} in *Figure 11*):

$$AM = \frac{\overline{AP}}{\overline{BP}} \sim \frac{1}{\cos \theta_z} \quad (12)$$

outside the atmosphere, $AM=0$, while when solar radiation enters the Earth's atmosphere, $AM>0$. When the sun is at the Zenit, the solar radiation travels the shortest possible path in the atmosphere (the least possible amount of atmosphere is encountered by solar radiation), thus the Air Mass is equal to 1.

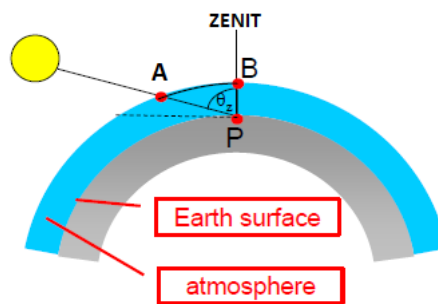


Figure 11: Definition of "Air Mass"

To understand the importance of the effect of the Air Mass on the spectral solar radiation, *Figure 12* shows different spectral distributions of solar irradiance $g(\lambda)$ considering different Air Mass values: the higher the value of AM and the lower the peak of solar irradiance.

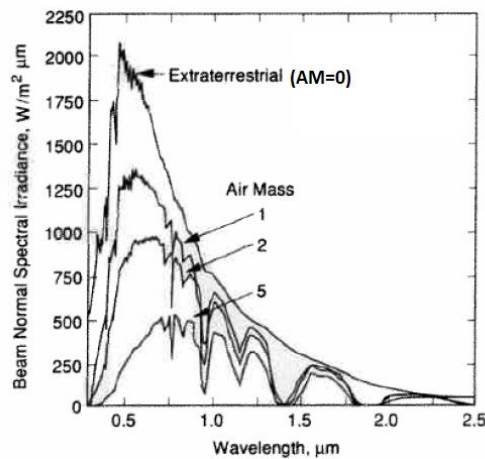


Figure 12: Spectral distributions of solar radiation $g(\lambda)$ for different values of Air Mass [18]

Considering the irradiance absorbed by a receiver on Earth, another component should be taken into account: the albedo. A small portion of the solar radiation that reaches the Earth, after being reflected from the Earth's surface, can reach a receiver on an inclined plane (albedo). The reflection coefficient ρ is defined as the ratio between the radiation reflected in

each direction from the Earth's surface and the radiation reaching the Earth's surface with direct and parallel rays. Therefore, the total irradiance that affects the surface of a terrestrial receiver consists of:

- direct irradiance;
- diffuse irradiance;
- albedo;

$$G_{\text{global terrestrial receiver}} = G_{\text{beam}} + G_{\text{diffuse}} + G_{\text{albedo}} . \quad (13)$$

- the influence of the clouds. This is the least quantifiable element because the cloud phenomenon is irregular in time and very variable in intensity. When conditions of intense cloud cover occur, the direct rays of the Sun are completely shielded from the clouds and the contribution to the measurement of the irradiance on the ground comes exclusively from "diffuse" radiation; the irradiance itself drops to values in the order of $50 \div 100 \text{ W/m}^2$ and even less. Therefore, the two contributions of direct and diffuse radiation are closely related to the metrological conditions; in case of clear sky, there is a diffuse radiation component of about the 20% of the total radiation.

1.2. Operation of a solar concentration panel

The solar collector is the most important component of systems that transform radiant solar energy into useful thermal energy. There is a transfer of energy by radiation between a radiant energy source (the sun) and a receiving body. As previously specified, sunlight carries with it a certain energy flow (amount of energy per unit of time and area, kW/m^2). For a given area, the sun delivers a certain amount of energy per unit of time, and, if the area is doubled, the amount of energy per unit of time is doubled. As a result, solar collectors should use a solar energy capturing area that is as large as possible. In the case of solar concentration systems, the collection area of the Sun's radiation is covered with mirrors that reflect this radiation on a smaller surface: the receiver. Solar concentration collectors focus only the direct radiation and they consist of:

- a concentrator;
- a receiver.

In *Figure 13*, considering a hypothetical irradiance equal to 1000 W/m^2 (maximum direct irradiance reaching the Earth), the scheme of a CSP panel is shown:

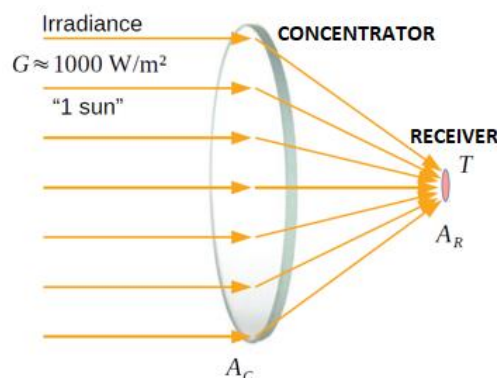


Figure 13: Concentrator-receiver scheme of a CSP panel

The mirror system concentrates the light on the receiver, causing the energy flow on the receiver to be significantly greater than the flow that naturally hits the earth. The ratio between the concentrated flux on the receiver and the environmental flux from the Sun is called “optical concentration ratio (C)”.

1.3. Concentration ratio: definition and limits

An important parameter of CSP systems is the optical concentration ratio C , which is indicated as the fraction between concentrated radiation intensity (I_r , or concentrated radiant flux) on the receiver and radiation intensity before concentration (I_o):

$$C = \frac{I_r}{I_o} \quad (14)$$

This ratio can be evaluated locally at any point of the system and it takes into account all the optical effects that occur in the collector (mirror reflectivity, shading, blocking, spillage). It is difficult and expensive to accurately evaluate this parameter, so it is often approximated to the geometric concentration ratio C_{geom} :

$$C_{geom} = \frac{A_a}{A_r} \quad (15)$$

with:

- A_a = aperture area of the concentrator, i.e. area of the capturing surface (mirror);
- A_r = receiver area;
- $A_r < A_a$.

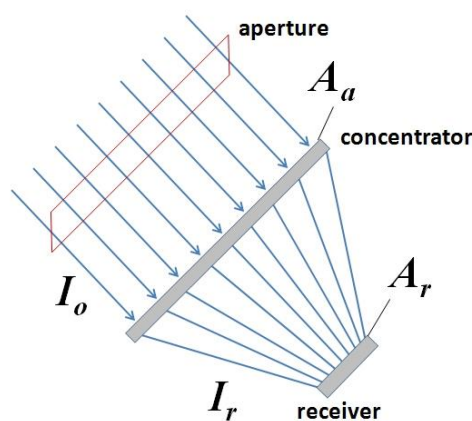


Figure 14: Aperture area and receiver area of a CSP panel [20]

The geometric concentration ratio is easy to be calculated given the areas of the concentrator and the receiver, but it is equal to the optical concentration ratio only if the radiation flow is uniform over the aperture of the receiver. Only some systems provide a uniform concentrated light flux, many others

with curved reflective surfaces (e.g. conical, parabolic, spherical) create a flux density distribution on the receiver and so they are characterized by a variable concentration ratio over the width of the receiver. In this case, the main parameter to characterize the performance of the concentrator is the local concentration ratio:

$$C_L = \frac{\text{Local intensity}}{\text{Incident intensity}} = \frac{I_r(y)}{I_o} \tag{16}$$

with $I_r(y)$ determined for any local position y from the centre of the produced image (as in *Figure 15*) and I_o equal to the incident radiation at the opening of the concentrator.

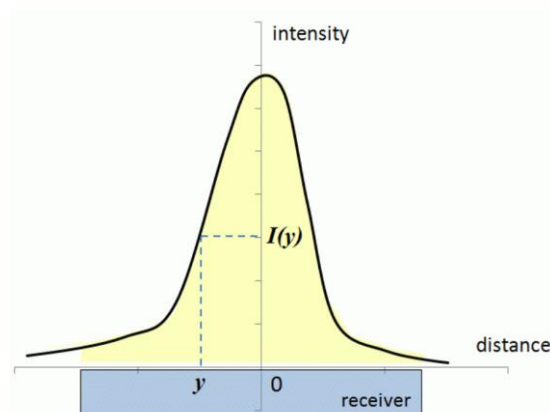


Figure 15: Example of distribution of local radiation intensity over the receiver in an imaging collector [20]

Another thing to be considered is that, for some concentrators, the available receiver surface area may be different from the image area produced by the concentrator on the receiver. If the image does not cover the entire receiver surface, the image area should be used to estimate the concentration ratio. The concentration ratio is very important to optimize the efficiency of a CSP solar system. Increasing the concentration, more light is focused on the collection area and more energy is produced on that area in a certain time interval. For a solar concentrator to be useful, it should be able to generate large amounts of energy, so the concentration should be increased as much as possible. However, this parameter is characterised by thermodynamic and optical limits. Thermodynamic limits are related to the fact that, for the second principle of thermodynamics, the receiver cannot reach the same temperature as the Sun; optical limits are related to: reflectivity of mirrors, blocking, shading and spillage. In *Table 1*, the maximum values of the geometric concentration ratio for different types of collectors are summarized considering both thermodynamic and optical limits and taking into account an ideal reflector and a receiver having the characteristics of a black body:

$C_{g,max}$	Thermodynamic limits	Optical limits
Dish with a flat receiver	46.25	11.6
Dish with a spherical receiver	46.25	11.6
Trough with a flat receiver	215	108
Trough with a cylindrical receiver	215	68.5

Table 1: Maximum value of the concentration ratio for different technologies

To sum up, optical effects impose much more restricting limits compared to thermodynamic effects.

1.4. Maximum receiver temperature

A further parameter to be taken into account in the solar concentration is the receiver temperature. Since large amounts of energy are deposited on the receiver quite quickly, the receiver heats substantially. There usually is a heat transfer fluid that removes heat from the receiver, keeping it at a stable temperature and transporting thermal energy to a thermal engine. Depending on the amount of refrigerant used to remove energy from the receiver, the operating temperature of the receiver itself is defined and this temperature also affects the efficiency of the solar collector. The connection between the operating temperature of the receiver and the efficiency of the collector is related to the loss of energy for thermal emission from the receiver. The receiver is designed to absorb light efficiently, so it can be approximated to a black body and any black body loses energy by emitting black body radiation. The amount of energy lost due to black body radiation rapidly increases with temperature. This concept is expressed more clearly later. In [Figure 16](#), the surface of a receiver is shown and it is characterized by:

- 1) incident flux equal to GC ;
- 2) absorbed flux equal to αGC ;
- 3) emitted flow equal to $\epsilon\sigma T^4$;
- 4) reflected flux equal to $(1-\alpha)GC$.

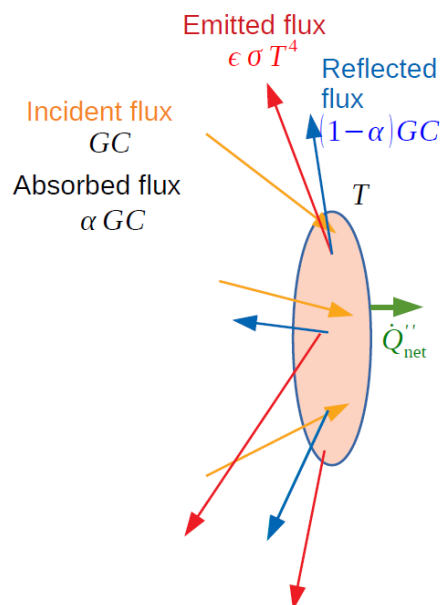


Figure 16: Receiver area as a black body [17]

When performing an energy balance at the receiver, the absorbed thermal power per unit of the surface area is:

$$\dot{Q}_{\text{net}}'' = \alpha GC - \epsilon\sigma T^4, \quad (17)$$

the thermal efficiency of the receiver is:

$$\eta_{th} = \frac{\text{absorbed flux}}{\text{incident flux on the receiver}} = \frac{\text{incident flux} - \text{reflected flux} - \text{emitted flux}}{\text{incident flux on the receiver}} \quad (18)$$

$$\eta_{th} = \frac{A_{rec} \dot{Q}_{net}''}{GC A_{rec}} = \alpha - \varepsilon \frac{\sigma T^4}{GC}.$$

From the formula of η_{th} , it can be stated that: increasing the temperature T of the receiver, the efficiency of the receiver itself is reduced due to emission losses and, approximating the receiver to a black body ($\alpha=\varepsilon=1$), in the extreme case in which the stagnation temperature is reached ($T_{st} = \sqrt[4]{\frac{GC}{\sigma}}$), $\eta_{th} = 0$. To sum up, to minimise such losses it is advantageous to limit the operating temperature. However, it is also necessary to examine the energy lost as heat in the conversion of thermal energy into mechanical work in the power unit. Carnot's theorem states that the maximum efficiency of a heat engine (η_{carnot}) is determined by the ratio between the high receiver temperature (T) and the cold temperature of the heat sink (T_0):

$$\eta_c = 1 - \frac{T_0}{T}. \quad (19)$$

The cold temperature of the heat sink is the ambient temperature of the earth (which is about 300 K); any temperature below this one will not produce any mechanical energy and the efficiency of the power cycle would be equal to 0. To maximize the efficiency in the heat engine, the temperature should be much higher (if there was an infinite temperature, for example, the efficiency would be equal to 1). The overall efficiency of the system for the conversion of solar energy into mechanical energy is:

$$\eta_{global} = \eta_{th} \cdot \eta_{th \text{ engine}} \quad (20)$$

with:

- η_{th} which reduces increasing T ;
- $\eta_{thermal \text{ engine}}$ which increases as T increases and it is lower than η_c .

Figure 17 shows the overall efficiency of a CSP system coupled with a Carnot cycle. This graph underlines that the thermal power absorbed by the receiver increases as the concentration ratio increases ($\dot{Q}_{net}'' \propto C$) because a high concentration ratio produces high temperatures on the receiver itself.

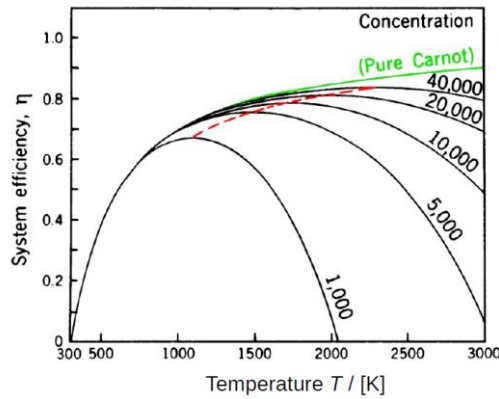


Figure 17: Global efficiency of a CSP system coupled with a Carnot cycle [17]

1.5. Geolocation of CSP systems

As previously written, CSP collectors only concentrate on direct radiation because its direction is well defined and it is not scattered by the atmosphere. This radiation reaches the Earth's surface in rays parallel to the surface itself and so it can be easily concentrated. Diffuse radiation cannot be used in these systems because its direction varies randomly and unpredictably. The predictability of the direction of the sun's rays is important for the design of CSP panels to capture as much solar radiation as possible. This feature limits the possible location of CSP systems, which can only be installed in sites with high direct solar radiation values, normally above 2000 kWh/m² per year. As a result, cost-effective energy production from CSPs takes place in sunny and arid regions between 15° and 40° latitude north or south of the equator. In general, equatorial regions are not particularly suitable for the installation of CSP systems because of cloudiness and frequent rainfall. High direct insolation values are also found in locations at high altitudes above sea level, where the atmosphere is very clear (as shown in [Figure 18](#)) [21].

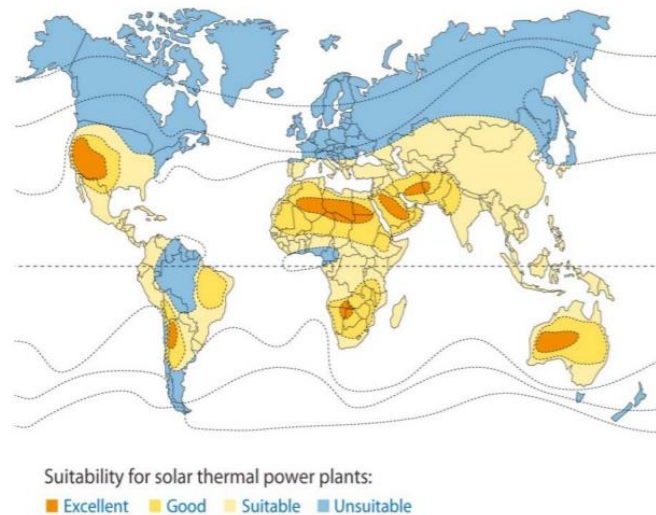


Figure 18: Geolocation of CSP systems

In high altitude deserts, such as the Atacama desert in Chile, which has an average altitude of 4000 m above sea level, direct radiation can reach levels of 3000 kWh/m² per year. In the most favourable locations, with DNI of 2200 kWh/m² per year, electricity production can reach values of 120÷140 GWhe/km² per year. Latitude is not the only parameter that characterizes the optimal location of CSP plants. Other important factors include general weather conditions (annual rainy and foggy days), frequency and speed of prevailing winds (affecting the design of collector supports), orography (the proximity of mountains can induce meteorological instability) and site altimetry (affecting the installation of collectors). As it can be seen in *Figure 18*, most of the Italian territory falls within the geographical area classified as "suitable"; only the Po Valley (partially) and the Alpine region are excluded.

1.6. Classification of concentrators

Four different CSP plant technologies, depending on the type of concentration system, are used (see *Figure 19*):

- 1) parabolic trough collector (PT);
- 2) linear Fresnel reflector (FR);
- 3) solar tower and heliostats (ST);
- 4) parabolic dish collector (SD).

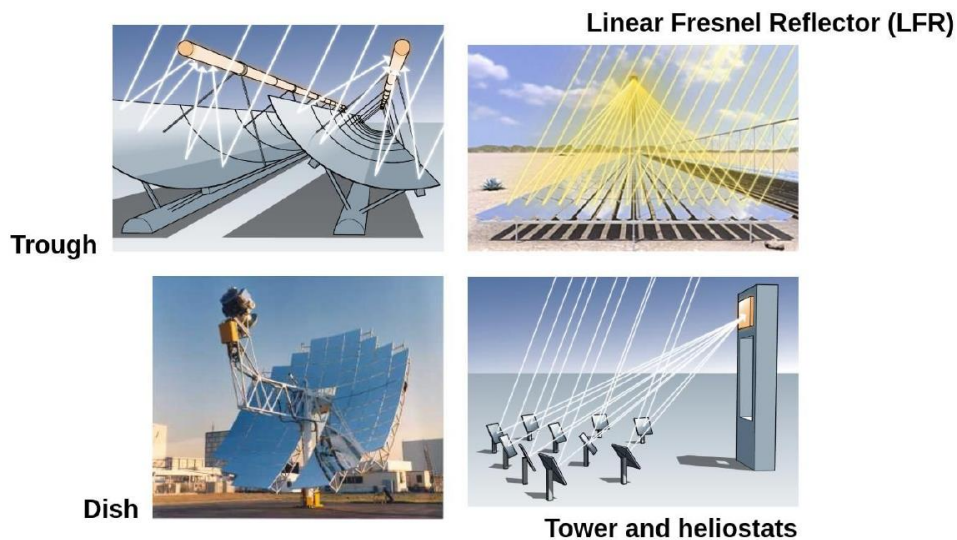


Figure 19: CSP plant technologies

Each technology is characterized by a different capacity of concentration of solar energy, so by different reachable operating temperatures. In the first two types (PT and FR), mirrors concentrate solar radiation on a focal line (linear concentrators), with concentration factors in the order of 60-80 and a maximum operating temperature of around 550°C. In the other two types (ST and SD), mirrors concentrate the radiation on a single focal point (point concentrators), with much higher concentration factors and higher operating temperatures. The following tables (*Table 2*, *Table 3*) show some characteristic values of concentration, efficiency and operating temperatures that can be associated with the various types of CSP systems [21]. It has to be noted that:

- 1) solar efficiency is the ratio between net electric production and direct solar radiation;

- 2) temperatures and efficiencies are evaluated in an ideal condition, the receiver is considered as a black body.

SYSTEMS	Concentration ratio	Peak solar efficiency (%)	Annual average peak solar efficiency (%)
Parabolic trough	70-80	24-28	12-16
Linear Fresnel	25-100	20	9-11
Solar tower	300-1000	22-24	16-18
Parabolic dish	300-2000	24-26	13-16

Table 2: Concentration factors and solar efficiencies characteristic for CSP technologies

SYSTEMS	Maximum temperature (°C)	Optimal temperature (°C)	Maximum efficiency (%)
Parabolic trough	750-850	350-450	46-50
Linear Fresnel	600-900	300-450	40-50
Solar tower	1250-1750	610-900	60-67
Parabolic dish	1250-2100	610-1080	60-70

Table 3: Characteristic temperatures and efficiencies for CSP technologies

1.6.1. Linear concentrators

1.6.1.1. Parabolic Trough (PT) collectors

Parabolic Trough (PT) technology is the most widespread and cost-effective in the industry. It accounts for over 90% of the installed CSP power worldwide. PT is characterized by linear parabolic mirrors that concentrate the solar radiation on tubular receivers placed on the focal line. A heat transfer fluid (e.g. water, synthetic oil, molten salt or gas) flows through the tubes and it is heated to high temperatures to be then used (generally) to produce steam in a steam generator. A single linear parabolic collector consists of mirrors mechanically connected to the receiver tube; this block rotates around an axis, concerning the support structure, to track the Sun.

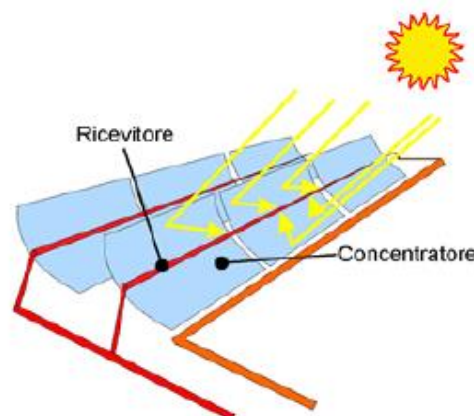


Figure 20: Scheme of Parabolic Trough collectors

The choice of a parabola shaped section can be explained by a property of the parabola itself: the tangent at any point belonging to a parabola is the bisector of the angle formed between the direction of a straight line parallel to the axis passing through that point and the conjunction of the point itself with a fixed point called focus. From this property, it can be deduced that: considering a plane tangent to the parabola at any point, this plane reflects the solar rays towards the fire provided that the rays themselves hit the plane with a direction parallel to the axis of the parabola.

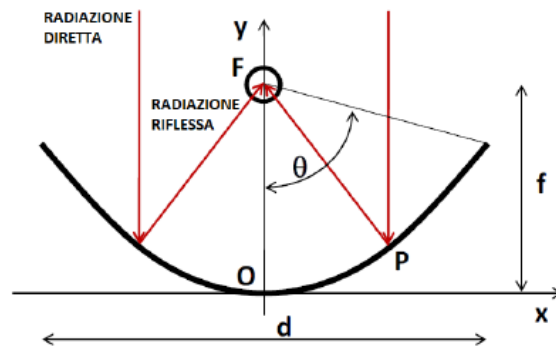


Figure 21: Parabola of the PT

As a result, the useful solar energy is given by the component of the solar radiation which is directed normally concerning the capturing surface (DNI, Direct Normal Irradiation), so a system that follows the solar trajectory is needed to ensure the orthogonality between the panels and the Sun's rays. For their geometric complexity, in parabolic trough collectors, a one degree of freedom device is used to rotate the horizontal axis of the collector from East to West or from South to North. However, with the rotation of the collector around a single axis, it is not possible to keep the collector surface oriented in a direction perfectly normal to the Sun's rays, which is, instead, possible using more complex tracking systems with movements on two axes.

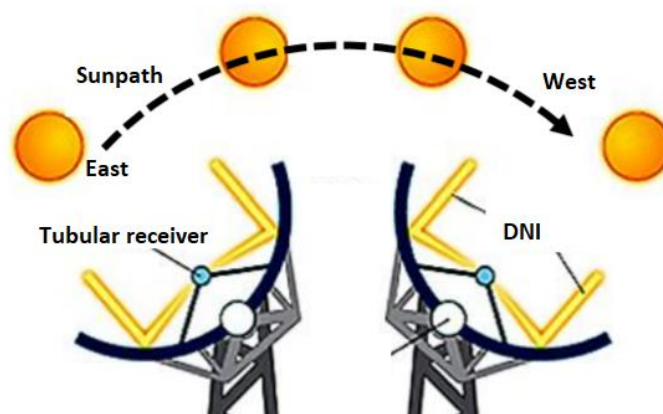


Figure 22: Tracking system of a PT

Most of the currently in operation PT systems produce electricity. These systems have the following properties:

- 1) powers from 15 to 100 MWe;

- 2) an average efficiency of 14-16% (efficiency expressed in terms of a ratio between net electricity produced and solar energy input);
- 3) a maximum operating temperature of 390°C, as a result of the stability limits of the fluid (synthetic oil), used as a means of transporting heat.

Some of these plants are designed to store high quantities of thermal energy through the storage of molten salts in special tanks.

1.6.1.2. Linear Fresnel Reflector (LF)

Fresnel collectors differ from parabolic trough collectors because the concentrator consists of flat or slightly curved mirrors. The receiver tube, positioned along the focal axis is, in this case, fixed: for the solar tracking, the movement only concerns the concentrator. In such systems, there also is a secondary concentrator (reflector) to recover the part of radiation which is dispersed because of the lower optical performance of this type of concentration system. The mirrors (or primary reflectors) can rotate along the longitudinal axis to follow the motion of the sun and keep the solar radiation constantly reflected on the receiver tube. They also are mounted close to the ground: this makes it possible to reduce the effects of wind action and to minimize the use of supporting structures.

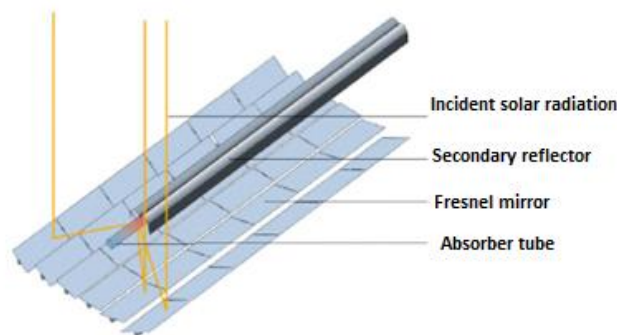


Figure 23: Linear Fresnel collector

Linear Fresnel collectors have some characteristics, which make them potentially competitive with parabolic trough collectors:

- 1) the shadow effect between nearby concentrators is negligible;
- 2) since the rows of the collectors do not have to be spaced, there is a better exploitation of the ground, 70% of exploitation of the ground against the 33% of parabolic trough collectors;
- 3) installation costs are much lower as a result of the lower commitment of materials.

However, their average efficiency is lower than that of parabolic trough systems because of the lower efficiency of both the collectors (temperature, non-vacuum insulated receiver tube, radiation concentration system) and the thermodynamic cycle. Typically, the concentration factors of such collectors vary between 25 and 40, while the attainable temperature is about 400 °C. This type of systems generally uses pressurized water as a heat transfer fluid, with direct steam production inside the receiver tube for applications at 270 °C and 40 bar. When temperatures above 270 °C should be reached, diathermic oils are generally used. The main features of these collectors (simple construction, lower maintenance costs, easy washing of flat reflectors, low wind loads, stationary receiver tube) make them particularly suitable for thermal applications at low-medium temperatures.

1.6.2. Point concentrators

1.6.2.1. Central tower collectors

The central tower system uses flat reflective panels (heliostats) that follow the sun with a rotation movement on two axes, concentrating the sunlight towards a single receiver, which is mounted on the top of a tower and inside which a fluid is circulated for the removal of solar heat. The obtained thermal energy can be used in various processes, for example in electricity production.

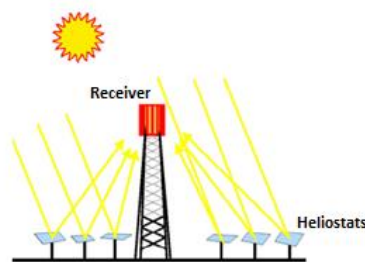


Figure 24: Structure of a Solar Tower system

The solar rays, which hit each heliostat, are reflected on a single point; this point is fixed in time and it acts as a focal point. The optical efficiency of the solar field is reduced by:

- shadowing (projection of the shadow of a heliostat on the rear one);
- blocking (incidence of the radiation reflected by a heliostat on the front one);
- spillage (fraction of radiation reflected by a heliostat leaving the receiver target).

The height of the focal point concerning the ground increases as the extent of the solar field increases and it can also exceed one hundred meters. Heliostats are installed in such a way to surround the tower or they are placed in a semicircle to the north. To avoid shading, they are increasingly spaced as they move away from the tower. Each heliostat could have an aperture area which varies from 40 to 170 m². In this type of plant, the heat transfer fluid circulating inside the receiver can reach high operating temperatures (565 °C using molten salts and 800-1000 °C using air). The available heat can be directly used in chemical processes that require high temperatures or in high-efficiency thermodynamic cycles for the production of electricity. The most recent tower systems are normally coupled to a thermal storage system, to cover more satisfactorily the energy demand of the user. Generally, around two hectares of the solar field are necessary for each installed MWe. The size of central tower solar systems is limited by the material possibility to keep the heliostats pointed with the necessary precision in the presence of wind as the distance from the receiver increases. Currently, the limit radius of a heliostat field is estimated to be in the order of 1000 meters, which corresponds to a tower with a height of 200-250 meters. The rated limit power for this type of systems is estimated at 50-100 MWe.

1.6.2.2. Parabolic dish collectors

Parabolic dish collectors consist of paraboloid-shaped reflective panels that follow the sun with a rotation movement around two orthogonal axes and concentrate the solar radiation on a receiver mounted at the focal point (see [Figure 25](#)).

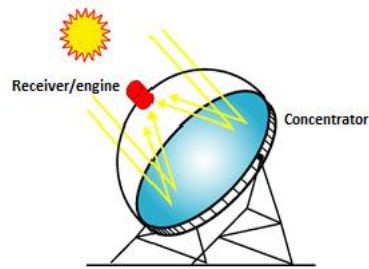


Figure 25: Structure of a parabolic dish collector

The ideal shape of the concentrator is a paraboloid of revolution; some concentrators approximate this geometric shape mounting a set of mirrors with a spherical profile on a support structure. For economic reasons, the size of the concentrator does not exceed 15 m in diameter, thus limiting the power of each collector to about 25-30 kWe. However, this technology is modular, allowing the construction of small/medium power plants. The heat at high temperature is normally transferred to a fluid and used to directly produce mechanical or electrical energy in a motor positioned above the receiver. The working fluid is compressed, heated and expanded through a turbine or piston to produce mechanical energy; this energy can be directly used by the user or transformed into electricity employing an alternator. Typically, a Stirling cycle, powered by air or hydrogen, is implemented and this cycle operates fully automatically (without continuous surveillance) in an isolated way or with clusters or solar farms with hundreds or thousands of units (as in [Figure 26](#)).



Figure 26: The Solar Card Plant in Peoria, Arizona (USA)

Concerning the operation of Parabolic Dish collectors, they start to operate in the morning, chase the sun during the daytime motion and return to their rest position at the end of the day. Another solution that can be implemented at the receiver is the Bryton microturbines. They are significantly less expensive than Stirling machines, but also less efficient, with efficiency values between 25% and 33%, compared to the 42% of the best Stirling engines. A penalizing limit of the current parabolic dish systems is the lack of a sufficiently efficient thermal storage system. At this state of the art, industrial applications of parabolic dish solar collectors allow to obtain:

- operating temperatures above 900 °C;
- the highest efficiencies of conversion of solar energy into electrical energy of all existing solar technologies (20% average daily efficiency with peaks of 25%).

Given the high conversion efficiency, the ease of installation and the possibility of cost reduction with mass production, it is easy to predict that these systems will become competitive even with large thermodynamic solar systems.

1.6.2.3. CSP system of the present study

In the present study, it is evaluated the use of concentrated solar power to supply both the reduction reaction of the chemical looping and the biomethane reforming reactor downstream the DME unit. For the high solar thermal requirements (around 294 MWt) of the system, there is the necessity of a very large CSP plant. Since also the required temperatures are very high (900°C for the reduction reaction and 800°C for the reforming reaction) a solar tower system is considered to be possibly used.

2. SYNTHESIS GAS (SYNGAS)

The production of synthesis gas is important for several aspects and it can be obtained through different processes which use a wide variety of raw materials.

Concerning the use of fossil fuels and biomass, gasification is one of the main processes to obtain synthesis gas. Gasification can be applied to carbon-rich materials (coal, oil, biomass, wood, organic waste) and it takes place at high temperatures (above 700-800°C) in the presence of a sub-stoichiometric percentage of an oxidizing agent, typically air (oxygen) or steam. The conversion of organic compounds into syngas has several advantages compared to their direct combustion:

- 1) pressurized syngas can be transported in a much easier way than a solid fuel;
- 2) syngas is very versatile. It can be directly burned in internal combustion engines, used to produce methanol or hydrogen or converted through the Fischer-Tropsch process into a synthetic fuel;
- 3) to reduce the contribution to pollution and greenhouse effect of the gasification plants, it is possible to couple to them sections of: treatment of syngas, removal of particulate matter and sulphur compounds and capture and sequestration of carbon dioxide.

As far as the exploitation of solar energy is concerned, synthetic gas can be used as an energy carrier for the storage of solar energy itself, as it is thought to do in the present work. This energy vector can be easily transported and used according to energy demand, thus solving the main problem of solar energy, linked to its intermittence.

2.1. Syngas composition and applications

Syngas is a mixture mainly consisting of varying amounts of hydrogen and carbon monoxide. It can be obtained by reaction of various sources (natural gas, coal, biomass and, in general, of a hydrocarbon charge) with steam (steam reforming), carbon dioxide (dry reforming) or oxygen (partial oxidation). The name "synthesis gas" derives from the fact that syngas is one of the most important intermediates in energy production it can be used as a fuel, as a reagent or as a hydrogen source. The main applications of syngas are power generation and synthesis of additional chemicals and fuels. In this study, syngas is used both for electricity and fuels production.

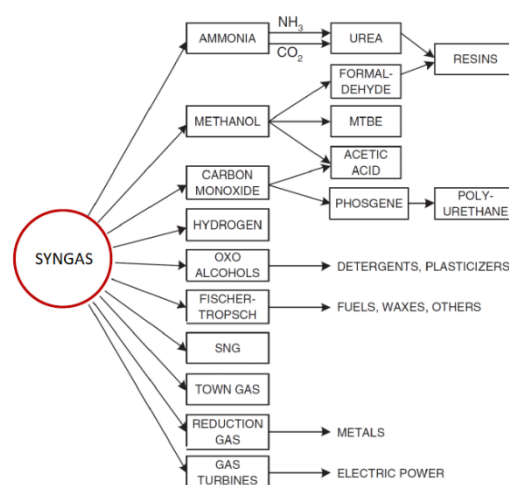


Figure 27: Syngas applications

2.1.1. Power generation through combustion or electrochemical oxidation

Syngas can be used as fuel in a gas turbine, in an internal combustion engine or in a fuel cell for electricity generation. As an example, an IGFC (integrated gasifier fuel cell) with CO₂ capture is reported [22]. In this plant, there is the coupling of a gasifier with a power island and a carbon capture system (see *Figure 28*). The primary fuel is fossil (coal) and it feeds a Shell-type gasifier, the produced syngas is introduced into a SOFC-type fuel cell, which works under pressure and at a temperature of about 800°C to produce electricity. Subsequently, CO₂ capture takes place according to the mechanism of oxyfuel combustion: the anode's exhausts are burned with pure oxygen to produce a hot, pressurised mixture of CO₂ and H₂O which is expanded in a gas turbine to produce electricity. Downstream the gas turbine, there is a condenser in which the mixture is cooled and separated from the water, so the carbon dioxide (with a purity of about 93vol.%) can then be compressed and prepared for transport and subsequent storage.

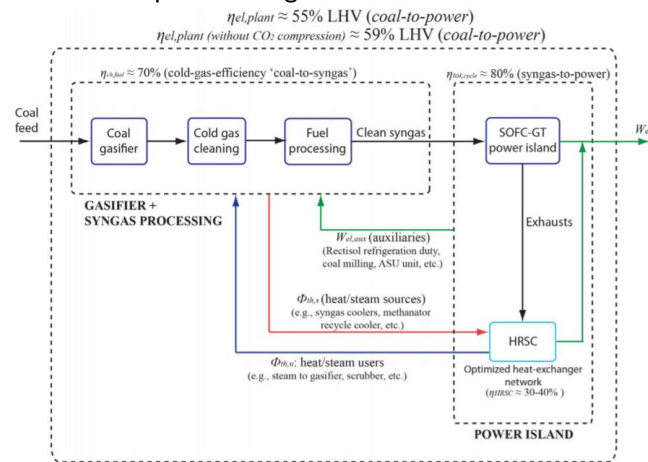


Figure 28: IGFC plant [22]

A similar scheme is also used in IGCC (integrated gasification combined cycle) plants, but, in this case, the high-temperature fuel cell (SOFC) power unit is replaced by a gas turbine. In the present study, the syngas produced in the reduction reaction of the CL is used to produce electricity in a SOFC.

2.1.2. Synthesis of chemicals and fuels

Most chemicals and fuels are conventionally obtained from the crude oil refinery. However, because of the rapid depletion of oil reserves and the more stringent environmental impact directives, alternative processes are needed. Therefore, the conversion of synthesis gas into fuels and other chemicals is one of the most important applications of syngas itself as it implements the strategy of the so-called "Green Carbon Science", which regards the production of high energy efficiency substances with low CO₂ emissions [23]. Different products can be obtained from syngas: pure hydrogen, carbon monoxide, ultra-clean gasoline, diesel, high-quality waxes, arenas, olefins, alcohols, aldehydes, carboxylic acids, carboxylic esters and dimethyl ether. One of the most important conversion processes of syngas is that of Fischer-Tropsch, mainly used for the synthesis of liquid hydrocarbon fuels such as kerosene, diesel and gasoline, which are easy to transport with current technologies. The Fischer-Tropsch process is performed at high temperatures and pressures, it requires high molar ratios H₂:CO (2:1 to 3:1) and it uses metallic catalysts. The reaction is as follows:



In the present study, the syngas produced in the oxidation reaction is injected in the DME synthesis and distillation unit for methanol and dimethyl-ether production.

2.2. Production of syngas with thermochemical processes powered by solar energy

Conventional industrial processes for the production of syngas/hydrogen are characterised by intensive use of fossil fuels. In such processes, the low energy content of carbon sources (coal, natural gas, biomass) is increased through the use of additional energy from the combustion of fossil fuels. However, the continuous combustion of fossil fuels in both industry and transport is having two serious effects: progressive depletion of fossil fuels and climate change. As regards the latter, in recent decades, the greenhouse effect has become an increasingly important phenomenon:

- 1) CO₂ emissions from fossil fuel combustion account for about 58% of global anthropogenic greenhouse gas emissions;
- 2) the concentration of CO₂ in the atmosphere is increasing by about 2 ppm/year, thus altering the natural carbon cycle, the amount of carbon emitted into the atmosphere is much higher than the amount that natural sinks can absorb.

To mitigate these phenomena, industrial processes for the production of syngas/hydrogen from solar energy have been developed, thus giving rise to the so-called solar non-fossil fuels. There are different methods for the production of solar fuels:

- 1) photochemical or photobiological conversion;
- 2) electrochemical conversion;
- 3) thermochemical conversion: reforming, gasification, splitting cycles.

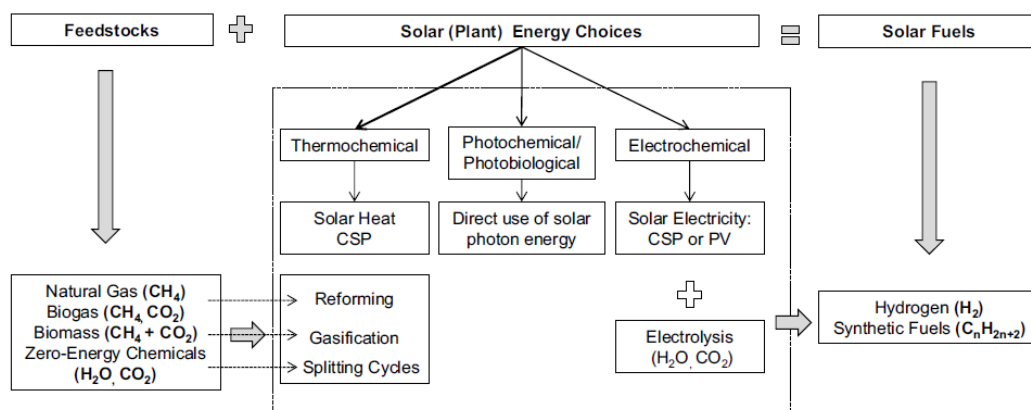


Figure 29: Syngas production technologies [7]

2.2.1. Photochemical or photobiological conversion

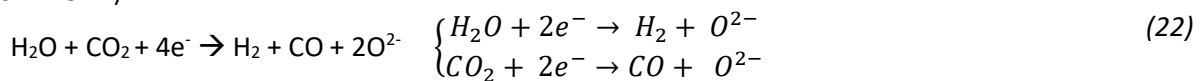
Photochemical and photobiological conversion processes take place at relatively low temperatures thanks to the direct use of solar energy from photons to feed photochemical or photobiological processes. In photochemical conversion, light is absorbed by a photo-catalyst to split a vapour/CO₂ mixture to produce syngas. Therefore, to give rise to this process, photo-catalysts are necessary: metal oxides are used and, considering current technologies, TiO₂ is the most stable and useful metal oxide, but it is characterized by a high energy gap between the bands. Photobiological conversion is based

on the so-called photosynthesis, which is carried out by a certain number of organisms. For example, in photolytic biological systems for hydrogen production, microorganisms (such as green microalgae or cyanobacteria) use sunlight to divide water into oxygen and hydrogen ions. Hydrogen ions can be combined through direct or indirect pathways and released as hydrogen gas. The problems related to these processes are: low rates of hydrogen production and the fact that water splitting also produces oxygen, which quickly inhibits the hydrogen production reaction and which can be a safety problem when mixed with hydrogen in certain concentrations. Researchers are working on developing methods to allow microbes to produce hydrogen for longer periods and to increase hydrogen production rates [24].

2.2.2. Electrochemical conversion

Electrochemical conversion processes consist in the co-electrolysis of CO₂ and H₂O for the production of syngas thanks to the chemical reactions that take place in an electrolyzer (usually in a SOEC) at the cathode and anode respectively:

CATHODE)



ANODE)



Electrolysis is a process that can only be carried out by supplying electricity from outside. In this case, for the production of solar fuels, electricity can be obtained from photovoltaic panels or thermal power stations. During electrolysis, the electrical energy supplied to the system is transformed into chemical energy in the form of H₂ and CO.

2.2.3. Thermochemical conversion

Thermochemical conversion processes take place thanks to the use of concentrating solar panels in which a concentrator concentrates the radiation on a point, the receiver. Energy is absorbed by the solar reactor where high temperatures are obtained, these temperatures can be used to give rise to specific reactions for the production of solar fuels. In this way, concentrated solar energy is stored in the chemical bonds of the produced solar fuels. Syngas can mainly be obtained through three thermochemical processes: reforming, gasification and splitting cycles [25]. Reforming and gasification, in general, use fossil fuels (or a mixture of fossil fuels, water and carbon dioxide) as raw materials to obtain hydrogen or syngas; thus they generally could contribute to greenhouse gas emissions and fossil fuel depletion. However, these two effects are mitigated by the use of solar energy as an energy resource while, in conventional methods, the energy source is given by the combustion of fossil fuels themselves. On the contrary, splitting cycles are emission-free as they only use concentrated solar energy and water or a mixture of water and CO₂.

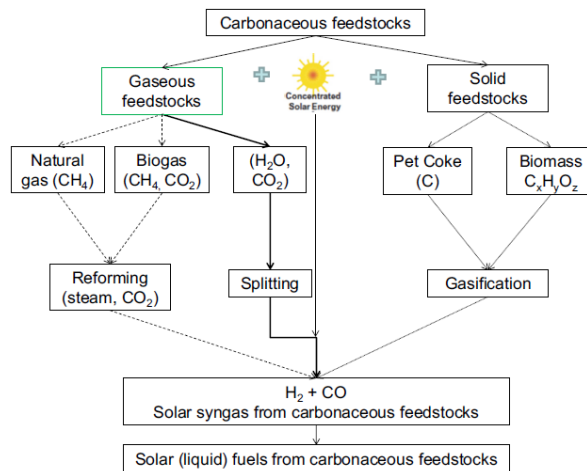


Figure 30: Thermochemical processes for syngas production [7]

2.2.3.1. Reforming

The most studied materials for the steam reforming of hydrocarbons are methane and natural gas (constituted of methane and other gases) because they contain a higher mass percentage of hydrogen than other hydrocarbons. In steam reforming, methane reacts with vapour at temperatures of about 800-1000°C in the presence of a catalyst (e.g. nickel). From this reaction syngas is obtained:



In natural gas reforming, CO₂ can also be used instead of steam as a gasifying agent (dry reforming):



This reaction is generally conducted at higher temperatures (800-1300 °C, depending on the stoichiometry of the reaction) in the presence of catalysts such as rhodium, palladium and nickel. The steam reforming of natural gas is one of the most used processes for the production of syngas due to the high speed of the reaction and the high chemical conversion that is obtained. For the reforming of methane coupled with solar concentration panels, research is mainly focused on the development of volumetric solar reactors because they are characterized by better thermal properties and efficiency than indirectly irradiated systems. However, the main disadvantage of these systems is related to the absorbing material, which has to be more resistant to thermal stress and the sintering of the catalyst must be reduced. In the present study, the dry reforming of biomethane at a temperature of 800°C is implemented downstream the DME unit to obtain a useful output (syngas) from the CO₂ separated partly from the anodic exhausts of the SOFC and partly from the exhausts of the DME distillation unit. Considering the reaction temperature of 800°C, it is considered to make it occur in a continuous flow receiver-reactor of a CSP system. Biomethane is produced through the pressure swing adsorption (PSA) mechanism applied to the biogas obtained from the organic fraction of the municipal solid waste (OFMSW), so it is a renewable energy source because it is not originated by fossil fuels.

2.2.3.2. Gasification

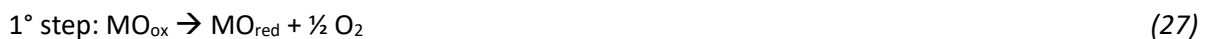
In the gasification reaction of coal, there is a partial combustion reaction of the coal itself with steam and oxygen at temperatures in the range of 800 and 1500 °C. The main product is a mixture of CO and H₂ (syngas) in different proportions:



In the case of biomass gasification, the process is more complex and it is characterized by many reactions, but the global process always is endothermic and it requires high temperatures. Research for the development of gasification systems coupled with solar concentration panels is still very active today; the study includes horizontal reactors indirectly and directly irradiated. Most of the solar reactors for gasification are laboratory or small-scale reactors (2 to 24 kW). As far as energy efficiency is concerned, the Packed Bed Reactor has better results. Vortex flow reactors allow a continuous supply of reactants, but they are characterized by lower energy efficiencies, which may be due to limitations in the smaller amount of particles that are irradiated (less irradiated surface area). The main disadvantage of the latter reactors lies in the need for high gas flow to maintain a continuous gas-particle flow. This increases the costs of the process.

2.2.3.3. Splitting cycles

The analysis of splitting cycles began around the 1960s with a project called "Energy Depot", which aimed at producing fuels from materials such as earth, air and water. The first proposed cycles were characterized by a high number of steps, but these processes were too complex for solar applications. The simplest thermochemical cycles are characterized by two steps; they require higher temperatures, but they also are much more efficient. Considering a metal oxide (MO) and the hydrogen production, the two steps are:



The first reaction is endothermic and requires temperatures above 1000 K. In this reaction, the metal oxide is reduced at high temperatures and oxygen and the reduced metal oxide are produced. The second reaction is exothermic and takes place at temperatures below 1000 K. In this reaction, the reduced oxide is used for the dissociation of H₂O; H₂ and the initial oxide (MO_{ox}) are obtained. The net result of the two steps is the splitting of H₂O (hydrolysis). The most important difference between thermochemical cycles and other thermochemical processes is that starting from certain compounds, these compounds are regenerated and reused (hence the term "cycle"). One of the main advantages of these cycles is that H₂ is produced without contaminants (such as carbon monoxide, which occurs when H₂ is obtained from fossil fuels). This pure hydrogen can be directly used in a PEMFC (proton exchange membrane fuel cell). Thermochemical cycles can also be used for carbon monoxide production:

SYNTHESIS GAS (SYNGAS)



or for syngas production:



The research aims to obtain thermochemical cycles with high efficiency and continuous reactant feeding.

3. THERMOCHEMICAL SPLITTING CYCLES

In the present work, beyond the reforming unit, thermochemical cycles are considered for the production of syngas. They consist of a series of consecutive chemical reactions to form a closed loop: these processes start from and produce the same compounds with one or more intermediate steps in which a useful effect is obtained.

3.1. History of thermochemical cycles

The study of thermochemical cycles began in the 1960s [6] with different proposals of usable components and feasible cycles. At the beginning, this study was started for the production of hydrogen. Thermal dissociation of water in a single step (thermolysis) is, conceptually, the simplest reaction which can be executed to directly and quickly obtain hydrogen:



However, it is characterized by two problems: very high operating temperatures (water thermolysis completely occurs at temperatures higher than 4000°C [26]) and difficulties in the separation of H₂ and O₂ to avoid explosive mixtures. Thermochemical cycles are a series of chemical reactions (≥2) that can result in the splitting of H₂O into H₂ and O₂. The main advantages in the use of such cycles for the hydrogen production are that: the step at maximum temperature is characterized by a much lower temperature than water thermolysis reaction and, with thermochemical cycles, the problem of H₂ and O₂ separation is overcome because they are produced in different stages of the cycle. Since these cycles also involve a highly endothermic step, they require an amount of energy supplied from outside, which can be given by CSP systems, characterized by high operating temperatures. During the 1970s and 1980s, several studies were carried out to identify the most promising cycles, different aspects were considered: thermodynamics, efficiency and cost. By the end of the 1980s, interest in these cycles was drastically reduced and until the late 1990s little progress had been made in this regard. In-depth research on thermochemical cycles started again in around 2010. The impetus to this reborn interest was given by the need for hydrogen production as a green energy vector, i.e. clean and without greenhouse gas emissions, to meet the Kyoto Protocol (which came into force in 2005, [27]). Among the various thermochemical cycles, those consisting of two steps operating with a redox pair are of particular interest: there is the transition of a metallic oxide (with more oxidation states) from the oxidized state (with higher valence, MeO_{oxidized}) to the reduced state (with lower valence MeO_{reduced}). The first step consists of an endothermic reaction and it takes place at a higher temperature (1600-2100 K). Thanks to the heat supplied from outside, the metal oxide with a higher valence are subjected to a thermal reduction reaction; the products of this reaction are constituted by the same metal oxide with a lower valence and oxygen. The reduced metal oxide is, in general, separated from the oxygen through an inert sweep gas and transported to the second reactor, in which the second step of the cycle takes place. The second step is oxidation, it takes place at a lower temperature (800-1100 K) and it is exothermic. The reduced metallic oxide, with a lower valence and produced in the previous step, acquires oxygen and the metallic oxide at the initial higher valence is reproduced to close the cycle. During the oxidation, oxygen can be supplied by:

- H₂O for hydrogen production, water shift (WS);
- CO₂ to produce CO, carbon dioxide shift (CDS);
- an H₂O/CO₂ mixture to produce syngas.

Therefore, the following reactions occur:

1) REDUCTION:



2) OXIDATION:

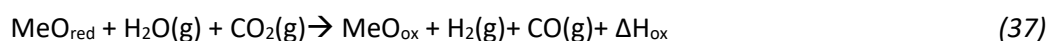
- with H₂O to produce hydrogen



- with CO₂ to produce carbon monoxide



- with an H₂O/CO₂ mixture to produce syngas



As shown in the previous reactions, it is important to highlight that, through the thermochemical cycles, CO can also be produced. Even in the case of CO production, the simplest and quickest reaction would be the carbon dioxide thermolysis:



However, as in water thermolysis, very high temperatures are required (carbon dioxide thermolysis completely occurs at temperatures higher than 3000°C [26]) and the problem of CO and O₂ separation is still present. To sum up, the global process of a two-step thermochemical cycle produces H₂ and/or CO with the net material input of only H₂O and/or CO₂, while the other compounds are recirculated cyclically. The involved reactions require a lower temperature than thermolysis and, since O₂ and CO/H₂ are produced in different stages, there are no separation issues and the production of H₂/CO/syngas can take place:

- on-demand;
- in certain places;
- independently from the availability of solar energy.

3.2. Carbon capture and utilization (CCU)

As specified in [Chapter 3.1](#), the production of syngas through a thermochemical cycle (and, in general, as seen in [Chapter 2.2](#), through the highest amount of processes fed by solar energy) requires the injection of carbon dioxide, which has to be shifted (simultaneously with steam) in the second step of the cycle itself. Thus, thermochemical cycles are a means of the utilization of captured carbon in the process of Carbon Capture and Utilization (CCU). Different pathways were proposed to reduce the anthropogenic emissions of CO₂ and to restrict the global warming to 1.5°C above pre-industrial temperatures (target set by Intergovernmental Panel on Climate Change, IPCC, in 2018). Among these pathways, Carbon Capture and Utilization is gaining an important role as an alternative and complementary process concerning Carbon Capture and Sequestration (CCS). CCS is an interim

solution to stabilize GHG emissions while still relying on fossil fuel power plants. The future of energy production is decarbonized (without the use of fossil fuels), but, at present, lots of fossil plants are still in operation and will be built in the close future years, so CCS is a way to mitigate the increasing CO₂ emissions. The generic CCS process consists of:

- 1) CO₂ capture;
- 2) compression;
- 3) pipeline transportation;
- 4) underground, or undersea, carbon sequestration (or storage) in a permanent geological reservoir.

The alternative CCU path is characterized by the fact that CO₂ is not stored but it is exploited to produce valuable and useful products. Three different types of Carbon Capture (CC) processes exist:

- 1) post-combustion carbon capture (suitable for existing infrastructures);
- 2) pre-combustion carbon capture (suitable for new infrastructures);
- 3) oxyfuel combustion.

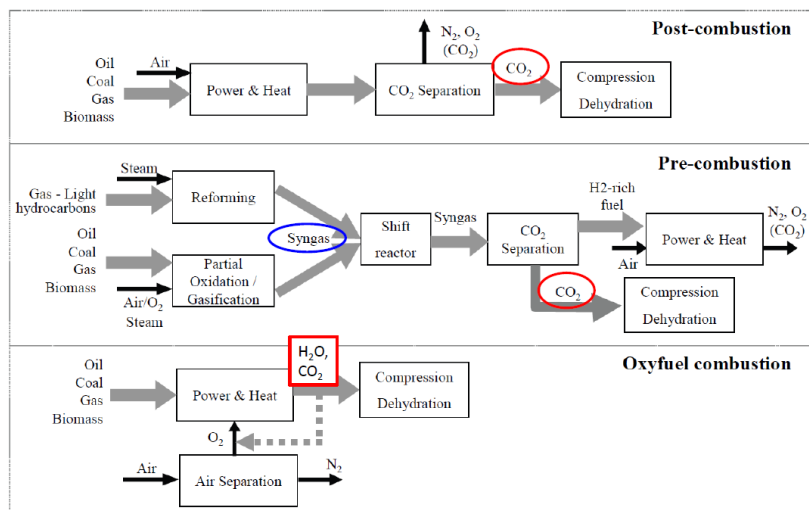


Figure 31: Different pathways for Carbon Capture [28]

In the post-combustion capture, exhausts of a combustion process are properly treated to remove CO₂. It is based on a chemical absorption process called “chemical wash”: the flue gas is treated with a chemical solvent to selectively extract CO₂ from nitrogen and water vapour. This process takes place in an absorption column operating at atmospheric pressure in which the chemical solvent is, in general, chilled water solution with amines and it is sent in counter-flow concerning the flue gases.

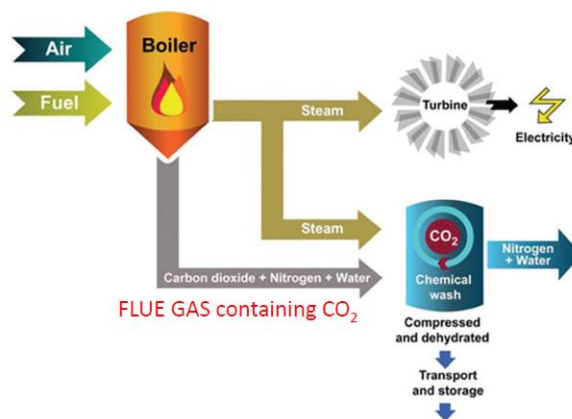


Figure 32: Post-combustion Carbon Capture [28]

Pre-combustion capture process has to be combined with gasifying systems because it is designed to work with syngas. An Air Separation Unit is used to make coal react with pure oxygen to produce a syngas which is already concentrated in CO₂ (without being contaminated with nitrogen compounds). The produced syngas is not directly used to produce electricity or chemicals but it is firstly pre-treated with steam in a water gas shift reactor to obtain an H₂/CO₂ stream. Then, a separator is used to extract CO₂ from H₂, the two resulting streams can be further stored or used in different applications respectively.

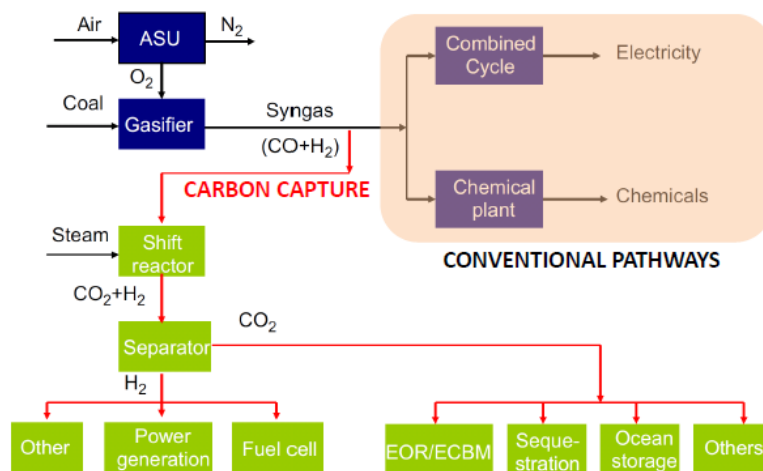


Figure 33: Pre-combustion Carbon Capture [28]

In the oxyfuel combustion process, the fossil fuel is directly burnt with oxygen instead of air, so nearly stoichiometric combustion is executed. This process aims at obtaining a resulting flue gas which is only composed of H₂O, CO₂ and a negligible amount of O₂. In this way, CO₂ can be easily separated: the exhausts are cooled down, condensed and an almost pure CO₂ stream is obtained. This process is used in the two attempts made to increase the electricity production of the polygeneration plant in this work. The additional thermal requirements of these two systems are satisfied with the oxyfuel combustion of biomethane.

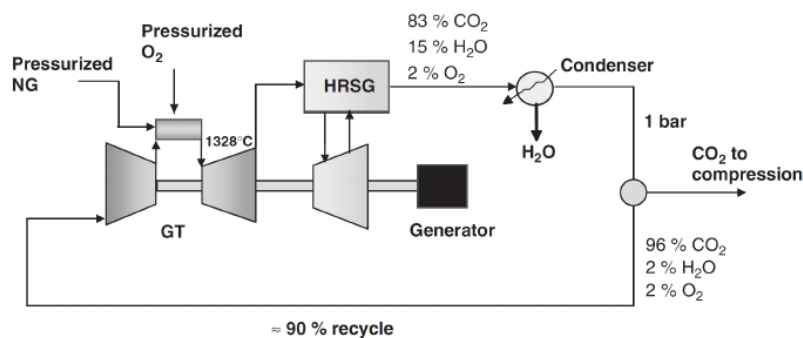


Figure 34: Example of an Oxy-combustion combined cycle [28]

Carbon capture in power plants produces a high energy penalty and loss of efficiency of the system due to:

- 1) the high amount of thermal energy required by the re-boiler of the separation unit of a post-combustion CC;

- 2) the high amount of energy to cool methanol (physical solvent used in the separation unit) to -20°C in a pre-combustion CC;
- 3) high energy expenditure to produce pure oxygen in the ASU of an oxyfuel combustion.

As a result, CCU could be a means to twice exploit CO_2 to produce a net gain and to reduce the plant losses. In the present study, CCU and CCS are applied in two different sections of the solar energy fed polygeneration plant:

- 1) the anodic exhausts of the SOFC are separated into two streams (water and carbon dioxide) in a flash unit. The stream of CO_2 is:
 - integrated with additional CO_2 and sent to the oxidation reactor of the CL during the presence of a high amount of irradiance that makes the CL operate properly;
 - stored (sequestered) at 25 bar and 80°C in a steel tank during those periods in which the CL does not work. This CO_2 is, then, reused both in the oxidation reactor of the CL and in the reforming reactor downstream the DME unit when a high value of irradiance is present;
- 2) the exhausts of the distillation unit of the DME reactor are burnt and separated through a flash unit (a very low amount of nitrogen is present, so it is not convenient to implement a chemical wash). The CO_2 stream is sent to the reforming reactor of biomethane to produce additional syngas that is partly reused in the plant and partly sent to a syngas-duct.

3.3. Classification of two-step solar thermochemical cycles (STC)

Three different types of thermochemical cycles can be distinguished based on the used redox pairs [29]:

- 1) stoichiometric volatile cycles;
- 2) stoichiometric non-volatile cycles;
- 3) non-stoichiometric non-volatile cycles.

In volatile cycles, the reduction temperature is higher than the boiling temperature of the metal oxide, therefore there is a solid-gas transition of the metal or the reduced metal oxide (e.g. $\text{M}_x\text{O}_y (\text{s}) \rightarrow x\text{M} (\text{g}) + \frac{1}{2} y\text{O}_2$). Among the volatile cycles the most studied are:

- ZnO/Zn cycle;
- SnO_2/SnO cycle.

The large-scale implementation of the volatile cycles is limited by the possibility of recombination between the products of the reduction reaction, the reduced metal oxide can also be transported by the sweep gas with the released oxygen. A separation between the products of the reduction has to be executed. At the high temperatures at which the first step of the STC takes place, the simplest way to separate the compounds is to solidify the reduced metal oxide. A rapid quenching process is necessary between the reduction and the oxidation reactors. However, during the quenching, there is the recombination of a certain amount of oxygen with the metal oxide and this decreases the overall efficiency of the system. Nevertheless, due to their lower molecular weights, volatile materials, have a higher oxygen atom share and so a better oxygen storage capacity per unit of mass. In non-volatile cycles, the reduced metal oxide remains in the solid or liquid phase throughout the entire process, thus avoiding the need for quench. Oxygen can easily be removed from the reduction of products through mechanical separators, e.g. cyclones. In the case of stoichiometric reactions, there is a variation in the crystal structure and the reduction of a cation to form solid compounds (e.g. $\text{M}_3\text{O}_4 \rightarrow 3\text{MO} + 0.5 \text{O}_2$). Examples of stoichiometric non-volatile cycles are iron oxide cycles. Stoichiometric reactions are characterised by a higher oxygen exchange capacity than non--stoichiometric reactions. The main characteristic of stoichiometric cycles is related to crystallographic (in non-volatile cycles) and phase (in volatile cycles) changes of the metal oxide during the reduction. These changes produce both negative and positive effects:

- the negative effects are related to the fact that these reactions are less stable and with much slower kinetics. To solve the stability problem, ZrO_2 has been used as a support of iron oxide

cycles, but this reduces the efficiency of the system due to the need for more heat to allow the thermochemical cycle;

- the positive effects lie in the greater variation in entropy that occurs during the reduction reaction (in which oxygen exchange takes place). Since the reduction process is not spontaneous (the Gibbs free energy variation is positive, $\Delta G_{\text{reduction}} > 0$), an increment of the ΔS reduces the Gibbs free energy of the reaction and, consequently, the required heat.

In non-stoichiometric non-volatile cycles, such as those with CeO_2 and perovskites LaMnO_3 , there is a partial reduction of metal oxide, which maintains its crystallographic structure (e.g. $\text{MO}_2 \rightarrow \text{MO}_{2-\delta} + 0.5\delta\text{O}_2$). Similar to iron oxide cycles, doping schemes with CeO_2 and perovskites were used to regulate thermodynamic parameters and redox efficiency.

3.3.1. Volatile cycles

3.3.1.1. ZnO/Zn cycle

Among the various systems of volatile metal/metal oxide pairs considered for the water (WS) and/or carbon dioxide (CDS) separation process, the ZnO/Zn system is the best from the thermodynamic point of view because Zn has a low atomic weight. This property produces a high energy content per unit mass (the oxygen storage capacity is around $0.197 \text{ kg}_{\text{O}_2}/\text{kg}$), that makes this energy carrier easy to be transported. However, the dissociation temperature of ZnO is higher than 2000 K, while Zn melts at 692 K and has a boiling point at 1180 K.

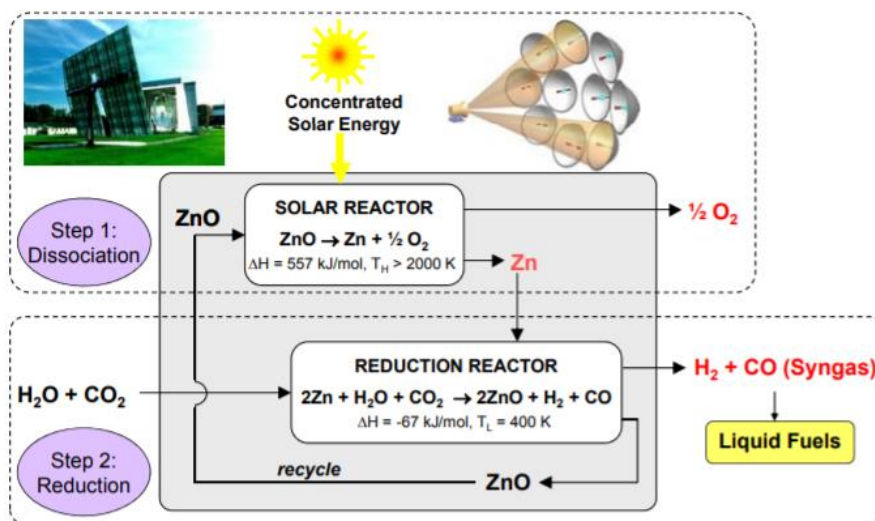
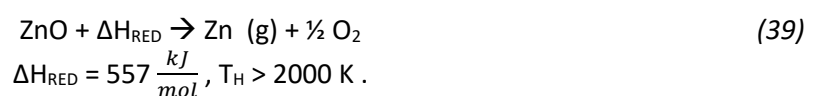
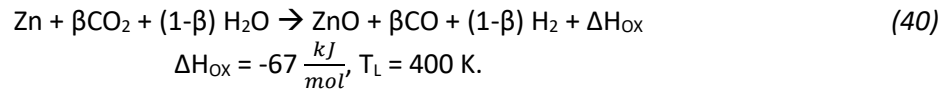


Figure 35: Scheme of the ZnO/Zn cycle for syngas production [30]

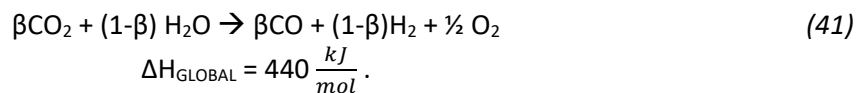
The first step is the thermal dissociation (reduction) of ZnO using solar process heat, it is an endothermic reaction:



The second step is an exothermic reaction (oxidation) and so it does not require solar heat. The purpose of this step is twofold, namely to produce syngas and regenerate ZnO, which is recirculated in the reduction step:



with $0 < \beta < 1$, which defines the molar fraction of CO_2 in the $\text{H}_2\text{O} + \text{CO}_2$ mixture. The H_2/CO and CO_2/CO ratios of the syngas are important to determine the quality of the syngas for its subsequent applications. The global reaction is given by:



The recovery of sensitive heat and latent heat from hot products and the exothermic reaction is essential to increase the efficiency of the system. This cycle presents several problems [31]:

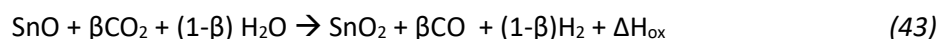
- 1) the main problem is the need for rapid cooling of the reduction reaction products to separate solid Zn from O_2 and avoid their recombination into zinc oxide. This is possible using rotary solar reactors, where ZnO has more functions: solar radiation receptor, thermal insulation and chemical reagent [32]. However, there is a reduction reaction efficiency that is limited due to the recombination of the chemical species during the quench phase;
- 2) the oxidation reaction is closely related to the surface area of the zinc metal, which is limited by the formation of oxide on the surface that inhibits the oxidation of the inner zinc;
- 3) there is the loss of metallic zinc during condensation due to the deposition of particles on the reactor walls;
- 4) the reduction temperature is very high, therefore there is a need for materials with high strength and durability. The temperature can be reduced with an inert gas that favours the reaction (e.g. argon, but this gas has high costs related to its separation from oxygen).

3.3.1.2. SnO_2/SnO cycle

The SnO_2/SnO thermochemical cycle was initially designed only for water splitting. The main advantage of this cycle compared to the ZnO/Zn cycle lies in the higher thermal dissociation yield during the reduction step at a lower temperature (of about 1900 K) [33]. Furthermore, the reactivity of SnO with O_2 is lower than the reactivity of Zn with oxygen, so the tendency to the recombination of SnO and O_2 in SnO_2 is lower. This characteristic is explained by the higher boiling temperature of SnO at atmospheric pressure: 1800 K compared to 1180 K of Zn. This causes SnO vapour to condense rapidly when the gas temperature decreases because there is a very small gap between the boiling temperature and the temperature of the reduction reaction. Therefore, SnO quench is much simpler than Zn quench. As far as the exothermic non-solar step is concerned, SnO hydrolysis takes place in a temperature range between 800 and 900 K. For the syngas production, the thermochemical cycle with the redox pair SnO/Sn is the following. The first step is the endothermic reduction reaction, which uses solar heat; the reaction products are gaseous SnO and O_2 :



The second step is exothermic and H₂, CO and SnO₂ are produced:

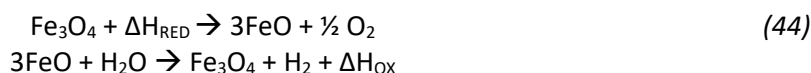


with $0 < \beta < 1$, which defines the molar fraction of CO₂ in the H₂O + CO₂ mixture. By making SnO react separately with H₂O and CO₂, the characteristics of these two reactions were identified. Hydrolysis of SnO for H₂ production can be performed efficiently in the temperature range of 800-900 K with an H₂ yield above 90%, that is higher than the yield of Zn nanoparticles (~55%), which, instead, showed a faster hydrolysis reaction rate [34]. Concerning carbon dioxide dissociation (CDS), it requires significantly higher temperatures (around 1073 K) than H₂O reduction to achieve the same conversion of SnO. In both cases, at these temperatures, the reaction product is H₂/CO and SnO₂. As a result, the simultaneous splitting of H₂O and CO₂ is not facilitated from a thermodynamic point of view precisely because of the greater reactivity of tin species with H₂O compared to CO₂. Parametric studies have shown that, as a global trend, both the conversion of chemical species and the reaction speed increase increasing the temperature and the molar fraction of the reagent gas (H₂O and/or CO₂). However, it is important to underline the influence of the disproportionation reaction of SnO to Sn and SnO₂ at temperatures above 773 K, which acts in parallel with the reduction reaction of H₂O and/or CO₂.

3.3.2. Non-volatile cycles

3.3.2.1. Iron Oxide Cycles

This type of cycles was first designed for water hydrolysis by Nakamura, who studied the redox pair Fe₃O₄/FeO (magnetite/wustite) in 1977 [35]. The thermochemical cycle with this redox pair is the following:



However, the required temperature for the reduction process is above 2200°C in air. This temperature is higher than the boiling point of both the Fe₃O₄ (1535°C) and the FeO (1370°C), so significant vaporization and sintering processes of the metal oxide take place. As a result, pure iron oxide cannot be used for cyclic reactions because, after a few cycles, due to the sintering, an increase in the particle size is experienced, thus reducing the total hydrogen yield and producing a progressive deactivation of the metal itself. To obtain an exhaustive conversion of Fe₃O₄ and the subsequent oxidation of FeO, granulation and grinding of the metal oxide are necessary. Over the years, studies aimed at solving the problems of the first step of the thermochemical cycle through the partial replacement of iron in Fe₃O₄ with M₃O₄/MO (M=Mn, Co, Mg, Ni, Zn...) to produce mixed metallic oxides (Fe_{1-x}M_x)₃O₄. The latter can be reduced at lower temperatures and the reduced phase (Fe_{1-x}M_x)_{1-y}O can perform the hydrolysis. Processes using solutions that include Fe₃O₄/FeO and M₃O₄/MO are known as "ferrite processes". Considering the best temperature range of the thermochemical cycle, process parameters and the yield in H₂ and O₂, Fresno et al. [36] reported studies performed on several commercially available ferrite powders (e.g. NiFe₂O₄, Ni_{0.5}Zn_{0.5}Fe₂O₄, ZnFe₂O₄, Cu_{0.5}Zn_{0.5}Fe₂O₄ and CuFe₂O₄). At the current state of the art, NiFe₂O₄ and CoFe₂O₄ are the best materials because, compared to the other ferrites, they are more active in cyclic ability and the production of hydrogen and carbon monoxide, they also are more reliable under real operating conditions in solar reactors:

- ferrites containing zinc have problems with zinc volatilisation;
- ferrites containing manganese have problems of stability at high temperatures and atmospheric pressure.

However, all these materials are still characterized by several problems:

- none of them has been shown to have high cycle activity and possible repeatability;
- their reduction temperature remains very high (1600-1700 K) and this represents an important disadvantage for the high sintering of the oxide that takes place at these temperatures.

Many attempts have been made to solve these problems, for example, by supporting ferrite metal oxides with zirconia and, in particular, with ZrO_2 particles (obtaining ferrite/m- ZrO_2), stable at high temperatures, and zirconia particles stabilized with yttrium (obtaining Fe_3O_4/c -YSZ). In these studies, the reaction between Fe_3O_4 and zirconia produced a very reactive compound, which could be used in a two-step thermochemical cycle for water splitting at temperatures below 1400°C. Studies on iron oxides and ferrites have recently been extended to the splitting of carbon dioxide [37], either separately or simultaneously with water. In particular, different temperature swings between the reduction reaction and the oxidation reaction in the thermochemical cycle in both WS and CDS have been considered. For both reactions, Fe ions are more reactive when dissolved in the YSZ lattice and the maximum amount of produced CO and H_2 per cycle is restricted by the limit of solubility of Fe in 8% of YSZ. Among the obtained results, it has to be noted that, in the simultaneous splitting of CO_2 and H_2O , the speed of water reduction is higher than carbon dioxide reduction, so the production of H_2 is favoured over the production of CO.

3.3.2.2. Cerium-based cycles

The first studies on the cerium cycles were carried out in the early 1980s by Japanese researchers. They proposed the reduced form of cerium oxide CeO_{2-x} for the cyclic splitting of H_2O and CO_2 in non-solar reactors in the temperature range of 773-973 K. These studies showed that the reduction of water by the reduced form of the cerium oxide was much easier to perform than the reduction of carbon dioxide [38]. Later, over the years, researchers focused on other thermochemical cycles, particularly on zinc oxide and on iron-based oxides. However, in zinc oxide-based thermochemical cycles, there are problems related to the recombination of the products of the reduction reaction to reproduce the reactants, while, in iron-based cycles, there are problems related to sintering during the cyclic operation, low hydrogen production rates and the need to use a reducing agent to reduce the dissociation temperature. Due to these limits of the other cycles, in 2006, when Abanades and Flamant (PROMES group) demonstrated the feasibility of a redox cycle for H_2 production, performed in a solar reactor and based on the stoichiometric reduction of CeO_2 in Ce_2O_3 at temperatures above 2220 K [39], the interest in cerium-based cycles reborn. The authors noted that the reduction of the cerium oxide started at temperatures just above 1700 K, but, to have a substantial reduction of the oxide, temperatures above 2220 K were required. At such temperatures, in the reduction reaction, CeO_2 is in the molten state and the redox material can vaporize producing a decrease in the amount of material available for recycling. At present, CeO_2 is the state of the art of used redox materials in thermochemical cycles thanks to:

- favourable thermodynamics of the oxidation reaction;
- rapid reaction kinetics;
- morphological stability of cerium oxide;
- selectivity in syngas.

For these ceria characteristics, this material is chosen in the chemical looping of the present work. However, the efficiency and feasibility of the cerium cycle are limited by the extremely high temperatures required for the thermal reduction step; these temperatures imply large heat losses, restrictions on the types of materials that can be used for the construction of thermochemical reactors and the need for high concentration ratios in the CSP system. Therefore, the research has focused on

the realization of the cerium oxide reduction reaction at temperatures lower than the melting temperature of the oxide itself. In this work, the strategy applied to decrease the reduction temperature of CeO₂ concerns the introduction of biomethane as a reducing agent in the reduction receiver-reactor. This allows to have the simultaneous reduction of CeO₂ and partial oxidation of CH₄ which is advantageous for two main reasons:

- 1) the pox of biomethane is exothermic, so it supplies a portion of the heat required for the reduction of CeO₂;
- 2) the presence of biomethane lowers the partial pressure of the oxygen shifting the equilibrium of the reduction reaction towards the products.

In the following chapters, a detailed analysis of cerium cycles is exposed starting from stoichiometric cerium cycles and proceeding to different techniques that can be applied to decrease the reduction reaction temperature.

3.3.2.2.1. Stoichiometric cerium cycle

As previously written, the interest in cerium oxide-based thermochemical cycles reborn in 2006 thanks to the studies of Abanades and Flamant, who proposed the following cyclic reactions for hydrogen production:

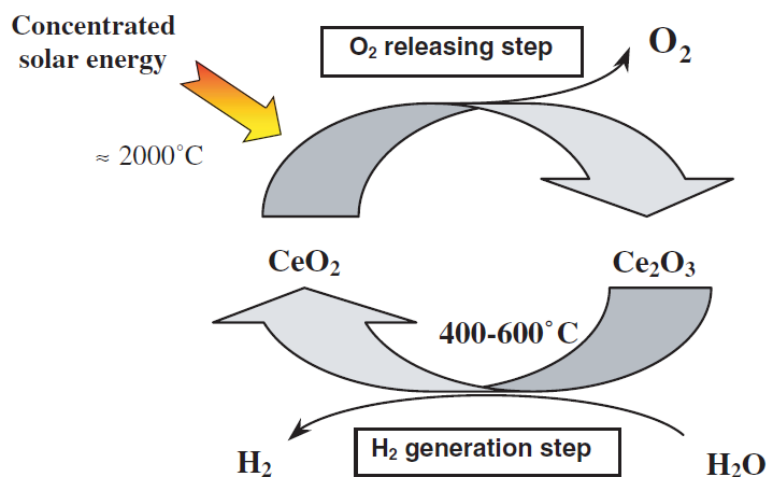
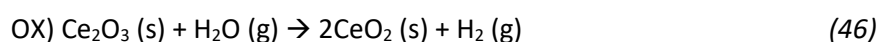
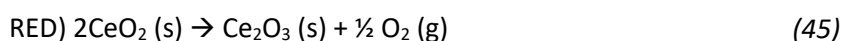


Figure 36: Scheme of the WS through the CeO₂/Ce₂O₃ thermochemical cycle

	MOLAR MASS [g/mol]	FUSION TEMPERATURE [°C]	DENSITY [kg/m ³]
Ce ₂ O ₃	328.2	1687-2230	6200
CeO ₂	172.1	1950-2400	7650

Table 4: Properties of cerium oxides

The description of the studies of Abanades and Flamant and their results follows. The first step of the thermochemical cycle is endothermic and involves the reduction of ceria:



with $x=0.5$, the reduction to Ce(III) is complete. This reaction was executed by the two researchers in a solar reactor with an atmosphere controlled by an inert gas (nitrogen, N_2) and the following operating conditions:

- reduction temperature of 2000°C;
- pressure equal to 100-200 mbar. This pressure was necessary to maintain a low oxygen partial pressure for the complete reduction of Ce(IV) without adding reducing agents (at higher pressures, there was no reduction) and it was regulated through the variation of the nitrogen flow. For the reduction reaction to occur, the nitrogen needed to be continuously flowing and pumped into the reactor with the aims to:
 - promote high mass transfers around the sample to allow the removal of O_2 and its separation from the sample without the recombination with the reduced oxide;
 - avoid the deposition of particles, which could be released by sublimation, on the glass. Deposition of these particles on the glass produces the absorption of a certain amount of solar radiation and this may inhibit the reaction due to a shading effect.

The reduced cerium oxide particles retained in the inert gas were collected in a filter at the exit of the solar reactor and recycled. In addition, it is important to control the exposure time of ceria particles to solar radiation. This time interval cannot be too long, otherwise, there is a non-negligible sublimation.

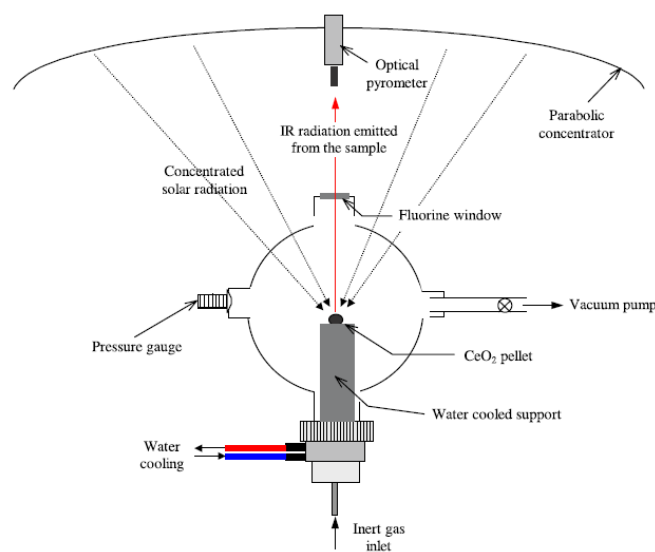


Figure 37: Scheme of the solar reactor used to reduce CeO_2 in a controlled atmosphere

The second step of the thermochemical cycle is the oxidation reaction:



This reaction was studied in a fixed bed reactor with reactive particles (with CeO_{2-x} composition) into which an inert gas containing steam was injected. At the beginning, argon was circulated in the reactor to eliminate air because the reduced oxide is very unstable at temperatures above 200°C and it is completely oxidized in CeO_2 by air in the temperature range 200-300°C. Then the reactor was heated to the desired temperature electrically and this T was controlled with a thermocouple (as in the diagram in [Figure 38](#)).

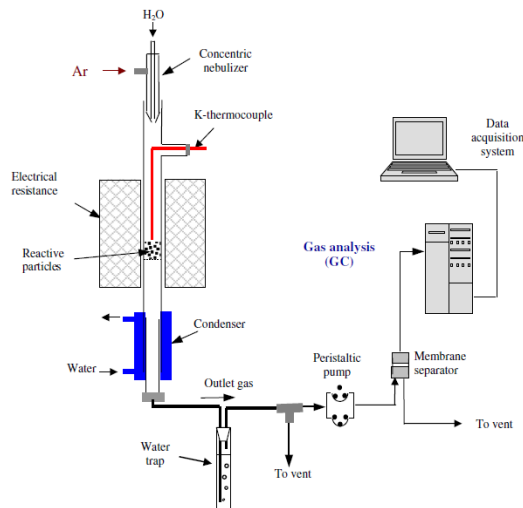


Figure 38: Scheme of the reactor used for the reduction of H₂O

At the thermal steady state, water and argon were injected through a nebulization system that produced an aerosol; water was then reduced by Ce(III) oxide to produce hydrogen and ceria. The outgoing gas was cooled and the steam in excess was eliminated in a bubbler, while Ce(IV) oxide was recirculated in the first step. To have a complete reaction with fast kinetics, the temperature range was between 400-600°C ($\Delta H_{ox} = -125$ kJ/mol at T=700 K). The scheme of the oxidation reactor is shown in [Figure 39](#), Ce₂O₃ particles in the solid phase entered the reactor through the green tube:

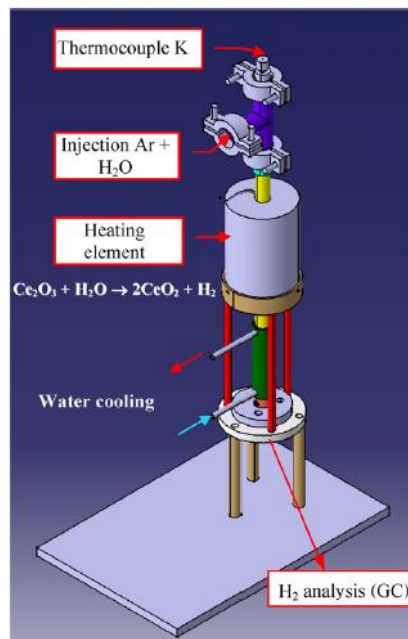


Figure 39: Experimental reactor for the production of H₂ from H₂O and CeO_{2-x}

It is important to highlight that CeO_{2-x} is reactive with water at moderate temperatures, while it is stable at room temperature: hydrogen could be produced quickly on-demand and with a complete reaction. Hydrolysis through cerium oxide quickly reached completion as the reaction took place as soon as the water was injected into the reactor. In this process, the only input material was water and the only input energy form was solar heat. The only outputs were O₂ and H₂ and these gases, as in the previous thermochemical cycles mentioned above, were obtained in two different steps, avoiding the production of explosive mixtures. Pure hydrogen (not contaminated by-products such as

CO and CO₂) was produced, so it could be directly used in a fuel cell. To sum up, different characteristics of the thermochemical cycle CeO₂/Ce₂O₃, compared to other two-step thermochemical cycles, can be indicated:

- 1) after the reduction reaction, no quenching of the products is necessary. Considering the above mentioned operating temperatures, the solar step proceeds in the liquid phase as soon as the melting point of the material is reached, but the reduced cerium oxide (with a high boiling point, 3200°C) remains in the condensed phase while O₂ is released and transferred from the liquid phase to the surrounding nitrogen and then flows with it. This mechanism causes O₂ to be separated from the reduced oxide and, during the cooling of the reduction products, the reverse reaction (oxidation of the reduced species) does not take place. On the contrary, in the ZnO/Zn cycle there is a significant quenching problem because both Zn(g) and O₂ are simultaneously produced at a temperature of about 2000°C and tend to recombine and form ZnO;
- 2) the high reactivity of the reduced oxide with water. The hydrolysis reaction is very quickly completed: the complete hydrolysis of Ce(III) oxide (with a 100% conversion) occurs after less than 5 min. Considering the hydrolysis of FeO or, more generally, of ferrites, instead, at 400°C and after 120 min, there is a conversion of only 32%. Therefore, in ferrite systems, there is very slow kinetics due to the formation of a layer of inert oxide on the surface of the particles, this inert oxide blocks the diffusion channels of the gaseous species;
- 3) the particle size of cerium oxide does not influence the efficiency of the hydrolysis reaction (diameters between 100-300 μm have been tested). On the other hand, particle size is of particular importance when considering the hydrolysis of Zn. To obtain an H₂ yield of 60%, Wegner et al. studied the formation of zinc nanoparticles with an average size of 70-100 nm. These dimensions allow:
 - high specific surface area, which increases reaction kinetics and heat and mass transfer;
 - high surface/volume ratio, which favours almost complete oxidation;
 - possibility to drag the particles in a gaseous stream to have a continuous and controlled refill of the reactants and optimal removal of the products. This process is not necessary for the ceria because hydrolysis proceeds in the solid-state regardless of particle size;
- 4) reduced cerium oxide is stable at room temperature and so it is easy to store. As a result, it could be thought of transporting the reduced cerium oxide to a hydrogen production site (on-site H₂ generation) by-passing the complications associated with long-distance transport and long-term storage of hydrogen;
- 5) the chemical components are non-corrosive, safe, clean and not toxic to both the environment and people.

The main problems and limitations of these cycles are:

- 1) maximum temperature slightly higher than 2000°C. The operating temperature of the endothermic step should be optimized to make it suitable for dish and tower concentrating solar technologies and to reduce sample vaporization;
- 2) the high molecular weight of cerium oxides, so the flow of solid particles in the process has to be minimized.

3.3.2.2.2. Non- stoichiometric cerium cycle

The interest in non-stoichiometric ceria reduction (CeO₂ → CeO_{2-δ}) was born from the need to perform this reaction below the melting point of the ceria itself to avoid the vaporization of the reactant with a subsequent decrease in the amount of available material for recycling. The main advantage of this partial reduction lies in the high rate of chemical diffusivity of oxygen which contributes to a faster reaction kinetics. Considering the production of syngas, the thermochemical cycle under analysis is as follows:





The first reaction is endothermic and non-stoichiometric, a portion of ceria atoms changes its oxidation state and the ceria particles maintain their crystalline structure. There is the formation of oxygen vacancies in the lattice structure and the release of O_2 , which produces a variation in the stoichiometry of the cerium oxide. The extent of the reduction depends on:

- the molar defect δ . The limit value of δ (equal to 0.35) for the crystalline structure preservation of the ceria was reported by Kümmerle et al. [40];
- the reduction temperature;
- the partial pressure of oxygen in the gaseous atmosphere where the reaction takes place (Le Chatelier Brown principle).

The second reaction is the oxidation of the previously reduced metal oxide and it proceeds with H_2O and CO_2 , H_2 and CO are released thanks to the reintroduction of oxygen into the cerium oxide lattice. As a result, the number of oxygen vacancies, created during the reduction, is directly related to the yield of fuel production. In general, the non-stoichiometric reduction is performed at 1773 K and the partial pressure of O_2 (p_{O_2}) is between 10^{-6} and 10^{-3} atm, while the oxidation step is performed at a temperature between 873 and 1273 K and at a p_{O_2} between 10^{-20} and 10^{-10} atm. Chueh and Haile [41] studied this cycle considering a solar reactor realized as in *Figure 40*:

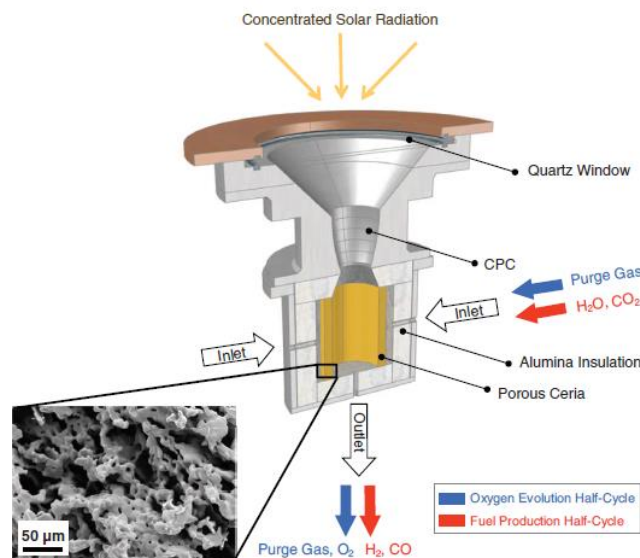


Figure 40: Solar reactor for the non-stoichiometric reduction of ceria

The solar reactor consisted of a cavity receiver with a window opening through which concentrated solar radiation entered. Thanks to this type of geometry, there were reflections inside the receiver and an efficient capture of solar energy. Monolithic porous ceria, assembled with a cylindrical shape, was inserted in the cavity and subjected to multiple heating and cooling cycles for the production of fuel through the injection of appropriate gases. The porous ceria cylinder was directly exposed to the concentrated solar radiation, which hit its internal walls. There also was an annular space between the ceria cylinder and the alumina insulation tiles to avoid chemical reactions between these two components. The reactive gases were inserted in this annular space and radially flew into the porous ceria cylinder to reach the inner part of the cavity, while the produced gases exited from the lower part of the reactor, characterized by an axial

outlet. To maintain a sufficiently low partial pressure of oxygen ($p_{O_2} = 10^{-5}$ atm), argon (purge gas) was made flow into the reactor. Considering an incident solar radiation of 1500 suns (1 sun = 1 kW · m⁻²), typical of a dish or of a tower CSP system, the temperature of the ceria tube rose in a range between 1420°C and 1640°C, with the exact temperature value depending on the reactor location and on the cycle. Below 1250°C, the temperature rose quickly, with an average speed of 140°C · min⁻¹, but this speed reduced to about 8°C·min⁻¹ when the temperature value began to reach the steady-state. This speed decrease was because of the increasing heat dissipation through the re-irradiation at the opening and the conduction in the insulation layer. The evolution of oxygen from ceria was studied at an initial temperature of about 900°C. The rate of evolution increased increasing the temperature, with a peak value of about 34 ml·min⁻¹ and an average value of about 16 ml·min⁻¹, averaged over the time needed to reach a 90% extent of the reaction (ξ = extent of the reaction) during the first cycle. When the oxygen diffusion rate dropped to about 20% of the peak value, the reduction reaction was stopped by decreasing the intensity of the incident radiation flux to achieve cooling down to about 900°C. At this point, CO₂ was injected into the solar reactor resulting in an immediate CO production with relevant peaks of about 1.5 x 10³ ml·min⁻¹ and an average rate of about 5.9 x 10² ml·min⁻¹. During the oxidation reaction, no appreciable amount of carbon was deposited on the cerium, thus confirming the 100% selectivity of cerium in CO. After the production of CO, the radiative flux was increased and the entire cycle was repeated. During the different cycles, there was a decrease in the temperature of the reduction reaction, which resulted in a lower amount of O₂ released and a lower CO yield. Further similar experiments were performed for H₂O dissociation to produce H₂. In this case, the peak production was about 7.6·10² ml·min⁻¹ with an average value of about 3.1·10² ml·min⁻¹. From these experiments, several conclusions could be assumed concerning the characteristics of ceria-based thermochemical cycles:

- 1) from mass balance considerations, there is a 2:1 molar (and, thus, volumetric) ratio between the produced fuel and the released oxygen by the non-stoichiometric cerium. In reality, for the production of CO, they obtained CO: O₂ which varied between about 1.6 and 2, while, for the production of H₂, H₂: O₂ was about 1.6. This small deviation of the real ratios from the ideal ratios is attributed to small system losses and the inaccuracy of mass flow control and gas composition measurements;
- 2) there is a fuel production rate which is much higher than the O₂ release rate;
- 3) reducing the purge gas flow by a factor of 4 has a minor impact on the oxygen release rate. This indicates that the convective oxygen transport in the reactor is not the step that limits the cycle speed. Confirmation of this deduction is also given by the fact that there is a CO₂ dissociation rate, which is much higher than the O₂ evolution rate. Therefore, the kinetics of the oxygen evolution is determined by the heat flow, which, instead, does not influence the production of fuel because the second step takes place in an isothermal way;
- 4) the solar-to-fuel conversion efficiency is defined as follows:

$$\eta = \frac{r_{fuel}\Delta H_{fuel}}{P_{solar} + r_{inert}E_{inert}} \quad (51)$$

with:

- r_{fuel} = molar fuel production rate;
- ΔH_{fuel} = higher calorific value of fuel;
- P_{solar} = incident solar radiation power;
- r_{inert} = flow of inert gas during oxygen evolution;
- E_{inert} = energy required to separate the inert sweep gas from the air.

From the experimental data, instantaneous peak efficiencies for the splitting of CO₂ and H₂O of 0.8% and 0.7% respectively (not considering heat recovery) were obtained. These

efficiencies consider the irreversibility of the cycle as a result of the intrinsic properties of the materials and the design and operation of the solar reactor. An energy balance revealed that 50% of energy lost was related to heat conduction through the reactor walls, while a further 41% of energy lost was due to re-irradiation through the reactor opening. The first form of energy loss could be reduced by improving the thermal insulation, while the last form of energy loss could be minimized by increasing the heat flow to reduce the size of the opening. A reduction in lost heat also means an increase in the rate at which the temperature increases in the reactor;

- 5) another important consideration concerns the stability of the materials. 500 thermochemical cycles in the temperature range between 800 and 1500°C were performed without interruption for water dissociation. After an initial period of stabilisation, lasting about 100 cycles, the rates of oxygen release and hydrogen production were recorded to be almost constant for the successive 400 cycles. During the stabilisation period, H₂ production was reduced by about 50%, this loss of reactivity was explained by the increase in the grain size. After stabilization, thanks to the significant variation in oxygen non-stoichiometry at moderate temperatures, ceria could perform cycles between the two oxidation states without a substantial loss of activity;
- 6) further important data concerning the reduction temperature follow:
 - at a reduction temperature of 1500°C, $\delta \approx 0.066$ and, with a subsequent hydrolysis at 800°C, there was an H₂ production rate of $4.6 \frac{ml}{g \cdot min}$;
 - at a higher reduction temperature of 1600°C, $\delta \approx 0.091$ and also a higher H₂ production rate of $6.2 \frac{ml}{g \cdot min}$ was obtained.

There also are the following advantages over other thermochemical cycles:

- 1) the solar-to-fuel conversion efficiency for CO₂ dissociation is about two orders of magnitude higher than the state of the art of photocatalytic processes;
- 2) the hydrogen production rate exceeds that of other thermochemical processes by more than one order of magnitude;
- 3) both efficiency and cycling speed in the reactor are limited by thermal losses;
- 4) a thermodynamic analysis of efficiency solely based on CeO₂ characteristics show that values between 16 and 19% can be obtained even in the absence of sensitive heat recovery;
- 5) the abundance of cerium makes this type of cycle applicable on a large scale for global energy consumption.

3.3.2.2.3. Doped-cerium cycle

With the non-stoichiometric reaction, oxygen is only delivered from the surface of ceria particles, so the thermal stability is one of the critical points to be analysed. As for iron, an implemented solution to this problem is the realization of doped-ceria particles, constituted of the pure ceria particles doped with metals (such as Mn, Ni, Fe, Cu...). The inclusion of these cations in the crystalline structure of the cerium oxide in substitution of Ce⁺⁴ produces the formation of O₂ vacancies in the lattice, this leads to the formation of solid non-stoichiometric cerium oxide solutions characterized by an OSC (Oxygen-Storage capacity) which increases by about the 40% compared to pure ceria and, consequently, by an improved oxygen-releasing capacity with no effect on the cubic structure of the ceria itself. Therefore, several favourable properties of these hybrid structures can be indicated: long-term thermal stability, high OSC, low sintering, high melting temperature and high reactivity in redox reactions. The oxygen storage capacity of the reduced cerium oxide decreases as the temperature of the reduction reaction decreases and increases as the partial oxygen pressure decreases. In 2007, Kaneko et al. [42] prepared a solid solution containing cerium oxide and various transition metal oxides MO_x (with, M= Mn, Fe, Ni, Cu). With these solid CeO₂-MO_x solutions, characterized by a molar ratio Ce:M equal to 9:1, the

thermochemical cycles were performed in a temperature range between 1000°C and 1500°C and the authors noted that the H₂ production capacity was higher than pure cerium oxide at thermal reduction temperatures above 1400°C. Specifically, CeO₂-NiO produced the maximum amount of H₂ (1.446 ml/g) at 1400°C, while CeO₂-MnO produced the maximum amount of H₂ (3.773 ml/g) at 1500°C. Above all CeO₂-MO_x solid solutions, CeO₂-Fe₂O₃ was the most stable in multiple thermochemical cycles: in 4 thermochemical cycles, the amount of O₂ released at 1400°C (1.33 ml/g) and the volume of H₂ produced at 1000°C (2.26 ml/g) remained constant. Miller et al. [43] studied the monolithic structures CeO₂-ZrO₂ (with a molar ratio of 0.25:0.75) for the thermochemical splitting of water (WS) and carbon dioxide (CDS). CeO₂-ZrO₂ structures were thermally reduced at a temperature of 1400°C and oxidized with H₂O and CO₂ at 1100°C. At this temperature, the production of CO was higher than that of H₂. A further study of solid CeO₂-MO_x solutions (M= Al, Mn, Fe, Co, Cu, Zn, Zr), with 25% added element, was performed by Abanades et al. [44]. Above all the materials, CeO₂-ZrO₂ show to have the best reactivity under certain operating conditions. By increasing the Zr content, the reactivity of the solid solution was increased with a higher yield of the reduction reaction. For example, considering (1-x)CeO₂-xZrO₂ with an x increase from 0 to 0.5, the following results were achieved:

- a reduction yield that increased by 70%;
- a decrease in the reduction temperature from 1150°C to 900°C.

Le Gal and Abanades [45] studied the effectiveness of the doping with zirconium considering different percentages of dopant in the crystalline lattice of CeO₂. They performed two successive redox cycles with thermal reduction at a temperature of 1400°C and hydrolysis at 1050°C. The higher the percentage of dopant with Zr, the higher the yield in terms of oxygen and hydrogen in both cycles. However, there also was a greater loss of reactivity of the mixture as the number of cycles increased. Another relevant result was that the hydrogen yield increased as the hydrolysis temperature increased. Meng et al. [46] tested samples with the structure Ce_{0,9}M_{0,1}O_{2-δ} (M = Mg, Ca, Sr, Sc, Y, Dy, Zr, Hf) considering nine thermochemical cycles for H₂O splitting with the thermal reduction reaction performed at 1500°C and hydrolysis at 500°C. The quantity of produced H₂ was entirely dependent on the quantity of released O₂ during the reduction reaction. Another relevant result was that, due to the sintering of Ce_{0,9}M_{0,1}O_{2-δ}, the volume of released O₂ and the produced H₂ decreased as the number of cycles increased.

3.3.2.2.4. Cerium cycle coupled with methane partial oxidation

As written before, non-volatile cycles have not problems with separation issues of the reduction products and, among these cycles, ceria-based oxygen carriers tend to have better performances in terms of thermal stability and reduction kinetics than ferrite oxides. For these reasons, ceria oxide has been chosen as oxygen carrier for the chemical looping process of this study. In addition, the strategy adopted in the present work to operate the cycle at a lower temperature and, as a consequence, to decrease the temperature swing between reduction and oxidation, is the combination of the CL with biomethane reforming. The introduction of a reducing agent (biomethane) effectively lowers the oxygen partial pressure shifting the equilibrium towards lower temperatures. In this way, the partial oxidation of biomethane (reaction (52), which is exothermic) is coupled with the solar-driven reduction step (endothermic) of the ceria redox cycle to attain high solar-to-fuel efficiency at a lower reduction temperature and, thus, at a lower solar concentration ratio:



This solution allows:

- the complete reduction of CeO₂ to Ce₂O₃, which is required to obtain a high H₂ and CO yield. This high yield is not reachable with the non-stoichiometric ceria;

- the isothermal and isobaric (the two-step redox cycle can operate near atmosphere) operation of the redox cycle, that guarantees low operation costs, enhanced stability and improved system efficiency as shown in *Figure 41*.

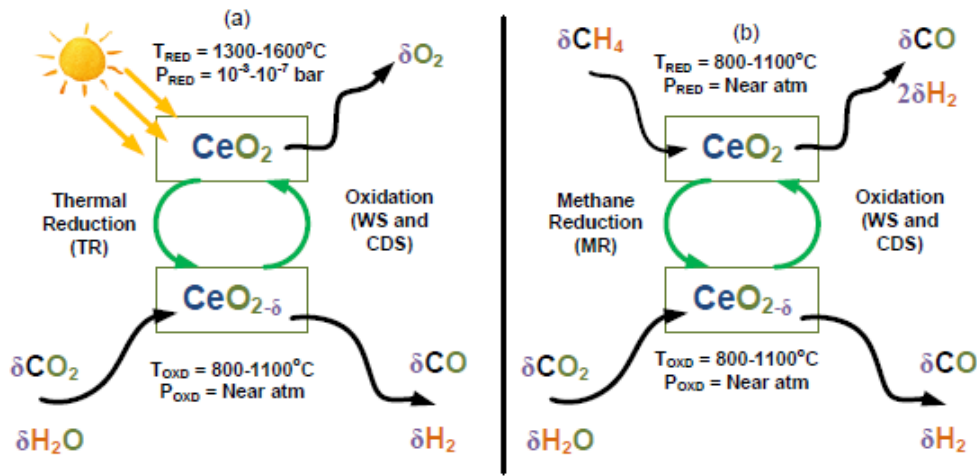


Figure 41: Conceptual scheme of the chemical looping syngas production through (a) solar thermal reduction and (b) methane reduction and corresponding splitting of water and carbon dioxide, usually present in waste gas from industrial applications [47]

- to obtain a simple and promising process for syngas production thanks to the usage of methane, which is abundant and cheap, or renewable biomethane;
- the production of streams of syngas from both the reduction and the oxidation reactors (as shown in *Figure 42*). By tuning in a proper way the operating conditions of the reactor, the obtained syngas streams can reach an $H_2:CO$ ratio of 2:1, ideal to produce methanol, or liquid fuels via the Fischer–Tropsch process.

The cycle is the following:

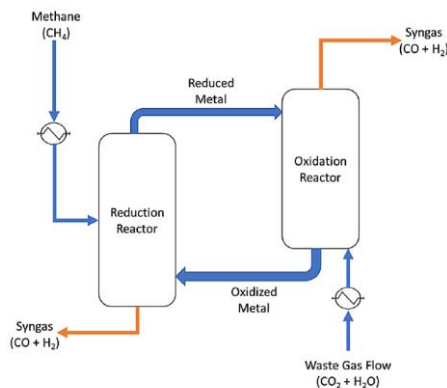


Figure 42: Conceptual scheme of the chemical looping for syngas production through methane reduction and corresponding splitting of water and carbon dioxide [48]

During reduction (53), ceria is reduced by methane and the moles of oxygen, which are released, produce CO and H₂ through the partial oxidation of CH₄. In the subsequent step of the cycle (54), the reduced metal oxide reacts with CO₂ and/or H₂O to reincorporate oxygen into the metal oxide lattice and CO and/or H₂ are obtained. Different investigations were made on this cycle. Bader et al. [49] reported a thermodynamic analysis of an isothermal redox cycling of ceria at 1500 °C, achieving efficiencies of 10% and 18% for hydrogen and carbon monoxide production, respectively. The efficiencies were considerably improved to over 30% for hydrogen production by introducing a temperature swing of 150°C between the reduction and the oxidation reactors. Many thermodynamic issues of this methane-driven cycle have to be considered and analysed:

- 1) carbon deposition in the reduction reactor through Boudouard reaction and methane dissociation mechanisms ((55) and (56)). This carbon is then transferred with the reduced ceria to the oxidation reactor. In this reactor, the carbon does not directly inhibit any reaction, but it reacts with H₂O (water gas reaction) and CO₂ (reverse Boudouard reaction) to produce syngas ((57) and (58)). As a result, the presence of carbon generates a set of reactions which compete against the oxidation of the reduced metal oxide. Steam and carbon dioxide preferentially react with solid carbon and this causes the metal oxide to remain at a reduced state. This process is more critical under a stoichiometric quantity of reactants because it lowers the utilization of the metal oxide:



- 2) at suitable thermodynamic conditions, the oxygen which is released from the reduced metal in the reduction reactor can react with the produced CO and H₂ to obtain CO₂ and water, respectively ((59) and (60)). This process reduces the effectiveness of the entire system because it lowers the calorific value of the syngas produced in the reduction reactor:



Due to the simultaneous presence of these components, water gas shift reaction (61) and methane reformation reaction (62) can also take place, but the chemical and thermodynamic conditions do not allow these reactions to become primary contributors to system thermodynamics:



Bose, A. Farooqui, A. Ferrero, D. *et al* [50] investigated the equilibrium composition of H₂, CO, CO₂, H₂O, O₂, CH₄, C, CeO₂ and Ce₂O₃ obtained from the reduction of methane over CeO₂ in a temperature range of 500°C-1000°C and CH₄/CeO₂ feed molar ratios from 0.4 to 4. Different results were obtained:

- 1) methane reduction reaction initiates over 600 °C. Lower methane to ceria ratios yield lower products than higher feed ratios at same temperatures. At stoichiometric conditions, that is with 0.5 mol CH₄ per mole of CeO₂, 50% of CeO₂ conversion occurs at around 800 °C, while the reaction yields 99.9% conversion at temperatures over 900 °C;

- 2) at lower temperatures (500–600°C) and for a lower CH₄/CeO₂ feed ratio (below 0.5), the metal oxide is poorly active for the reaction. In any case, even with higher CH₄/CeO₂ feed ratio, the complete reaction occurs at temperatures over 700°C, providing a thermodynamic limit to the reduction temperature of pure CeO₂ over methane;
- 3) an operation with 0.7–0.8 mol of CH₄ per mole of CeO₂ at around 900–950°C would provide the ideal operating conditions without the need to feed a high fraction of methane. A syngas stream of 31% CO and 63% H₂ can be obtained (balance 1% H₂O, 0.4% CO₂ and 4.6% CH₄) at around 950 °C and a CH₄/ CeO₂ feed ratio of 0.7 to 0.8;
- 4) for higher methane flows, the excess methane at the outlet of the reduction reactor would decrease the effectiveness of the chemical looping system.

In addition, an analysis of the molar fractions of unwanted chemical species obtained in the reduction reactor (carbon, CO₂ and H₂O, produced in the reactions (55)-(56) and (61)-(62)) at the different operating conditions was made:

- 1) at a higher temperature, and especially at a lower content of methane, there is an evident increase in CO₂ formation. A similar trend is observed for H₂O formation, but the yield of H₂O is considerably higher than CO₂, at corresponding temperature and pressure. At near stoichiometric operations, together they make up about 4% of the product gas flow. Reactions (61) and (62) mainly occur for the lower content of methane in the reduction step, so the oxygen which is released by the metal oxide lattice oxidizes the obtained CO and H₂ to produce CO₂ and H₂O;
- 2) carbon deposition starts at a methane to ceria feed ratios above 1.0 and with temperature above 900°C and it increases as the molar flow of methane and the temperature increase because these conditions favour the Boudouard and the methane decomposition reactions ((55) and (56)). The carbon deposition in the reactor has not negligible effects even at low contents; these effects limit the methane reduction to around 900 °C, and the molar feed ratio, to less than or around 1.0.

Considering the different studied factors, it could be concluded that the favourable operating zone of the reduction reactor has to be limited to around 900–950 °C with 0.7–0.8 mol of CH₄ per mole of CeO₂ to ensure complete reduction of CeO₂ without the need of high methane content and avoiding unwanted reactions to take place. In these operating conditions, the problem of sintering of ceria is solved because this process is not observed until 1623 °C (1900 K). In addition, in this operating range, the syngas obtained has the desired ratio of H₂/CO equal to 2. In the same study above mentioned [48], the oxidation reaction (second step of the thermochemical cycle) was also analysed considering:

- a temperature range of 500-1000°C;
- the complete reduced ceria (Ce₂O₃) to be introduced in the oxidation reactor with a constant flow of 0.5 kmol/h;
- an H₂O/CO₂ mixture (waste gas) composition which was made vary from 5% to 95% CO₂ and with a molar flow rate from 0.5 to 2 kmol/h.

The following results were obtained:

- water-splitting reaction peaks at temperatures between 600 and 650 °C, while a monotonic increase of CO production with the temperature was obtained for CO₂ splitting reaction;
- a minimum molar flow of 0.75 kmol/h of waste gas at the equimolar composition of CO₂ and H₂O would be required to completely oxidize a flow of 0.5 kmol/h of Ce₂O₃ to CeO₂ to close the redox cycle. This corresponds to a flow of 50% excess than the stoichiometric quantity. Sending above stoichiometric flows results in complete oxidation of Ce₂O₃, but also in a considerable drop of syngas fraction. This would decrease the effectiveness of the process by requiring additional downstream processes to separate CO₂ and water for obtaining pure syngas;
- as regards the ratio H₂/CO, at the outlet of the oxidation reactor with varying molar feed flows of the equimolar mixture of H₂O and CO₂, it was noted that the production of H₂ over CO is

favoured at lower temperatures and at higher molar feed rates. However, the ratio drastically decreases as the temperature increases ($H_2/CO \approx 0.6$ at around 1000°C);

- there is no specific peak for CO formation because it increases as the temperature increases.

As a result, for waste gases with large fractions of water content, it is better to make the oxidation reactor operate at a temperature of about $600\text{--}700^\circ\text{C}$ to ensure maximum reactivity of H_2O . On the other hand, for a higher CO_2 content, typically occurring for the exhausts of power plants, the temperature of the oxidation reactor can be set at higher values (around or above 900°C). This produces high conversion of CO_2 and also the possibility to operate the redox cycle at isothermal conditions. Taking into account these results obtained from literature, in the present study an isothermal and isobaric chemical looping is implemented in all the three different analysed plants. In the solar energy fed polygeneration system, both the reduction and the oxidation reactions operate at 900°C and 1.2 bar. In the reduction reaction, the CH_4/CeO_2 molar ratio is set at 0.76 and a syngas with H_2/CO molar ratio around 2 is obtained; in the oxidation reaction, an H_2O/CO_2 molar ratio equal to 1.13 is fixed to obtain a syngas with H_2/CO molar ratio around 1. In the other two studied systems, which are not supplied by solar energy, both the reactions of the CL occur at 800°C and 1.2 bar. The lowering of the cycle temperature makes necessary the increase of the biomethane molar flow rate sent to the reactor for ceria reduction, so the CH_4/CeO_2 molar ratio is increased to 0.95.

4. SOLAR RECEIVER-REACTORS

Solar thermochemical applications employ the same solar concentrating technologies of those systems which convert solar energy into power through the use of a conventional power cycle (Rankine, Brayton or Stirling) coupled with concentrating solar panels. The main difference is that the concentrated solar radiation is not focused on a “plain” receiver, but it is directed towards a receiver-reactor in which chemical reactions are performed. Since process temperatures of thermochemical cycles can reach 2300 K, only solar towers and dishes can be used. In addition, hydrogen/syngas production plants require a certain size and solar dishes are characterized by size limitations (as specified in [Chapter 1](#)), so most research and development work is executed on the implementation of thermochemical cycles coupled with solar towers (as in this study).

4.1. Directly and indirectly irradiated receivers

The first generic classification of solar receivers can be made based on the mechanism of transferring the solar heat to the heat transfer fluid and, therefore, two main types of receivers can be considered:

- 1) indirectly irradiated receivers;
- 2) directly irradiated receivers.

Indirectly Irradiated Receivers (IIRs) are characterized by absorbing surfaces which are exposed to the concentrated solar radiation. Then, the absorbed heat is conducted across the walls to the heat transfer fluid. An example of this type of receivers is given by tubular receivers with absorbing walls in which the heat transfer fluid (e.g. a gas or molten salts) circulates in a perpendicular direction concerning the incident solar radiation. Directly Irradiated Receivers (DIRs) use fluid streams or solid particles/structures which are directly exposed to the concentrated solar rays. These kinds of receivers are also defined “volumetric” receivers since they enable the concentrated solar radiation to penetrate and to be absorbed within the entire volume of the absorber. This absorber can have different geometries and properties, it can be:

- a stationary matrix (grid, wire-mesh, foam, honeycomb etc.);
- moving (usually solid) particles.

4.2. Structured and non-structured receiver-reactors

As explained in [Chapter 3](#), in thermochemical cycles, there is the reaction between a solid (metal oxide) and a gas. Based on the disposition of the solid material, two different types of reactors can be defined:

- 1) non-structured reactors. They are packed and fluidized bed reactors: solid particles are randomly distributed in the reactor;
- 2) structured reactors. Honey-comb, foam and membrane catalytic reactors belong to this category: solid particles are arranged in space in the reactor.

Both these two configurations of the solid particles can be obtained either within solar-heated tubular receivers (IIRs) or indirectly irradiated receivers (DIRs). However, in IIRs, there are several limits to the heat flux that can achieve the reaction site (in the inner region of the tube) due to the resistance to heat transfer and the maximum temperature reachable by the materials of the tube. As a result, the largest amount of reactors are DIRRs with solid particles or structures which are directly exposed to the concentrated solar radiation, but these particles have to be insulated from air and, consequently, receiver-reactors should be furnished with a transparent window that could also operate in pressure.

4.3. Temperature swing between the two steps of the thermochemical cycle

The two different steps of the thermochemical cycle are enhanced by different operating conditions:

- 1) the first step (thermal reduction of the solid oxide) is thermodynamically favoured at higher temperatures (typically in the range of 1600-1900 K) and low oxygen partial pressures. The solid metal oxide is fed with a purge gas;
- 2) the second step ($\text{H}_2\text{O}/\text{CO}_2$ splitting) is thermodynamically favoured by lower temperatures and high partial pressures of $\text{H}_2\text{O}/\text{CO}_2$. Concerning the temperature, a trade-off between thermodynamics (low temperatures are necessary to avoid the thermal reduction of the metal oxide simultaneously with the splitting of water and carbon dioxide) and kinetics of the reaction (the temperature cannot be too low, otherwise the reaction is not fast enough) has to be found, so temperature ranges between 1000-1300 K have to be considered. The solid metal oxide is fed with gaseous $\text{H}_2\text{O}/\text{CO}_2$.

To maximize the efficiency of the entire system, the temperature swing between the two reactions has to be considered and exploited to recover and reuse the sensible heat which is available after the first step. In fact, the dispersion of such thermal energy would produce a not negligible economic loss for the system itself.

4.4. Solar receiver-reactors for volatile and non-volatile cycles

Based on the chosen redox pair, another classification of the solar reactors can be executed:

- 1) solar reactors in which only thermal reduction takes place;
- 2) solar reactors in which both steps of the thermochemical cycle take place.

In volatile cycles, the products of the reduction reactions are in the gaseous phase and they consist of both the reduced phase (lower valence metal oxide/metal) and the oxygen. As a result, a quench is necessary to separate the two components of the mixture and avoid their recombination to the reactants, so the two steps of the cycle cannot be executed in the same reactor. Two different reactors are necessary: in one reactor, the reduction reaction is executed and supplied by solar energy, while in the other one (that does not necessitate to be a solar reactor) the WS/CDS takes place. In this kind of configuration, the following characteristics have to be highlighted:

- 1) the two steps of the cycle are decoupled and they could be executed in different periods: thermal reduction takes place during the day, when solar rays are present, while the syngas can be produced during the night;
- 2) solar reactors are designed only to perform the higher-temperature thermal reduction (TR) step. Thus, aerosol reactors are comprised in this typology of reactors because they only perform the TR step, even if they can work with both volatile and non-volatile cycles.

In the case of non-volatile redox pairs, reactants remain in the condensed phase during the whole cycle, thus there are no products separation problems. Both particle receiver-reactors and structured reactors can be used and, in these types of solar reactors, both the cycle steps can take place.

4.5. Solar reactors chosen in the present study

In the solar aided polygeneration system studied in this work, the thermochemical reduction of ceria and the biomethane reforming reaction downstream the DME unit are supplied by concentrated solar energy. The reduction reaction of CeO_2 necessitates of a temperature equal to 900°C , while the reforming reaction of biomethane occurs at a slightly lower temperature (800°C). However, the reforming unit only works simultaneously with the CL, so it operates in those periods in which a sufficiently high direct irradiance irradiates the receiver-reactor of the reduction to reach its operating temperature. In addition, a large solar thermal energy supply is required to simultaneously sustain the

two reactions ($W_{th,tot} \sim 294$ MWt). This makes not convenient the use of the Dish technology, thus it is considered to dispose of a Solar Tower system to feed with CSP both the reduction reaction of the CL and the biomethane reforming. It could be thought to realize only one tower with:

- the two receiver-reactors (reduction reactor and biomethane reforming reactor) installed at two different heights. A certain number of heliostats will point towards one receiver, while the remaining part will point towards the other receiver;
- beam down solar concentrator configuration. The two receivers will be installed on the ground next to each other and they will be invested by the re-reflected solar beams.

Furthermore, having available:

- 1) the data of the daily values of the direct normal irradiance in the neighbourhood of the Energy Center, measured by the meteorological station of the Politecnico;
- 2) the seasonal daily average temperature curves of the receiver-reactor at the focus of the Dish system installed on the roof of the Energy Center for different meteorological seasons (obtained from previous studies [51]);

the evaluation of the yearly periods of the chemical looping working is executed considering these data. Therefore, the CSP system which could be used in the present study is a Solar Tower system with two identical receiver-reactors which are similar (in a much larger scale) to the receiver-reactor of the solar Dish on the roof of the Energy Center both in terms of design and irradiance/temperature curves. When the receiver-reactor is at a temperature higher/equal to 900°C , the CL and, accordingly, the reforming unit is in ON-state. These receiver-reactors are non-structured tubes made of alumina (Aluminum Oxide: Al_2O_3). This material is highly resistant to abrasion and corrosion both in acid and alkaline environments, additionally, it is not subjected to oxidation, so it is particularly adapt to these applications.



Figure 43: Receiver-reactor at the focus of the Dish system of the Energy Center

In the solar receiver-reactor in which the reduction reaction of the CL occurs, ceria particles are placed in the reaction zone. When the CSP system starts to concentrate solar energy towards this reactor, a mass flow of argon is sent to clean the bed of the reactor itself, create inert zones, reduce the thermal stress at which the bed is subjected and avoid the formation of explosive mixtures. Then, a mass flow of biomethane is made circulate in the reaction zone for the occurrence of the solar thermal reduction of ceria. This reactor is a continuous flow reactor, this means that biomethane is continuously fed into the reactor and it emerges as a continuous stream of product. In this way, during the reaction of reduction of ceria, there always is a gaseous stream at the outlet of the reactor which can be sent to the SOFC anode. This reaction takes place with the heliostats of the CSP system perfectly focused to concentrate the highest amount of solar energy towards the receiver itself and reach the required reaction temperature (this temperature will be slightly higher than the 900°C chosen in the present study). When the reduction of CeO_2 is complete, the reduced particles are recirculated to the non-solar oxidation reactor to be re-oxidized. Even the oxidation reactor is a continuous flow reactor. These two reactors function simultaneously. During the reduction reaction in the solar receiver-

reactor, also the oxidation of other previously reduced ceria particles is taking place in the oxidation reactor. As a result, meanwhile, the just reduced ceria particles enter in the oxidation reactor, just re-oxidized ceria particles exiting the oxidation reactor enter in the reduction reactor. In the oxidation reactor, nebulized water and a CO₂ stream are sent to the reaction zone and the oxidation of ceria takes place. When the oxidation ends, the cycle restarts. The simultaneous functioning of these reactors allows the complete exploitation of solar energy when it is present thanks to the continuous operation of the reduction reactor itself which is not interrupted to make the re-oxidation take place. This is possible introducing in the chemical looping a number of ceria particles which is doubled compared to the net amount of particles which are recirculated between the two reactors at each cycle. This means that when the system is first started, in the reduction reactor ceria particles are introduced from the external environment and reduced through CSP. After the complete reduction of these particles, they are sent to the oxidation reactor and, meanwhile, other ceria particles are introduced from the external environment to the reduction reactor to be reduced. When the particles sent to the oxidation reactor are completely oxidized, they are recirculated to the reduction reactor and reduced through the concentrated solar power, while the particles just reduced in this latter reactor are sent to the oxidation reactor itself. The chemical looping operation reaches the steady-state with the two reactors functioning simultaneously when the receiver-reactor is at $T \geq 900^\circ\text{C}$, this is the condition analysed in the Aspen Plus model of the plant.

5. Fuel cells

Fuel cells are completely open electrochemical cells: reactants and products are exchanged between the cell and the external environment, the two electrodes support the reactions without taking part to them. In addition, in a fuel cell, a spontaneous reaction takes place ($\Delta\bar{g} < 0$) and so electric power is produced (chemical to electrical energy conversion, it is a galvanic cell).

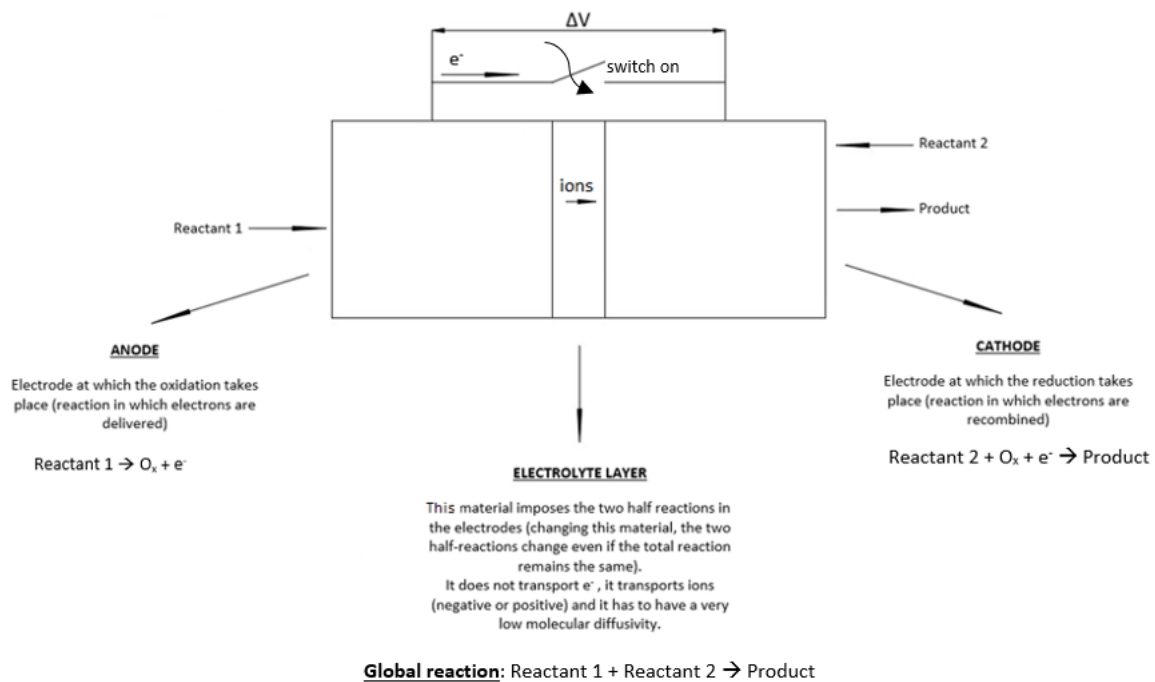


Figure 44: Generic scheme of a fuel cell

In a fuel cell, the electrolyte layer separates the two reactants and guarantees that they do not enter in contact with each other, but the reaction occurs anyway because:

- ions are transferred by the electrolyte;
- electrons travel through an external circuit (when it is closed), this creates a coherent flow of electrons, which (by definition) is current.

Current (I) is the first element which contributes to the electric power, the second element is a voltage gradient (ΔV). The ΔV is generated by the separation of charges in the anode, which produces an electric field and so a voltage. As a result, electric power can be defined as:

$$W_{el} = I \cdot \Delta V \quad (63)$$

In the present study, the device chosen to generate electric power is a fuel cell and not a gas turbine for three main reasons:

- 1) higher fuel flexibility. In this regard, a solid oxide fuel cell is chosen because it can be fed with many different fuels;
- 2) higher electrical efficiency, a thermal machine has efficiencies in the range of 15%-60%. While an electrochemical cell in the range of 50%-75%. It results from the lower generation of entropy that takes place in a fuel cell than a gas turbine (and, in general, to a thermal machine). The highest amount of irreversibilities in the gas turbine is produced by the

combustion chamber, which is not present in a fuel cell because the latter directly converts chemical energy into the electric one without the intermediate conversion into heat (as shown in *Figure 45*)

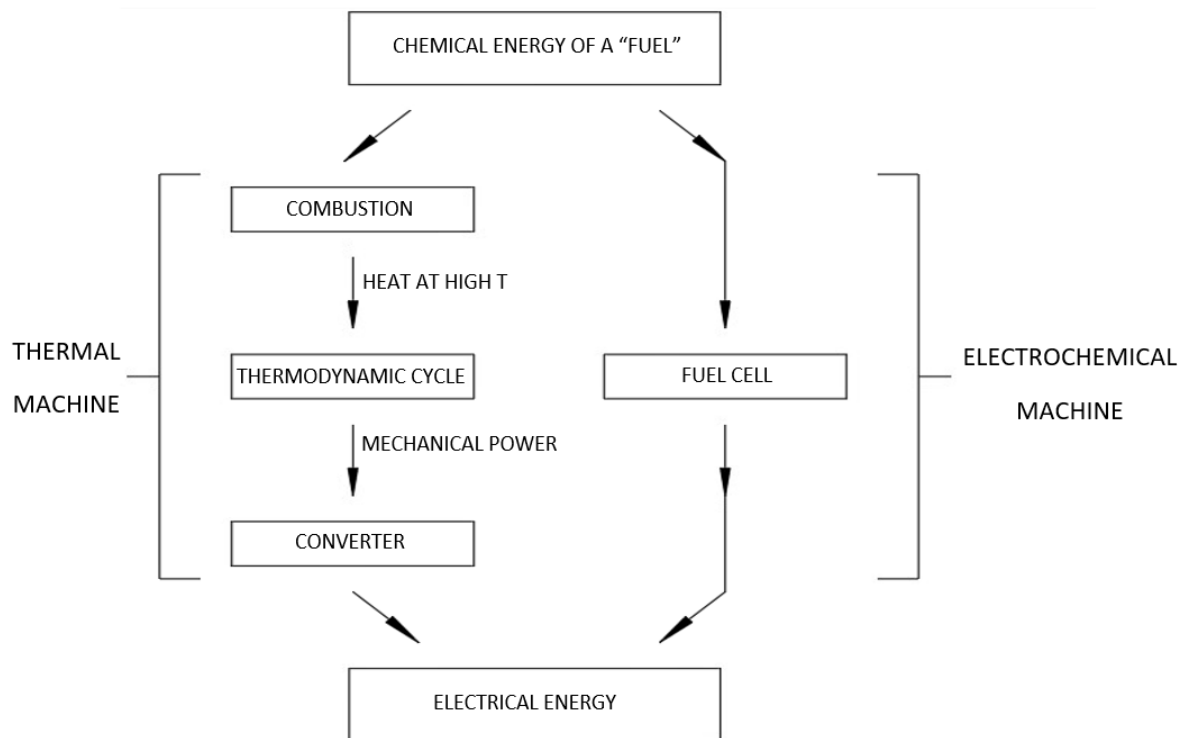


Figure 45: Comparison between a thermal machine and an electrochemical machine

- 3) in a fuel cell, there are no moving parts, so there is not the problem of noise of the components.

5.1. Focus on the SOFC

In the present work, the Solid Oxide Fuel Cell is chosen to generate electric power. This fuel cell is characterized by a high operating temperature ($T > 700^{\circ}\text{C}$). This high temperature produces both advantages and disadvantages. The main advantages, which are the reasons why this typology of fuel cell is chosen, are:

- 1) all transport processes are improved (charge transfer, charge conduction and mass transfer). This characteristic allows to obtain a highly efficient fuel cell without the need of a precious catalyst (usually nickel is used). At present, SOFC is the most efficient fuel cell, Elcogen's SOFC stack holds the world record of 74% of electric efficiency [52];
- 2) very good fuel flexibility. Many different fuels can be used such as H_2 , hydrocarbons, alcohols, ethers, biogas, natural gas, syngas, ethanol and methanol. In this study, the syngas produced in the reduction reactor of the chemical looping process is used to feed the FC;
- 3) availability of high-temperature heat as a by-product ($T > 250^{\circ}\text{C}$). In this work, this heat is exploited in different ways:
 - in the solar energy fed polygeneration plant, the produced heat is exploited to generate steam and to combust the waste products of the DME synthesis reactor;

- in the other two analysed systems, this heat is used to supply the reduction reactor of the chemical looping.

The main disadvantages are:

- 1) SOFCs are not dynamic machines. They have slow startups and the slowest dynamic; they are not suitable for automotive applications, but they can be used for CHP systems and power production. They are ideal to cover base loads and it is important to avoid thermal cycles of switch-on and switch-off of the FC, it is better to switch on the machine and never switch it off (it takes time, also hours, to switch on the machine). This characteristic may be a problem in the coupling of the SOFC with solar energy because this energy is highly intermittent and discontinuous. To solve this problem, in the solar aided polygeneration plant analysed in the present paper, a storage system of the fuel that feeds the FC is considered. In this way, it is possible to make the SOFC work at base load throughout the entire year;
- 2) high temperature needs good quality materials for the auxiliaries, this implies high costs of the components.

An anode supported planar SOFC with the structure shown in *Figure 46* is chosen because it has a thin electrolyte (there is not a so high ohmic drop), a thin cathode (it facilitates the diffusion of the O₂) and a thicker anode which guarantees a large three-phase-boundary (TPB). The TPB is the zone in which the fuel is oxidized, so there is the coexistence of the porous phase, electronic phase and ionic phase: the molecule of the reactant has to be fed to the point of the reaction (this takes place in the porous phase) and the ions and the electrons have to be removed from the point of the reaction (in the ionic phase and in the electronic phase respectively).

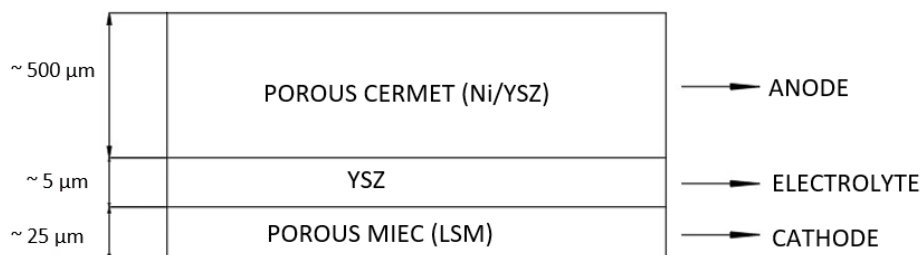


Figure 46: SOFC structure

As shown in *Figure 46*, the SOFC layers are constituted by different materials:

- 1) the electrolyte is composed by yttria-stabilized-zirconia (ZrO₂ + 8%Y₂O₃, Zr⁴⁺ is doped with Y³⁺). The doping of Zr⁴⁺ with Y³⁺ produces O²⁻ vacancies in the lattice and so a good mobility of O²⁻ ions. Zirconium is not expensive, yttrium is less available but it is only used for doping, so this FC is not expensive. In addition, the ionic resistivity of YSZ decreases with the increase of the temperature and starts to have very low values at around 650°C, that's why the SOFC has to operate at T>700°C;
- 2) the anode is made of a porous cermet, alloy of a metal (nickel) and a ceramic material (yttria-stabilized zirconia, YSZ). At this electrode, the three-phase-boundary is constituted by YSZ at 30% of porosity (ionic and porous phase) and nickel (electronic phase), which also acts as a catalyst;
- 3) the cathode is realized in an MIEC (Mixed Ionic Electronic Conductor). The MIEC is LSM (Lanthanum Strontium Manganite Oxide, La_{1-x}Sr_xMnO₃, perovskite structure) because it has the closest behaviour to YSZ in terms of volumetric modification with temperature.

In the stack, interconnectors between the cells are constituted by Crofer 22 which is tight (very dense to avoid molecular diffusion), a good e⁻ conductor and with a volumetric modification with temperature similar to YSZ, guaranteeing mechanical strength to the SOFC.

5.1.1. SOFC voltage and polarization curve

The produced electric power is the product between voltage and current. Current is obtained by the coherent flow of electrons which circulate in the external circuit, while the voltage can be evaluated as follows. At the open circuit, the current is equal to zero, but voltage (E) is not null and it can be calculated through the Nernst equation.

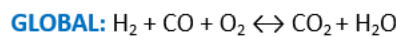
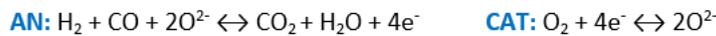
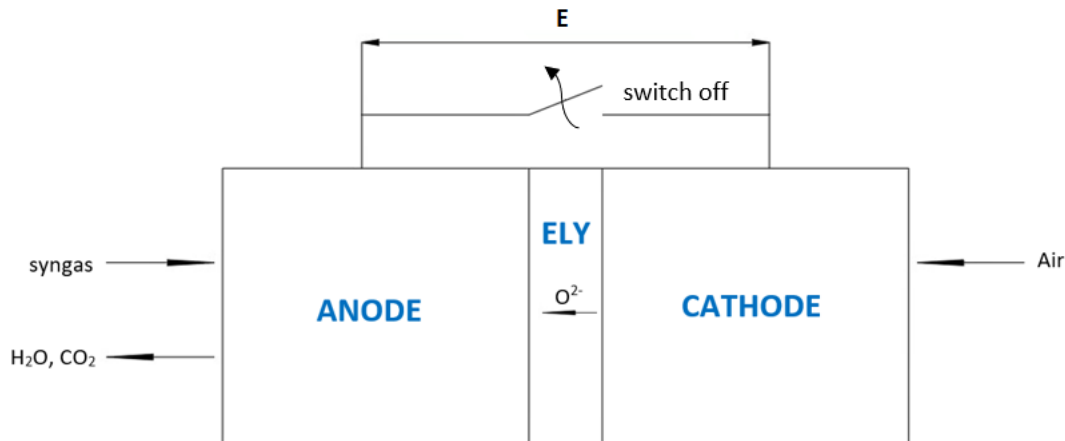


Figure 47: SOFC at open circuit

E is related to the gradient of Gibbs free energy between the anode and the cathode (in the anode the H₂/CO is present, while at the cathode there is O₂), so it is linked to the chemistry and not to the transport process because the reactions at both the cathode and the anode are in equilibrium (the rate of the forward reaction is equal to the rate of the reverse reaction, $r_{forward} = r_{reverse}$). Writing the first and the second laws of thermodynamic at the steady-state for the fuel cell under the hypothesis of ideal gases, the Nernstian voltage is obtained:

$$E = - \frac{\Delta\bar{g}((T, P_0))}{Z_F \cdot F} + \frac{RT}{Z_F \cdot F} \cdot \ln \frac{\prod_{reactants} \left(\frac{P_i}{P_0}\right)^{\nu_R}}{\prod_{products} \left(\frac{P_i}{P_0}\right)^{\nu_P}} \quad (64)$$

in which:

- 1) $\Delta\bar{g}((T, P_0))$ is the average molar free energy variation of the reaction at the real operating temperature and at the reference pressure P_0 ;
- 2) Z_F is the charge number of the fuel (in case of the SOFC fed by syngas, $Z_F = 4$);
- 3) F is the Faraday number, equal to 96485 c/mol;

- 4) R is the universal gas constant, equal to $8.314 \text{ kJ}/\text{K} \cdot \text{mol}$;
- 5) P_i is the partial pressure of the i-th component of the reaction.

In an FC, the aim is to produce power and, accordingly, to increase the voltage. The increase of the Nernstian voltage can be obtained through the:

- 1) increase of the reactants' partial pressures ($P_{i,\text{reactant}}$) that can be obtained increasing either the molar fraction of the reactant, either the total operating pressure of the cell or both:

$$P_{i,\text{reactant}} = y_{i,\text{reactant}} \cdot P_{\text{tot}} \quad (65)$$

In the present work, the Nernstian effect is made increase setting the operating pressure of the SOFC at 5 bar;

- 2) decrease of the products' partial pressures ($P_{i,\text{product}}$). It is important not to have the accumulation of the products in the FC because it would push the reaction towards the reactants;
- 3) reduction of the operating temperature of the FC (the higher the operating temperature and the lower $\Delta\bar{g}((T, P_0))$). This is why the PEMFC has a Nernstian voltage that is higher than the SOFC.

Closing the external circuit, the current is produced by the conduction of electrons from the anode to the cathode.

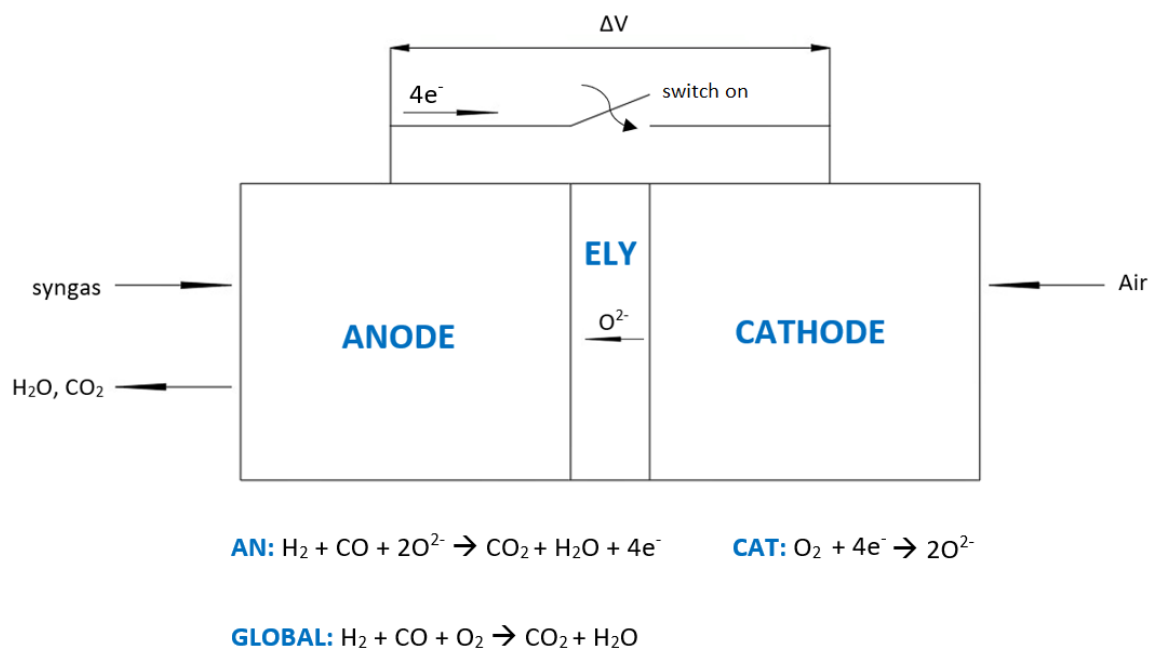


Figure 48: SOFC operation at a close circuit

During this operation of the FC, transport phenomena take place and they produce overvoltages which lower the value of the FC voltage:

- activation overvoltage (η_{act}). It is linked to the charge transfer effect and it prevails at low values of current;
- ohmic overvoltage (η_{ohm}). It is due to the conduction of electrons in the external circuit and the transport of ions in the electrolytic material. It prevails for intermediate values of the current;

- diffusion overvoltage (η_{diff}). It is related to the mass transport and, accordingly, to the diffusion of the reactants into the electrodes and it prevails at high values of the current.

As a result, the cell voltage (V_{cell}) can be written as:

$$V_{cell} = E - \sum_{j=1}^3 \eta_j \quad (66)$$

Actually, in a SOFC, thanks to the high operating temperatures, η_{act} and η_{diff} are negligible:

$$V_{cell,SOFC} \approx E - \eta_{ohm} \quad (67)$$

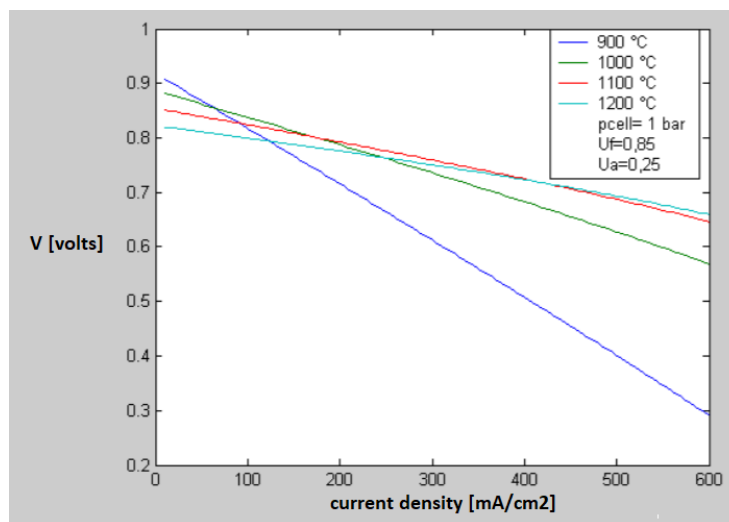


Figure 49: SOFC polarization curve at different temperatures and fixing a $FU = 0.85$, an $AU = 0.25$ and a pressure $P=1$ bar [53]

5.1.2. Thermal balance in a SOFC

The produced electric power is strictly related to the enthalpy gradient between the products and the reactants of the FC. However, not the whole gradient is transformed into power, there also is a thermal exchange between the cell and the external environment so a portion of the chemical energy of the fuel is lost in heat. A thermal balance of the cell is fundamental to correctly control the cell's temperature. In particular, there are two sources of heat:

- 1) heat connected to the electrochemistry and thermodynamics of the reaction:

$$\phi_{reaction} = T \cdot \Delta \bar{S}_{reaction} \cdot \dot{n}_{reactants} \quad (68)$$

since in an FC $\Delta \bar{S}_{reaction} < 0$, the reaction is exothermic;

- 2) heat connected to transport processes, which generate heat from irreversibilities. This thermal dispersion can be evaluated considering the three different overvoltages (voltage drops) that take place in the FC from the open circuit:

$$\Phi_{\text{irrev}} = -I \cdot \sum_j \eta_j \quad (69)$$

As a result, the total amount of heat released by the FC during its operation is:

$$\Phi_{\text{total}} = \Phi_{\text{reaction}} + \Phi_{\text{irrev}} \quad (70)$$

and, developing the expressions (68), (69) and (70):

$$|\phi_{\text{total}}| = \left(-\frac{\overline{\Delta h_{\text{reaction}}}}{Z_F \cdot F} - V_{\text{CELL}} \right) \cdot I = \left(-\frac{\overline{\Delta h_{\text{reaction}}}}{Z_F \cdot F} \cdot I - W_{\text{EL}} \right) \quad (71)$$

In a SOFC, the control of the temperature is executed by sending a high excess of air in the cathode of the fuel cell which absorbs the heat released by the cell (Φ_{total}). In general, an air utilization (AU) of around 20% (and, consequently, an air excess ≈ 5) is considered:

$$\text{AU} = \frac{\text{amount of air used in the stoichiometric reaction}}{\text{total amount of air sent to the cathode}} \quad (72)$$

6. CASE STUDY: POLYGENERATION PLANT

This study focuses on a polygeneration plant. Polygeneration plants are gaining increasing attention in the last years because of their high overall efficiency. This high efficiency is related to the use of the heat rejection streams, which, otherwise, would be wasted in the environment, for the production of useful heat or the feeding of other devices to obtain useful outputs. As a result, these units generate multiple products like electricity, cooling, heating, freshwater and chemicals. Particularly, the present analysis combines a solar energy system with a polygeneration unit, producing many useful outputs:

- thermal power;
- electric power;
- dimethyl-ether (DME);
- methanol;
- syngas.

To sum up, a sustainable plant is obtained because it is characterized by high efficiency and the use of a clean energy source.

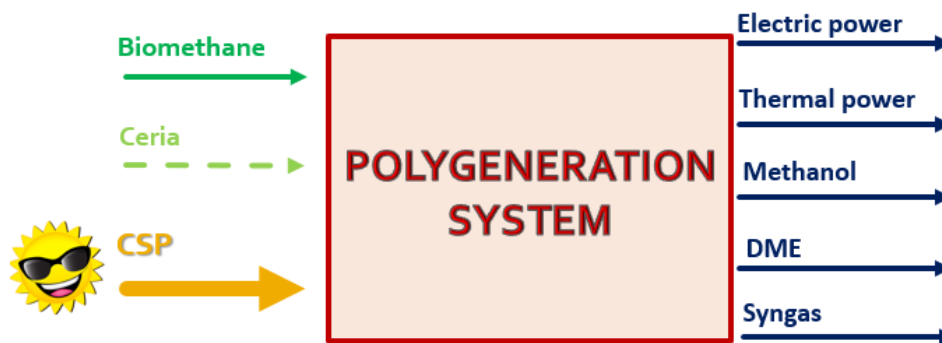


Figure 50: Inputs and outputs of the polygeneration plant

Generally, polygeneration systems have one prime mover, which is the most important device; it is fed by heat and/or fuel inputs and it acts as the “manager” of the system feeding with flue gases (or heat input) other secondary devices to produce additional useful outputs. In most plants, the prime mover produces electricity, but, in the plant analysed in the present study, the prime mover is given by the chemical looping, that has the function to produce syngas. The produced syngas feeds a solid oxide fuel cell and a catalytic reactor for the production of electricity and DME respectively. Additionally, it is important to highlight that the reduction reaction of the chemical looping is endothermic, therefore it needs external heat to take place properly. To satisfy the thermal requirements of the prime mover, the reduction reaction is made occur in the receiver-reactor placed at the focus of a CSP system, while the oxidation reaction takes place in a non-solar reactor simultaneously with the reduction reaction. The temperature curves of the reduction receiver-reactor are considered equal to the ones of the receiver installed at the focus of the Dish system on the roof of the Energy Center. However solar energy is highly intermittent and the effects of yearly seasonal alternation and meteorological conditions are not negligible, consequently, two different situations with different operating conditions of the plant have to be analysed:

- 1) operation during a clear sky day with an irradiance which is sufficient to make the chemical looping operate properly;
- 2) operation during a low-irradiance day.

In the first operating condition, all the components of the plant can work properly, as shown in *Figure 51*. Solar energy feeds the reduction reaction, CeO_2 is reduced simultaneously with the partial

oxidation of biomethane and two main outputs are obtained: Ce_2O_3 and syngas. Ce_2O_3 is re-oxidized, while the syngas is partly sent to the Solid Oxide Fuel Cell and partly stored in an AISI316L tank to be then used as the fuel of the SOFC during those days in which solar irradiance is not sufficient to make the CL operate. For the continuous operation of the SOFC throughout the year (the SOFC has to work at base-load conditions as written in [Chapter 5.1](#)), the SOFC itself is under-sized compared to the reduction reactor of the chemical looping. During its operation, in the reduction reaction, it is produced an amount of syngas which is much higher than the syngas flow rate that effectively feeds the fuel cell and the surplus of produced syngas is stored to be used in those periods in which a lack of production from the CL is registered. In the Solid Oxide Fuel Cell, air from the external environment is also introduced for the oxidation of H_2 and CO into H_2O and CO_2 and electric power is obtained. The anodic exhausts of the cell (H_2O and CO_2) are split into two streams of H_2O and CO_2 respectively. H_2O is directly sent to the oxidation reactor, while the CO_2 stream is firstly integrated with an additional amount of CO_2 , coming from the CO_2 tank (refilled when the CL does not work), and then it is entirely sent to the oxidation reactor (which is not a solar reactor). Ce_2O_3 is re-oxidized to CeO_2 and syngas is produced. This latter syngas stream is integrated with additional syngas produced in the reforming unit and feeds the DME unit whose aim is to produce DME. Methanol and a further amount of syngas, obtained from the reforming unit, fed by solar energy and placed downstream the DME unit, are additional outputs of this section. Additionally, water is introduced in the plant to produce steam from the waste heat of the system components. This steam is partly recirculated in the plant to cover heat loads and partly used to obtain another important output of the system: thermal power. This heat can be used for auto-consumption or it could be sold to other users.

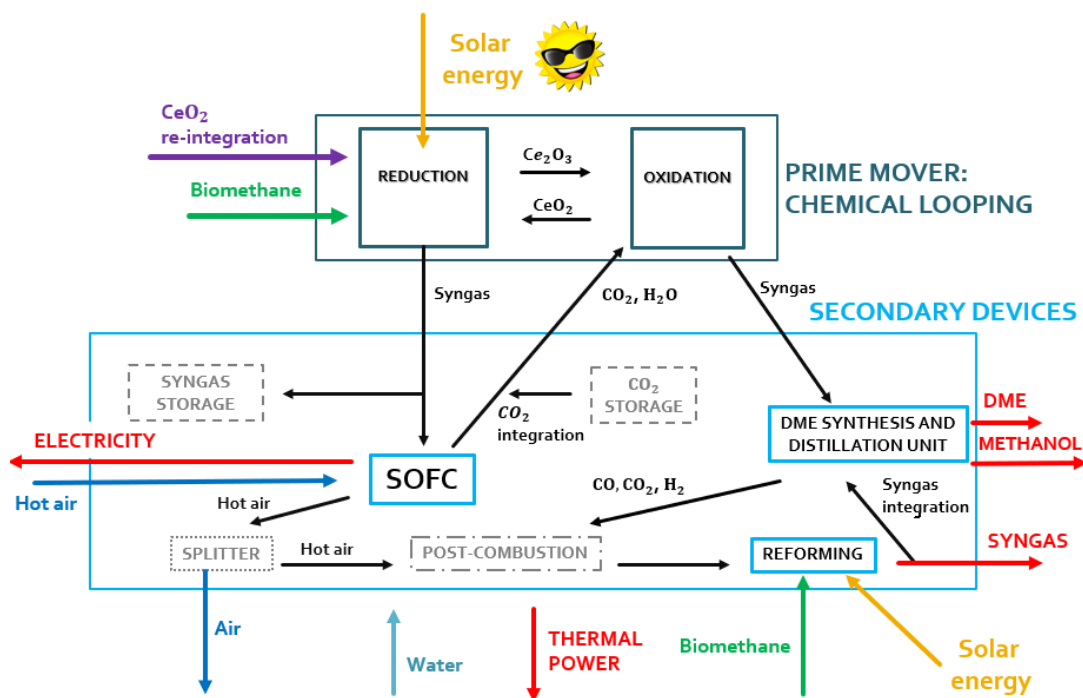


Figure 51: Prime mover and secondary devices of the polygeneration plant during a clear sky day

In the second operating condition of the plant, only the SOFC can operate. Due to the lack of solar energy, the chemical looping does not work and the Solid Oxide Fuel Cell is fed by the syngas stored during the previous operating condition of the system. In this case, the streams of the anodic exhausts of the SOFC, separately H_2O and CO_2 , are stored to be then reused when the CL restarts to operate, as shown in [Figure 52](#).

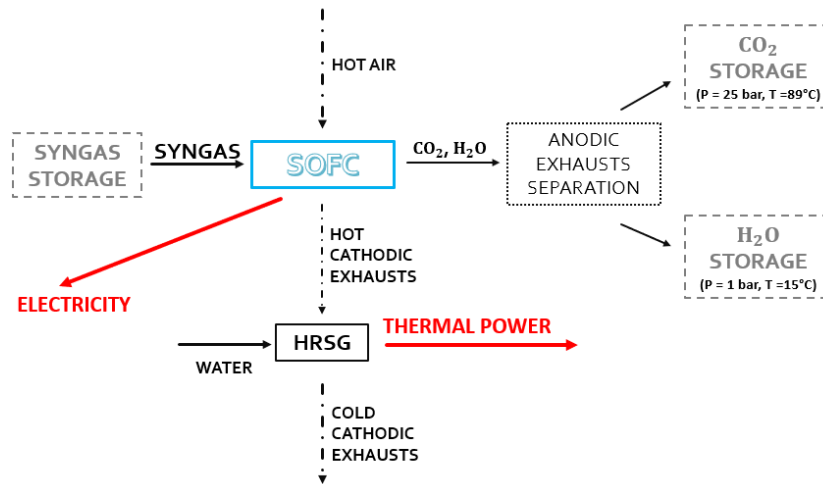


Figure 52: Operating components of the plant in the absence of solar irradiance

These two different operating situations of the polygeneration plant can be defined taking into account the measured seasonal temperature of the receiver-reactor of the Dish solar system installed on the roof of the Energy Center (shown in [Figure 53](#)). Since the chosen temperature of the reduction reaction is 900°C when the receiver is irradiated by enough amount of solar radiation and reaches 900°C, the chemical looping works and the plant operates as shown in [Figure 51](#), otherwise only the SOFC functions, as shown in [Figure 52](#).

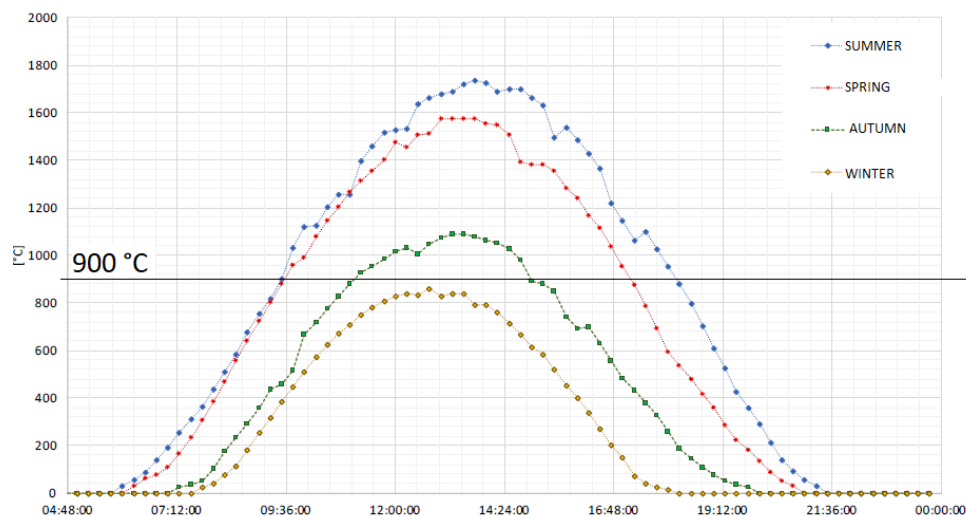


Figure 53: Seasonal daily average temperature curves of the solar reactor for the different meteorological seasons. Values were obtained from a 2D modelling on Comsol [51]

In [Figure 53](#), it can be seen that the outermost curves, in particular the summer one, offer considerably higher values of the temperature reached by the receiver-reactor for longer time intervals because it absorbs a higher amount of solar energy (thanks to the registered higher values of solar irradiance for longer daily time intervals), this means higher plant yields in the warmer months, thus making the entire analysed technology very interesting and valuable. In addition, it can be seen that the temperature higher/equal to 900°C is reached:

- 1) for 8h and 30min per day in Summer;
- 2) for 7h and 40min per day in Spring;

- 3) for 3h and 40min per day in Autumn;
- 4) never in Winter.

To sum up, the chemical looping can work for around 110010 minutes per year (around 1833 hours and a half, so around 77 days). On the other hand, the SOFC works for the whole 365 days of the year.

6.1. Plant scheme and components

As written before, the analysed plant is constituted of four main sections:

- 1) chemical looping. It is the prime mover and its aim is to produce syngas, it works only under the presence of a sufficient amount of irradiance hitting the receiver-reactor of the considered CSP system, in which the reduction reaction takes place. Therefore, its operation is for around 1833 hours and a half in one year;
- 2) SOFC. It is a secondary device fed by the syngas produced in the reduction reaction of the CL, this syngas is directly sent to the SOFC when the CL is correctly operating, otherwise, it is obtained from the syngas storage (the chemical looping is over-sized compared to the SOFC). The fuel cell aims at producing electric power and it works for the entire 8760 hours of the year;
- 3) DME production. In this section, dimethyl-ether is directly obtained starting from the syngas coming from the oxidation reactor of the CL. As a result, this section of the plant only operates simultaneously with the CL and it is also integrated with a reformer, supplied by solar energy, to treat the exhausts and obtain an additional output (syngas);
- 4) steam production. In the plant, five heat recovery steam generators (HRSG) are inserted for exploiting the waste heat fluxes of the system. Steam is obtained heating cold water coming from the external environment and from different sections of the plant (H_2O from the anodic exhausts of the SOFC stored during those periods in which the chemical looping is not able to operate, H_2O from the dehydration of the syngas sent to the DME synthesis reactor, H_2O from the dehydration of the products of the DME reactor) sent in counterflow to hot streams of the system that have to be cooled (syngas sent to the SOFC prior the storage, syngas sent to the DME synthesis reactor, products of the DME reactor, cathodic exhausts of the SOFC, products of the biomethane reforming reactor). This steam is partly used to heat different streams of the system and partly can be considered as an output of the plant.

The fuels of the entire plant are:

- 1) solar energy. It is used to make the reduction reaction of the CL and the reforming reaction in the reforming unit take place, they are endothermic reactions, so high-temperature heat is required;
- 2) biomethane. It is necessary to introduce methane in the reduction reactor of the CL as a reduction agent, this lowers the reduction temperature of the cerium oxide (CeO_2) making this reaction suitable to be fed by concentrated solar energy (partial oxidation of methane is exothermic, so it lowers the amount of solar energy required to feed the reduction reactor). Another stream of biomethane has to be sent in the reforming reactor, where the CO_2 exhausts of the distillation unit of the DME and a portion of CO_2 from the exhausts of the SOFC (stored and not sent to the oxidation reactor of the CL) are made react with the biomethane itself to obtain syngas (CCU is executed). This syngas is partly recirculated to the DME synthesis reactor and partly sent to a syngas duct;
- 3) cerium oxide (CeO_2). This fuel has to be inserted in the reduction receiver-reactor of the CL during the first cycle and then it is recycled as the chemical loop takes place. Actually, in the plant, a refill of this oxide at each cycle is also forecasted to cover the possible losses of this material in the different components of the plant and, in particular, in the cyclones, which do not have a unitary efficiency;

- 4) air. In the cathode of the SOFC, the air is necessary to make the oxidation of CO and H₂ take place;
- 5) additional water for steam production.

The core of the plant is the chemical looping, in which the fuel for the other sections of the system is generated. As written before, the redox-couple chosen for the CL is CeO₂/Ce₂O₃ and the reduction of CeO₂ takes place simultaneously with biomethane partial oxidation to exploit the large advantages of this kind of cycle than the other ones ([Chapter 3](#)). It is important to highlight that this reaction only occurs during the periods of the day/year in which a sufficient amount of solar irradiation irradiates the CSP system in which it is considered to be installed the receiver-reactor that hosts the reduction reaction of the chemical looping. The oxidation reaction of the CL occurs in a non-solar reactor and it is fed through the anodic exhausts of the SOFC, which are mainly composed of H₂O and CO₂. This scheme allows to execute the so-called CCU (Carbon Capture and Utilization). The Carbon Capture takes place through the separation of the anodic exhausts in the two different streams (water and carbon dioxide) in a flash unit at around 15°C and 1 bar. Then, proper amounts of water and carbon dioxide are sent to the oxidation reactor of the CL. As a result, beyond being a polygeneration plant with optimized operating conditions and different outputs, this kind of system is also characterized by an optimization in the materials and streams used. These characteristics, coupled with the use of renewable energy sources (the sun and biomethane), make the plant sustainable, green and ideally emission-free.

6.1.1. Modelling and simulation of the plant in Aspen Plus

The modelling and the simulation of a plant using appropriate informatic tools is fundamental during the plant design. These tools solve safely and efficiently real-world problems through the mathematical replication and prediction of the behaviour of the analysed system. In general, the model is inserted in a simulation tool that is based on the application of energy and mass balance equations. Giving to the program certain input values (ex. molar flow rate of the fuel, maximum operating temperature, desired electric power output...), it returns an accurate map of the operating conditions of each component and stream of the system. Valuable solutions are provided by giving insights to simple or complex systems and, through these results, it is easy to understand if the plant operates properly or not, what are the weak components and where an optimization of the system is necessary. In the present study, Aspen Plus®, made by AspenTech, is used as a simulation tool. It is a market-leading process modelling tool for conceptual design, optimization and performance monitoring of an engineering process, it is widely used in the industrial sector for chemical, petrochemical and oil refining process analysis or in the academic field. There are both built-in equipment models (like compressors, turbines, reactors or exchangers) and FORTRAN subroutines which can be used to include further information in a certain block or create new models from the beginning. This simulation tool also uses mass and energy equations balance, reaction kinetics and reaction equilibrium combined with reliable thermodynamics databases and realistic operating conditions, so the plant operation can be reliably simulated. In the present study, two different schemes of the plant are analysed considering its two different ways to operate depending on the presence or not of solar energy and, consequently, on the activity or not of the chemical looping. In both the plant schemes, the polygeneration plant is modelled mainly using built-in components and the entire modelling is realized with the assumption of chemical equilibrium except the DME reactor, for which a kinetic approach is used. As a result, the characteristic components of the plant are:

- compressors, turbines, valves, mixers, splitters, heaters, coolers, heat recovery steam generators, cyclones and flash units;
- RGIBBS reactor blocks for the reduction and the oxidation reactors of the chemical looping, for the anode of the SOFC, for the post-combustion unit and for the biomethane reforming reactor;
- a separator for the cathode of the SOFC;

- RADFRAC columns for the DME distillation columns;
- an RPLUG reactor coupled with the Langmuir-Hinshelwood Hougen-Watson (LHHW) kinetic model to simulate the catalytic behaviour in the DME synthesis reactor. Soave-Redlich-Kwong (SRK) equation of state (EOS) is used for the thermodynamic properties of the DME reactor because, according to Graaf et al. [54], the chemical equilibrium of the methanol reaction and of the water gas shift (WGS) reaction can be well described at high-pressure by using the SRK-EOS. This model is, generally, applied to binary components [55].

The material streams used in the model are both conventional (H₂O, CO₂, H₂, CO, CH₄, N₂, O₂, CH₃OH, CH₃OCH₃) and solid streams (oxygen carriers of the chemical looping, CeO₂ and Ce₂O₃); for this latter type of streams, the Barin equation is used [56]. In addition, the Peng-Robinson-Boston-Mathias (PR-BM) property method is used for those components acting on conventional streams. This approach is recommended for hydrocarbon processing applications such as gas processing, refinery and petrochemical processes [57] and it is based on the Peng-Robinson cubic equation of state combined with the Boston-Mathias alpha function for all the thermodynamic properties [58]. In the plant simulation also calculator blocks are used to execute calculations with variables of the simulation. In each calculator block, it is necessary to define:

- input variables. They are taken from the flowsheet and used in the calculator block;
- export variables. They are calculated in the calculator block and exported to the flowsheet.

In the following *Table 5* the main assumptions and hypothesis used in the process simulation are listed.

Biomethane		95% CH₄, 5% CO₂
Oxidation and reduction reactors		Model: RGIBBS, no heat losses
Compressors, pumps and turbines		$\eta_{is,comp} = 0.9$ $\eta_{mech,comp} = 0.98$ $\eta_{is,tur} = 0.9$ $\eta_{mech,tur} = 0.98$ $\eta_{is,pump} = 0.9$ $\eta_{driver,pump} = 0.9$
SOFC		Model: RGibbs for the SOFC anode, Separator for the SOFC cathode
Methane reforming		Model: RGibbs, no heat losses
Oxygen carrier		CeO ₂ , Ce ₂ O ₃ , temperature drop of 20°C from OXY-CL to RED-CL
DME reactor		Model: RPLUG multi-tube reactor, Operation T=250°C P=50 bar
Distillation unit		Model: RADFRAC, Reboiler type: Kettle
DIST-CO2	DIST-DME	DIST-MET
P = 10 bar	P = 9 bar	P = 2 bar

Table 5: Main assumptions and hypothesis used in the process simulation

6.1.2. Plant operating components in a high irradiance and clear sky day

6.1.2.1. Chemical looping

The chemical looping is the prime mover of the analysed polygeneration plant. In this study, the redox couple CeO₂/Ce₂O₃ with the addition of biomethane as a reduction agent is chosen for its benefits compared to the other cycles. The chemical looping consists of two steps:

- 1) reduction reaction. This step is endothermic, so it necessitates of heat to be executed. It occurs in the receiver-reactor of the chosen CSP system, that, as previously written, is considered to be characterized by the same seasonal daily average temperature curves of the receiver installed on the roof of the Energy Center. Heat is given by concentrated solar energy,

which is the main fuel of the overall plant, but it is intermittent and available only in certain periods of the year and of the day, as it can be seen from the daily seasonal evolution of the receiver-reactor temperature in *Figure 53*. The intermittence of this fuel makes the chemical looping able to operate only for around 1833 hours and a half per year;

- 2) oxidation reaction. This reaction is exothermic, so heat is released towards the external environment and it occurs simultaneously with the reduction reaction in a non-solar reactor.

Both the reduction and the oxidation reactions work at the same operating conditions:

- temperature = 900°C;
- pressure = 1.2 bar (to avoid that pressure drops in the components downstream produce the operation at a pressure under the atmospheric one).

The isothermal and isobaric operating conditions of the CL increase the efficiency of the process reducing both heat losses and expenditures for the pressurization of the reactors and the heating of the CeO₂ entering in the reduction reactor. However, this kind of operation is possible only with the addition of a proper quantity of CH₄ in the reduction of the CL. In particular, a CH₄/CeO₂ molar ratio equal to 0.76 is set to obtain:

- the complete reduction of the oxygen carrier to Ce₂O₃ at the specified operating conditions;
- an H₂/CO molar ratio of the produced syngas in the reduction reaction equal to around 2. This molar ratio between the hydrogen and the carbon monoxide contents in the syngas makes it adapt to feed a SOFC because H₂ is a better FC fuel compared to CO. H₂ is characterized by a higher exchange current ($i_{0,CO} \approx \frac{1}{8} \cdot i_{0,H_2}$), so the activation overvoltage of the FC is lower when it is fed with a higher amount of H₂ than CO, and H₂ also diffuses quicker in the anode than CO (the effective diffusion coefficient of H₂ is higher than CO), so the diffusion overvoltage is lowered.

Concerning the oxidation reaction, it occurs with the Ce₂O₃ (previously reduced through the solar thermal reduction) and a mixture of H₂O and CO₂ (coming from the anodic exhausts of the SOFC, CCU is applied in the plant to reduce greenhouse emissions and make the system green and sustainable).

The H₂O/CO₂ molar ratio is properly defined to obtain:

- the complete re-oxidation of Ce₂O₃ to CeO₂;
- an H₂/CO molar ratio of the produced syngas in the oxidation reactor around 1, ideal for the successive DME production in the DME reactor.

To meet these requirements, a molar ratio H₂O/CO₂ ≈ 1.13 is chosen. As written before, the reduction reaction is fed with biomethane. This biomethane is produced through the pressure swing adsorption (PSA) mechanism applied to biogas obtained from the organic fraction of the municipal solid waste (OFMSW). For the sake of simplicity, in the analysed plant, it is assumed that all the necessary treatments (including sulphur removal) for the biomethane production take place upstream and the composition of the produced biomethane is: 95% CH₄ and 5% CO₂ [59], [60].

6.1.2.1.1. Simulation of the chemical looping in Aspen Plus

In Aspen Plus, the above described chemical looping is simulated as shown in *Figure 54*.

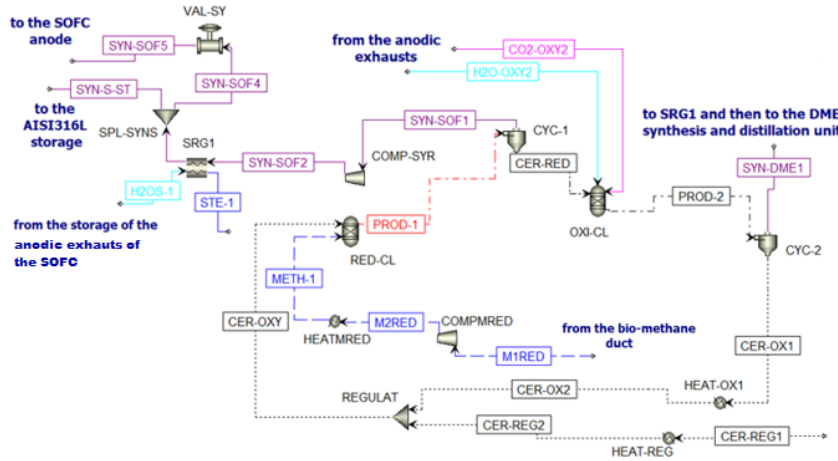


Figure 54: Chemical looping in Aspen Plus

The first component is a Gibbs reactor (RGibbs), used to simulate the reduction reaction (RED-CL), and its operating conditions are set at 1.2 bar and 900°C. The inlet streams are constituted by CeO₂ and biomethane at 900°C and 1 bar. The ceria stream is a solid material stream, so a particle size distribution is implemented to define the size of the particles themselves [61]:

Particle diameter	Frequency of particles (%)
95 nm–264 nm	11.4
264 nm–384 nm	17
384 nm–616 nm	35
616 nm–953 nm	23
953 nm–1.61 μm	9
1.61 μm–2.4 μm	3
2.4 μm–4.01 μm	1
4.01 μm–6.71 μm	0.23
6.71 μm–9.96 μm	0.37

Table 6: Particle size distribution of the ceria as a function of the frequency obtained from ELPI measurements [61]

The biomethane stream is assumed with a composition of 95% CH₄ and 5% CO₂ and its molar flow rate is evaluated in a calculation block (C-RED-CL) in which the molar ratio $\frac{\text{biomethane}}{\text{ceria}}$ is set at 0.8. In the same calculator, a refill of ceria is implemented to maintain a constant molar flow rate of the ceria stream feeding the reduction reactor, equal to $0.59 \frac{\text{kmol}}{\text{s}}$. In [Table 7](#), the streams entering the reduction reactor and their properties are shown.

FLOW	PRESSURE [bar]	TEMPERATURE [°C]	MOLE FLOWS [kmol/s]	MOLAR FRACTIONS		
				CeO ₂	CH ₄	CO ₂
CER-OXY	1	900	0.590	1	0	0
METH-1	1	900	0.472	0	0.95	0.05

Table 7: Inlet streams of the reduction reactor

At the outlet of the reduction reactor, a stream mainly constituted by Ce_2O_3 , H_2 and CO is obtained. This stream (PROD-1) is separated in the cyclone CYC-1 to obtain the solid and the gaseous fractions in two different streams. The first is the Ce_2O_3 stream, sent to the oxidation reaction, while the second is the syngas stream, as shown in [Table 8](#).

FLOW	PRESSURE [bar]	TEMPERATURE [°C]	MOLE FLOWS [kmol/s]	MOLAR FRACTIONS					
				Ce_2O_3	CH_4	H_2O	CO_2	CO	H_2
CER-RED	1.1985	900	0.2655	1	0	0	0	0	0
SYN-SOF1	1.1985	900	1.1372	0.0259	0.1148	0.0005	0.0002	0.3001	0.5585

Table 8: Outlet streams of the cyclone after reduction reactor

The syngas (SYN-SOF1) is compressed (in COMP-SYR) and cooled in the heat recovery steam generator (SRG1) to be stored at $800^\circ C$ and 10 bar in an AISI316L tank. This tank cannot be simulated in Aspen Plus, so in [Figure 54](#) downstream the compressor and the SRG1, there is a splitter (SPL-SYNS), which regulates the flow entering the anode of the SOFC (SYN-SOF4), and a valve (VAL-SY), that reduces the pressure of the portion of syngas sent to the SOFC at 5 bar (SYN-SOF5). As a result, as specified before, to make the SOFC operate during the whole year, regardless the intermittence of solar energy, only a portion of the syngas produced in the reduction reaction during its correct operation flows through the valve to the anode of the fuel cell itself (SYN-SOF4) while the remaining syngas is stored in the tank (SYN-S-ST). The portion of the syngas entering the SOFC is evaluated as follows. The difference between the operating period (during the year) of both the SOFC and the chemical looping is considered:

- 1) operating minutes of the chemical looping in one year = 110010 min/year;
- 2) operating minutes of the SOFC in one year = 525600 min/year.

Therefore, the SYN-SOF1 mole flow is spread over the whole year of operation of the SOFC and the stream SYN-SOF4 is obtained:

$$\dot{n}_{SYN-SOF4} = \dot{n}_{SYN-SOF1} \left[\frac{kmol}{min} \right] \cdot \frac{\text{operating minutes of the CL}}{\text{operating minutes of the SOFC}} : 60 \frac{s}{min} = 0.2381 \frac{kmol}{s} \quad (73)$$

Going back to the chemical looping simulation unit, the oxidation reaction is simulated through another Gibbs reactor (OXY-CL) and it is fed by the reduced cerium oxide (CER-RED) and a mixture of H_2O and CO_2 ($H_2O/CO_2 \approx 1.13$) coming from the anodic exhausts of the SOFC, as shown in [Figure 54](#). The H_2O produced by the SOFC simultaneously with the operation of the CL is sufficient to feed the oxidation reactor, while the amount of produced CO_2 is too low, so it has to be integrated with additional carbon dioxide coming from the storage of the CO_2 after its heating and expansion (CO2-INT5), this storage is fulfilled by the anodic exhausts during the periods in which the CL is not able to operate. The properties of the streams entering the oxidation reactor are listed in [Table 9](#).

FLOW	PRESSURE [bar]	TEMPERATURE [°C]	MOLE FLOWS [kmol/s]	MOLAR FRACTIONS						
				Ce_2O_3	CeO_2	CH_4	H_2O	CO_2	CO	H_2
CER-RED	1.1985	900	0.2655	1	0	0	0	0	0	0
CO2-OXY2	1	900	0.1963	0	0	0	0.0137	0.7861	0.0724	0.1278
H2O-OXY2	1	900	0.1838	0	0.0672	0	0.9328	0	0	0

Table 9: Inlet streams in the oxidation reactor

The product of the oxidation reactor (PROD-2) is mainly constituted by CeO_2 , H_2 and CO and it is sent to a cyclone CYC-2 to separate the solid fraction (CeO_2), sent to the reduction reactor to close the cycle (CER-OX1) after a re-integration of the lost ceria for the not unitary efficiency of the cyclones (CER-REG2) in a regulator (REGULAT), and the gaseous fraction (SYN-DME1), sent to the DME production section of the plant.

FLOW	PRESSURE [bar]	TEMPERATURE [°C]	MOLE FLOWS [kmol/s]	MOLAR FRACTIONS					
				CeO_2	CH_4	H_2O	CO_2	CO	H_2
CER-OX1	1.1941	900	0.4890	1	0	0	0	0	0
SYN-DME1	1.1941	900	0.4218	0.1288	0.0003	0.0880	0.0615	0.3377	0.3838

Table 10: Outlet streams of the cyclone after the oxidation reactor

FLOW	PRESSURE [bar]	TEMPERATURE [°C]	MOLE FLOWS [kmol/s]	MOLAR FRACTIONS					
				CeO_2	CH_4	H_2O	CO_2	CO	H_2
CER-REG2	1	900	0.1010	1	0	0	0	0	0

Table 11: Re-integration of ceria at each cycle

The implementation of the cyclones is made considering the following data [62]:

Calculation method	Leith-Licht
Type	Stairmand-HE
Separation efficiency	0.9
Maximum pressure drop	0.015 bar
Maximum number of cyclones	100

Table 12: Cyclones' characteristics [62]

Therefore, the simulation of the chemical looping operation in Aspen Plus is executed considering to reach the thermodynamic equilibrium of the reactions because Gibbs reactors are chosen to image both the reduction and the oxidation reactors of the CL. In this way, the yields of the reactions are overestimated concerning the real reactions yields, for which also the kinetics of the reactions should be considered. Thermodynamic fixes what is possible to happen, for example, the chemical composition at equilibrium, but equilibrium needs time to be obtained. In most of the cases, it is not possible to reach the composition of the products at equilibrium. Kinetics is mainly affected by:

- 1) temperature. The higher the temperature, the higher the kinetic energy of the molecules and the higher the probability to have collisions between molecules at sufficient energy;
- 2) concentration of the reactants. A higher concentration means a higher probability of collisions;
- 3) presence of a catalyst. A catalyst is a material which participates to the reaction without being modified by it and it helps the reaction to occur fastly.

6.1.2.2. Storage system

In the analysed plant, a storage of the syngas produced in the reduction reactor of the chemical looping has to be considered. This storage system is fundamental for the correct functioning of the SOFC, which has a very high sensibility to load variations and transients due to its high operating temperature. The idea is to oversize the chemical loop (and, accordingly, the amount of syngas produced in the reduction reaction) compared to the SOFC so that it is possible to store the surplus of syngas obtained from the reduction reaction of the CL concerning the molar flow rate of syngas which

is necessary to feed the SOFC. Through this expedient, it is possible to make the FC work at baseload with a constant molar flow rate of fuel, solving the problem of intermittence of the solar energy and, consequently, of the production of syngas in the CL. As a result, the storage system is mandatory to couple the discontinuous solar energy source with the base-load operating Solid Oxide Fuel Cell. The material chosen to realize the tank for the storage of the syngas can be AISI316L (ss316L), which stands for “stainless steel, type 316L” [63]. To improve the properties of stainless steel, alloys are often added to the ss itself. The ss316 (stainless steel type 316) is an austenitic chromium-nickel stainless steel that contains between 2 and 3% molybdenum. The molybdenum content increases corrosion resistance, improves resistance to pitting in chloride ion solutions, and increases strength at high temperatures. There are different types of ss316, the most common are the L, F, N and H ss316; each type has certain properties and is used for a specific aim. The “L” designation indicates a lower amount of carbon than ss316; the maximum carbon content in type 316 is 0.08%, while the carbon content is controlled to a maximum of 0.03% in 316L, this minimizes the problem of carbide precipitation during the welding process. Both ss316 and ss316L have the following properties:

- high corrosion resistance;
- strength at elevated temperatures;
- similar cost;
- durability;
- high-stress resistance.

However, 316L is chosen in this present work because the purpose is to realize a storage system at high temperature and pressure and ss316L is:

- less susceptible to weld decay than ss316;
- high-temperature resistant.

According to the physical and mechanical properties of ss316L, the storage of the syngas is considered at the operating conditions of 10 bar and 800°C (this temperature is also a good compromise for the operation of the SOFC, which is at 850°C). The stored syngas is then expanded to 5 bar and used to feed the SOFC.

6.1.2.2.1. Simulation of the storage system in Aspen Plus

In Aspen Plus, there is not a model for the simulation of the storage system. As a result, the analysed plant in Aspen Plus is planned to be possibly coupled with a storage system thanks to the presence of:

- 1) a compressor (COMP-SYR) that pressurizes to 10 bar (storage pressure) the syngas exiting from the reduction reactor of the CL;
- 2) a heat recovery steam generator (SRG1) that cools the syngas to 800°C (storage temperature) producing steam;
- 3) a valve (VAL-SY) which makes the syngas expand from the storage pressure (10 bar) to the SOFC pressure (5 bar) prior the feeding of the anode of the SOFC maintaining more or less not varied the temperature of the stream.

In the practical realization of the plant, the storage unit should be placed between the heat recovery steam generator and the valve. In the scheme realized in Aspen, this component is not present, but there is a splitter which divides the compressed and cooled syngas obtained in the reduction reactor into two streams: SYN-SOF4 and SYN-S-ST. The first stream is sent to the anode of the SOFC, while the second one should be stored and used when the CL does not operate for the unavailability of enough solar energy irradiating the receiver-reactor.

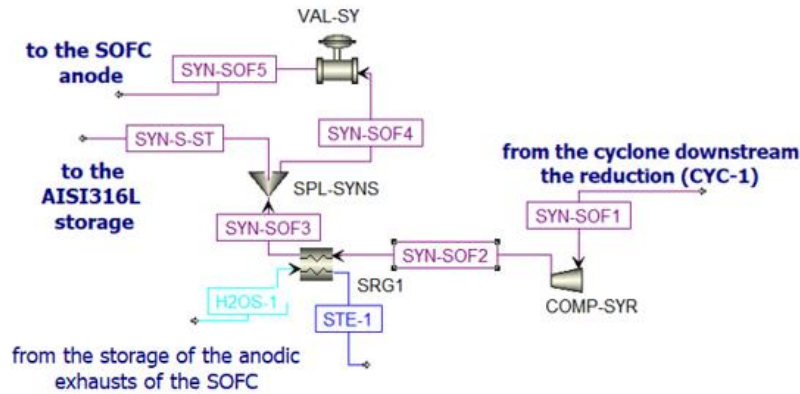


Figure 55: Storage system in Aspen Plus

6.1.2.3. Solid oxide fuel cell (secondary device)

As written in [Chapter 5.1](#), in the present plant, a SOFC for the production of electricity is chosen to take into account its advantages compared to a thermal machine and its wide fuel flexibility. However, the Solid Oxide Fuel Cell is a high-temperature fuel cell, this means that it has very slow startups and shutdowns. As a result, to have a high efficiency of this system, it is important to make it work at baseload conditions: the SOFC should operate at constant operating conditions continuously throughout the year. This characteristic of the SOFC is totally in contrast to the intermittence of solar energy availability, consequently, there cannot be a direct connection between the fuel cell and the chemical looping, whose functioning is strictly dependent on the value of the solar irradiance that irradiates the receiver-reactor of the CSP system in which it is imagined to make reduction reaction of the CL itself take place. To solve this problem, an under-sizing of the SOFC compared to the reduction reactor is made. During its correct functioning, the reduction reaction of the CL produces an amount of syngas which is much higher than the syngas stream necessary to feed the anode of the SOFC; the surplus between the produced syngas in the receiver-reactor and the SOFC fuel stream is stored and used during those periods in which the CL is not in operation. The yearly periods of operation of both the SOFC and the CL (equal to the all 365 days of the year and around 77 days per year respectively) are evaluated in the introduction of this [Chapter 6](#).

6.1.2.3.1. Simulation of the SOFC in Aspen Plus

The Solid Oxide Fuel Cell is simulated in Aspen Plus both when the CL is in ON-state and OFF-state as shown in [Figure 56](#) and [Figure 57](#).

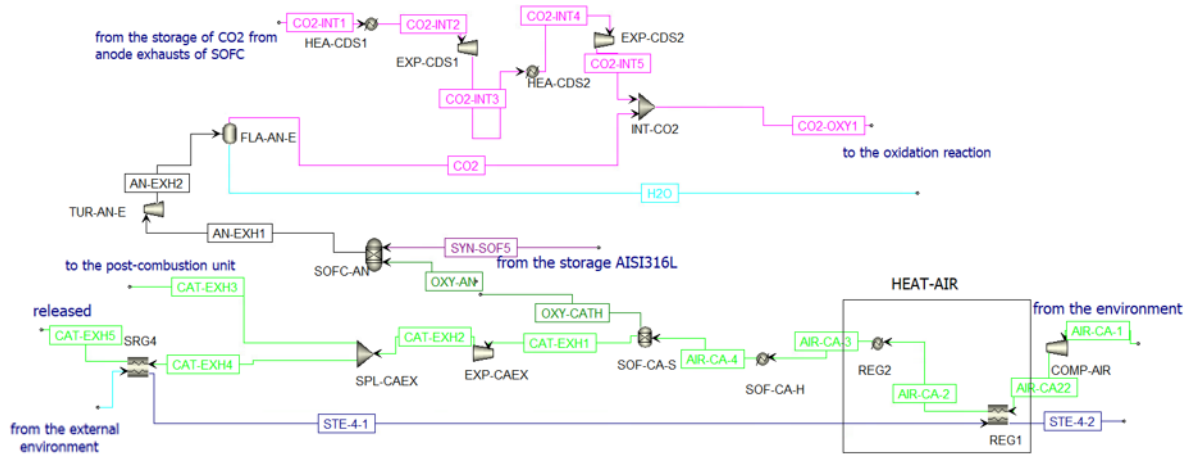


Figure 56: SOFC scheme in Aspen Plus when the CL is in ON-STATE

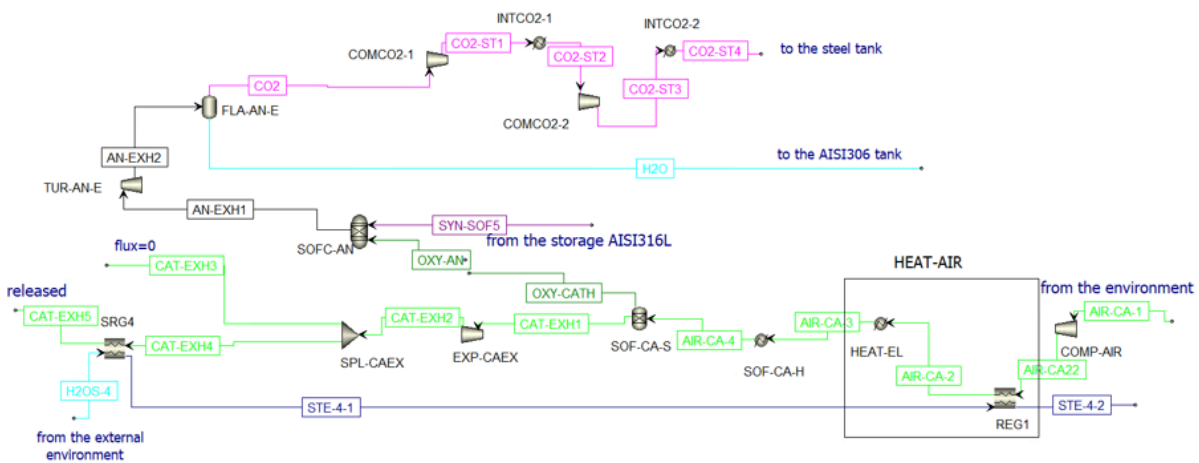


Figure 57: SOFC scheme in Aspen Plus when the CL is in OFF-STATE

Thus, the components of the SOFC are represented in this way:

- 1) the anode is schematized through a Gibbs Reactor (RGibbs), SOFC-AN;
- 2) the cathode is schematized through a separator (Sep) and a heat exchanger (Heater), SOF-CA-S and SOF-CA-H.

The operating conditions of the SOFC are set at:

- 1) temperature = 850°C. It is a high-temperature FC and this T is chosen also taking into account the T at which the syngas should be stored in the tank (defined by the thermal limits of the ss316l) to avoid the expenditure of further thermal energy to heat the syngas before the feeding of the anode;
- 2) pressure = 5 bar. The FC is made to operate under pressure to improve its performance, in fact, the higher the P and the higher the Nernstian voltage, so the higher the produced electric power. However, too high pressures cannot be chosen for the limit in the mechanical strength of the materials constituting the cell itself, so the chosen pressure is a compromise between the cell's performance and mechanical stability.

As specified in Chapter 6.1.2.1.1, the syngas mole flow entering the anode of the SOFC to guarantee its yearly continuous operation at constant conditions according to the availability of syngas guaranteed by the reduction reaction of the CL is: $\dot{n}_{\text{SYN-SOF5}} = 0.2381 \frac{\text{kmol}}{\text{s}}$. Another inlet stream in the anode is given by the oxygen ions (OXY-AN), the value of the molar flow rate of this stream is evaluated in the Aspen Plus section "Flowsheeting options-Calculator". In this Calculator block (C-IN-SO), it is

imported the molar flow rate of the stream of syngas entering the anode (stream SYN-SOF5, $\dot{n}_{\text{SYN-SOF5}}$) and it is used to calculate the total current produced by the cell (C_{tot}) according to the Faraday law:

$$C_{\text{tot}} = \dot{n}_{\text{SYN-SOF5}} \cdot Z_{\text{fuel}} \cdot \text{FU} \cdot F \cdot \% \text{H}_2/\text{CO} \quad (74)$$

with:

- 1) $\dot{n}_{\text{SYN-SOF5}}$ and $\% \text{H}_2/\text{CO}$ defined by the properties of the stream SYN-SOF5, exiting from the reduction reactor of the chemical looping and equal to $0.2381 \frac{\text{kmol}}{\text{s}}$ and 0.8 respectively;
- 2) $Z_{\text{fuel}} = 4$;
- 3) $\text{FU} = \text{fuel utilization} = 0.8$;
- 4) $F = \text{Faraday number} = 96485 \frac{\text{C}}{\text{mol}}$.

In the same Calculator block (C-IN-SO), knowing C_{tot} , the stoichiometric molar flow rate of the oxygen O_2 (OXY-AN), needed to generate in the cathode an amount of ions O^{2-} which is sufficient to oxidize the fuel, is evaluated according to the Faraday law:

$$\dot{n}_{\text{OXY-AN}} = \frac{C_{\text{tot}}}{Z_{\text{O}_2} \cdot F} \quad (75)$$

with: $Z_{\text{O}_2} = 4$, so $\dot{n}_{\text{OXY-AN}} = 148.42 \frac{\text{mol}}{\text{s}}$.

In another Calculator block (C-OXY-SO), the previously calculated molar flow rate of oxygen ($\dot{n}_{\text{OXY-AN}}$) is set equal to the molar flow rate of the stream OXY-CATH exiting from the component SOF-CA-S (separator constituting the cathode of the FC) to simulate the conduction of the ions from the anode to the cathode in the electrolytic layer of the SOFC. The cathode is supplied by air which is made enter the plant at ambient conditions ($T_{\text{AIR-CA-1}} = 15^\circ\text{C}$ and $P_{\text{AIR-CA-1}} = 1 \text{ bar}$), then it is compressed to 5 bar (in COMP-AIR) and heated to 600°C (in HEAT-AIR) to let this air (AIR-CA-3) enter in the hot FC without producing a thermal shock of the cell itself. It is important to highlight that the molar flow rate of the air stream is calculated iteratively in the Aspen Plus section "Flowsheeting options-Design Specs", in a block named DS-AIR. These iterations aim at finding out the value of the molar flow rate of air which can be heated from 600°C to 850°C (in SOF-CA-H) absorbing the entire heat rejected by the SOFC, equal to $\phi_{\text{total}} = \phi_{\text{reaction}} + \phi_{\text{irrev}}$ = heat duty of the Gibbs reactor representing the anode of the SOFC + electric power produced by the SOFC (W_{el}):

$$\dot{n}_{\text{AIR-CA-3}} = 3.0441 \frac{\text{kmol}}{\text{s}} \quad (76)$$

Once the air stream (AIR-CA-3) enters in the cathode, it firstly encounters a heater (SOF-CA-H) that simulates the heating of the air that removes the thermal energy released by the FC during its operation and then it encounters a separator (SOF-CA-S) in which the streams OXY-CATH (that simulates the oxygen ions which are conducted from the cathode to the anode) and CATH-EXH1 are produced. The latter represents the cathodic exhausts, they are at high pressure (5 bar) and at a high-temperature T (850°C), so they are expanded to 1 bar producing electric power and then they are split into two streams (this splitting takes place only during the operation of the DME synthesis and distillation unit, which is simultaneous with the operation of the CL. When these units do not work, the whole stream of air is directly cooled and rejected to the external environment). One stream (CAT-EXH4) feeds an HRSG (Heat Recovery Steam Generator, SRG4) to produce steam and then it is released to the external environment (CAT-EXH5), the other stream (CAT-EXH3) feeds the post-combustion unit. In the post-combustion unit, the $\text{CO-CO}_2\text{-H}_2$ rich stream (H_2COCO_2), obtained from the vapour-gas separation of the product of the DME synthesis reactor (PROD-3) after being heated ($\text{H}_2\text{COCO}_2\text{H}$) and expanded ($\text{H}_2\text{COCO}_2\text{E}$), is combusted to produce a $\text{H}_2\text{O-CO}_2$ rich stream ($\text{H}_2\text{OCO}_2\text{-1}$).

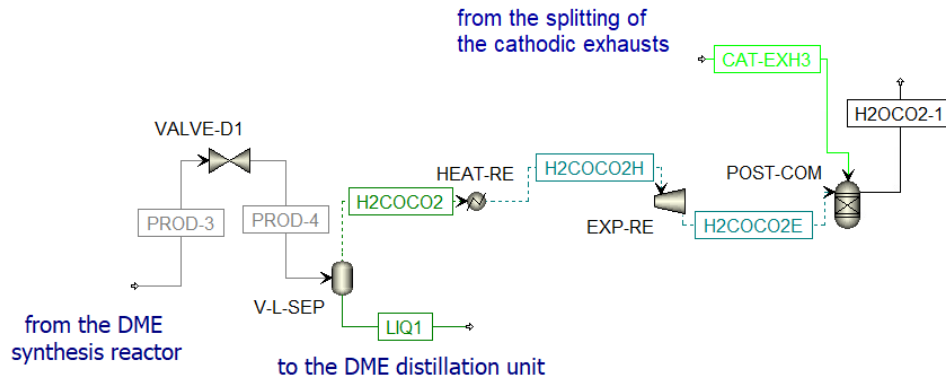


Figure 58: Post-combustion unit in Aspen Plus

The anodic exhausts (AN-EXH1) are mainly constituted of H₂O and CO₂. They are firstly expanded in a turbine (TUR-AN-E) to produce electric power and bring them to 1 bar, so they are sent to a flash separator (FLA-AN-E) with operating conditions of 15°C and 1 bar to obtain two different streams of CO₂ and H₂O. During the correct operation of the chemical looping:

- the H₂O stream is heated and directly sent to the oxidation reactor;
- the CO₂ stream is firstly integrated with additional CO₂, coming from the CO₂ storage (fulfilled by the anodic exhausts when the CL does not operate) after being heated and expanded, and then it is sent to the oxidation reactor.

When the chemical looping does not operate, these streams are stored in two different tanks:

- the H₂O stream is directly stored at 1 bar and 15°C in an AISI 306 tank;
- the CO₂ stream is compressed and cooled to 25 bar and 80°C and stored in a steel tank.

With this kind of operating conditions and scheme and considering a cell voltage equal to around 0.8 V, the Solid Oxide Fuel Cell can produce continuously throughout the year an electric power equal to:

$$W_{el} = V_{cell} \cdot C_{tot} = 45.82 \text{ MW} \quad (77)$$

However, in the practical realization of the plant, a SOFC size of 45.82 MW does not exist; the connection of different stacks of fuel cells should be realized. Considering the Bloom Energy Servers [64], characterized by an electric power production of 200 kW each, the number of necessary cells is:

$$N_{cells} = \frac{W_{el, present plant}}{W_{el, Energy Servers}} = \frac{45.82 \text{ MW}}{0.20 \text{ MW}} \sim 230 \text{ stacks} \quad (78)$$

6.1.2.4. DME production (secondary device)

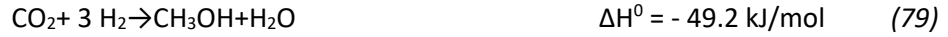
6.1.2.4.1. DME synthesis

In this section of the plant, the syngas obtained from the oxidation reactor of the CL is used to produce DME, a liquid fuel, in a catalytic reactor, so this unit only operates when the chemical looping properly produces syngas and, consequently, when a sufficiently high irradiance is present (for around 77 days per year). DME synthesis can take place through two different pathways:

- 1) two steps pathway. Methanol and DME are produced in two different reactors, two independent catalysts, with two different functions, are required (a methanol forming component and a dehydration component);
- 2) single-step pathway. A dual catalyst should be used.

The two steps pathway has as main disadvantage the limit of the conversion of syngas to methanol by equilibrium and thermodynamic constraints, while, in the co-production of methanol and DME, this

limit is alleviated, thus a significant increase of the total methanol yield [65]. In the present study, the single-step pathway is chosen because it is thermodynamically and economically preferable than the two steps process. The process can be described through three main reactions: the syngas conversion to methanol (reaction (79)), water gas shift (reaction (80)) and methanol dehydration to DME (reaction (81)):



The global reaction is:



As a result, the overall reaction is exothermic and generates two molecules of products from six molecules of reactants; hence, according to the Le Châtelier principle [66], it is favoured at high pressure and a low temperature. In addition, a molar fraction H_2/CO equal to one of the feeding syngas is preferable for a high yield of the reaction of DME production. The catalytic reactor chosen in this study is a multi-tube fixed bed reactor which is kept at a constant temperature of 250°C by a water jacket cooler. The operating conditions of the reactor itself are obtained from the study of Pozzo et al. [67]:

- 1) pressure=50 bar;
- 2) temperature=250°C.

The bi-functional catalyst $\text{Cu}/\text{ZnO}/\text{Al}_2\text{O}_3: \gamma\text{-Al}_2\text{O}_3$ is selected considering a loading ratio of 1:2 from literature. $\text{Cu}/\text{ZnO}/\text{Al}_2\text{O}_3$ is necessary for the methanol synthesis, while $\gamma\text{-Al}_2\text{O}_3$ is the catalyst of the methanol dehydration.

6.1.2.4.2. Simulation of the DME synthesis reactor in Aspen Plus

The syngas produced in the oxidation reactor of the chemical looping (SYN-DME2) during its correct functioning, before being sent to the DME synthesis reactor, is:

- 1) cooled in the heat recovery steam generator (SRG2) producing steam;
- 2) separated from water (in FLA-SYDM) at 30°C and 1 bar;
- 3) integrated with additional syngas (SYN-RE3R) produced in the reforming reactor with a molar ratio $\text{H}_2/\text{CO} \sim 1$;
- 4) compressed to the operating pressure of the reactor (50 bar) through a two-stages intercooled compression. The final stream SYN-DME6 is at 50 bar and 250°C, so it feeds the DME reactor.

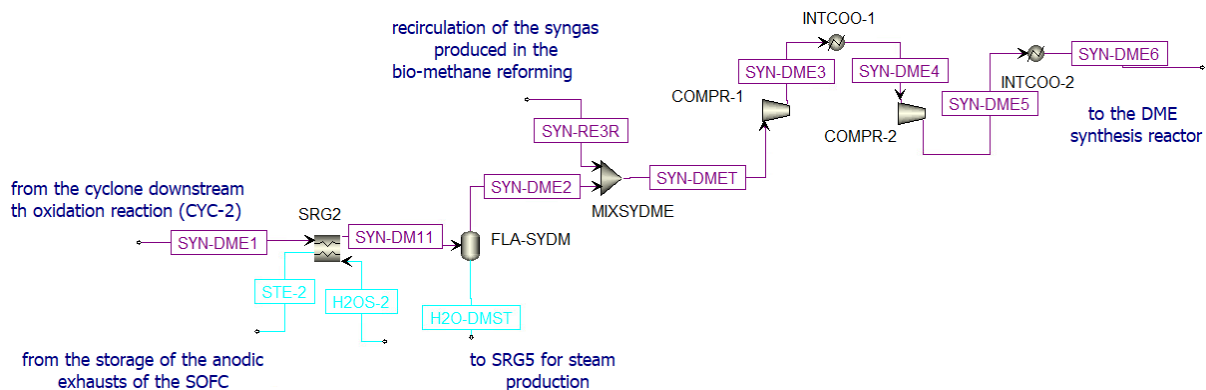


Figure 59: Pre-treatment of the syngas sent to the DME reactor in Aspen Plus

The properties of the resulting syngas stream (SYN-DME6) entering in the DME synthesis reactor are shown in *Table 13*:

FLOW	PRESSURE [bar]	TEMPERATURE [°C]	MOLE FLOWS [kmol/s]	MOLAR FRACTIONS					
				CH ₄	H ₂ O	CO ₂	CO	H ₂	N ₂
SYN-DME6	50	250	1.1783	0.0036	0.0413	0.0580	0.4560	0.4323	0.0087

Table 13: Syngas stream entering the DME reactor

The DME reactor is simulated in Aspen plus through a plug reactor (Rplug), constituted of 5500 tubes and solved with the SRK-EOS property method.

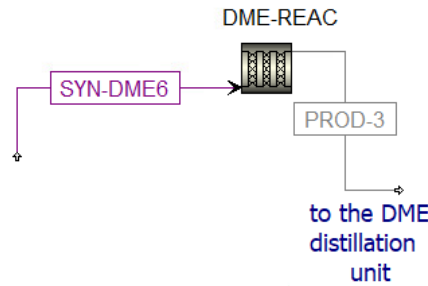


Figure 60: Simulation of the DME reactor in Aspen Plus

The parameters inserted in Aspen Plus for the DME reactor modelling are the following in *Table 14* [4]:

N° tubes	Diameter [m]	Bed voidage	density Cu/ZnO/Al ₂ O ₃ [kg/m ³]	density γ-Al ₂ O ₃ [kg/m ³]	ρ _{average} [kg/m ³]	Temperature [°C]	Pressure [bar]	Length [m]
5500	0.02	0.45	1200	1470	1380	250	50	15

Table 14: Parameters of the DME reactor

In addition, a Langmuir-Hinshelwood Hougen-Watson (LHHW) kinetic model is implemented taking into account the three simultaneous reactions defined above ((79), (80), (81)). The expressions of the rates for CO₂ hydrogenation, WGS and methanol dehydration are calculated according to equations (83), (84) and (85) [68], [69], [70]. These reaction rates are expressed in $\frac{kmol}{kg_{cat} \cdot s}$:

$$r_{CO_2,hydrogenation} = \frac{k_1 (p_{H_2} \cdot p_{CO_2}) \left[1 - \left(\frac{1}{k_{eq,1}} \right) \cdot \frac{p_{CH_3OH} \cdot p_{H_2O}}{p_{CO_2} \cdot p_{H_2}^3} \right]}{\left(1 + k_2 \cdot \frac{p_{H_2O}}{p_{H_2}} + \sqrt{k_3 \cdot p_{H_2}} + k_4 \cdot p_{H_2O} \right)^3} \quad (83)$$

$$r_{WGS} = \frac{k_5 \cdot p_{CO_2} \left[1 - \left(\frac{1}{k_{eq,2}} \right) \cdot \frac{p_{CO} \cdot p_{H_2O}}{p_{CO_2} \cdot p_{H_2}} \right]}{1 + k_2 \cdot \frac{p_{H_2O}}{p_{H_2}} + \sqrt{k_3 \cdot p_{H_2}} + k_4 \cdot p_{H_2O}} \quad (84)$$

$$r_{MeOH,dehydration} = \frac{k_6 K_{CH_3OH}^2 \left[C_{CH_3OH}^2 - C_{H_2O} \cdot \frac{C_{DME}}{K_{eq,3}} \right]}{\left(1 + 2 \sqrt{k_{CH_3OH} \cdot C_{CH_3OH}} + k_{H_2O} \cdot C_{H_2O} \right)^4} \quad (85)$$

with:

- p equal to the partial pressure of the gases in Pa;
- C equal to the concentration expressed in kmol/m³.

The equilibrium constants K_i and the constant rates k_i are listed in the following *Table 15* and taken from the literature [4]. These parameters refer to the Arrhenius equation (86):

$$k_i = (\text{Pre})_i \times \exp\left(\frac{B_i}{RT}\right) \quad (86)$$

in which B_i could represent the activation energy, the reaction enthalpy or a combination of the two.

	Pre	unit	B	unit
k_1	$1.07 \cdot 10^{-13}$	(kmol/(kg·s·Pa ²))	$3.6696 \cdot 10^7$	(J/kmol)
k_2	8.1416	-	0	(J/kmol)
$k_3^{0.5}$	-6.452	Pa ^{-0.5}	2068.44	(J/kmol)
k_4	-34.9513	Pa ⁻¹	14928.9	(J/kmol)
k_5	6	(kmol/(kg·s·Pa))	$9.4765 \cdot 10^7$	(J/kmol)
k_6	$1.486 \cdot 10^{11}$	(kmol/(kg·s))	$1.43666 \cdot 10^8$	(J/kmol)
$k_{\text{CH}_3\text{OH}}$	-15.05	m ³ /kmol	16974	(J/kmol)
$k_{\text{H}_2\text{O}}$	-2-4686	m ³ /kmol	5070	(J/kmol)

Table 15: Kinetic parameters used in DME synthesis

Other used expressions are [4]:

$$\log_{10}K_{\text{eq},1} = 7059.73 - \frac{24.3889}{T} \quad (87)$$

$$\log_{10}(1/K_{\text{eq},2}) = -4.67 + \frac{4773}{T} \quad (88)$$

$$\ln K_{\text{eq},3} = -1.7 + \frac{3220}{T} \quad (89)$$

The resulting stream obtained from the DME reactor (PROD-3) has the properties shown in *Table 16*:

FLOW	PRESSURE [bar]	TEMP [°C]	MOLE FLOWS [kmol/s]	MOLAR FRACTIONS							
				CH ₄	H ₂ O	CO ₂	CO	H ₂	N ₂	CH ₃ OH	DME
PROD-3	50	250	0.5830	0.0073	0.0153	0.4201	0.1082	0.1556	0.0177	0.0413	0.2346

Table 16: Stream PROD-3 exiting from the DME synthesis reactor

6.1.2.4.3. Distillation unit

The DME synthesized in the DME reactor (PROD-3) is characterized by a high amount of impurities, so a separation and a distillation are necessary to obtain pure DME. Prior to the distillation columns, there is a vapour-liquid separation unit at -45°C and 10 bar. The gaseous stream (H₂CO₂) exiting from this separator is mainly constituted of H₂, CO and undissolved CO₂ (uncondensable gases) and it is treated and sent to the biomethane reforming reactor. This reactor is also fed by a stream of CO₂

obtained from the first distillation column of the distillation unit (CO₂-D2) and a stream of CO₂ (CO₂-RS-3) obtained from the anodic exhausts of the SOFC, stored at 80°C and 25 bar during the period in which the chemical looping does not work and not further used in the oxidation reactor of the CL itself.

The mole flow of this latter stream is evaluated as follows:

- the molar flow rate of CO₂ produced by the SOFC during its operation is obtained after the separation of the anodic exhausts from water in a flash unit at 15°C and 1 bar: $\dot{n}_{\text{CO}_2, \text{SOFC}} = 5.4282 \frac{\text{kmol}}{\text{min}}$. During the operation of the CL, this mole flow is integrated with an additional amount of CO₂, $\dot{n}_{\text{CO}_2, \text{INT}} = 3.8300 \frac{\text{kmol}}{\text{min}}$, coming from the CO₂ storage, and sent to the oxidation reactor of the CL (the total mole flow of pure CO₂ to the oxidation reactor is $\dot{n}_{\text{CO}_2\text{-OXY}_2} = 9.2589 \frac{\text{kmol}}{\text{min}}$);
- since the chemical looping only operates for 110010 $\frac{\text{min}}{\text{year}}$, in one year, it can reuse, in the oxidation reactor, an amount of CO₂ equal to:

$$n_{\text{CO}_2, \text{OXY}_2} = \dot{n}_{\text{CO}_2\text{-OXY}_2} \cdot 110010 \frac{\text{min}}{\text{year}} = 1018568.03 \frac{\text{kmol}}{\text{year}} \quad (90)$$

- since the SOFC operates continuously during the year, the amount of pure CO₂ produced in one year is equal to:

$$n_{\text{CO}_2, \text{SOFC}} = \dot{n}_{\text{CO}_2, \text{SOFC}} \cdot 525600 \frac{\text{min}}{\text{year}} = 2853508.68 \frac{\text{kmol}}{\text{year}} \quad (91)$$

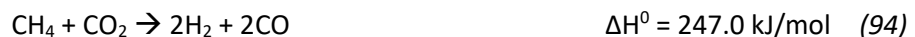
- the surplus of CO₂ produced in the SOFC compared to that one used in the oxidation reactor (ΔCO_2) has to be exploited in the reforming reactor:

$$\Delta\text{CO}_2 = n_{\text{CO}_2, \text{SOFC}} - n_{\text{CO}_2, \text{OXY}_2} = 1834940.65 \frac{\text{kmol}}{\text{year}} \quad (92)$$

Since the reforming reactor only works simultaneously with the chemical looping (for 110010 $\frac{\text{min}}{\text{year}}$), to exploit ΔCO_2 , a mole flow of CO₂ equal to $\dot{n}_{\text{CO}_2\text{-RS-1}}$ has to be sent to the reforming reactor itself:

$$\dot{n}_{\text{CO}_2\text{-RS-1}} = \frac{1834940.65 \frac{\text{kmol}}{\text{year}}}{110010 \frac{\text{min}}{\text{year}}} = 16.6798 \frac{\text{kmol}}{\text{min}} \quad (93)$$

It is important to notice that these calculations are executed considering only the presence of CO₂ in the evaluated streams, actually, these streams are not made of pure CO₂, they also have small amounts of other components that contribute to increase their mole flow value. Another stream entering the reforming reactor is biomethane (METH-2, 95% CH₄ and 5% CO₂) taken from the pipeline, pressurized and heated. The aim of the biomethane reforming reactor is to make reforming of biomethane take place according to the reaction (94):



This reaction is endothermic and from 2 moles of reactants, 4 moles of products are obtained. As a result, the methane reforming is favoured at low pressures and high temperatures; in the present study, it takes place at 800°C and 1 bar, so it can be fed by solar thermal energy. In this regard, it is imagined that this reforming reaction takes place in an additional receiver-reactor placed in the neighbourhood of the reactor in which the reduction reaction of the CL takes place. This additional receiver is identical to the first one, so the distribution of the temperatures is equal to [Figure 53](#) and, consequently, the reforming reactor works simultaneously with the CL unit. It is important to highlight that the introduction of the biomethane reforming reactor is mainly executed in the view of minimization of greenhouse emissions of the plant (which, thanks to this trick is emission-free). Consequently, this reactor makes it possible for the so-called Carbon-Capture and Utilization avoiding the re-introduction of CO₂ in the atmosphere and allowing the utilization of CO₂ in a useful way [71]. From this reaction (94), a syngas stream with a molar ratio H₂/CO equal to 1 is obtained, so it can be partially sent to a syngas duct and sold and partially recirculated to the DME synthesis reactor as this molar ratio between hydrogen and carbon monoxide is the best for a high yield production of DME. The liquid stream at the outlet of the previous mentioned vapour-liquid separation unit is, instead, mainly constituted of dissolved CO₂, DME and CH₃OH, so it is further treated in three different distillation columns:

- 1) column for CO₂ separation;
- 2) column for DME production;
- 3) column for methanol separation from water. Methanol is an additional fuel obtained from the plant.

6.1.2.4.4. Simulation of the distillation unit in Aspen Plus

In Aspen Plus, the vapour-liquid separator (V-L-SEP) inserted prior the distillation section is simulated through a flash reactor which has the following operating conditions:

- 1) temperature = -45°C;
- 2) pressure = 10 bar.

In this component, the stream produced in the DME reactor PROD-3, after its depressurization through a valve (VALVE-D1) to 10 bar, is sent (PROD-4), as shown in [Figure 58](#). The output streams of this component are:

- 1) a stream of uncondensable gases (H₂CO₂), treated as follows. It is pre-heated to 400°C (in HEAT-RE) and expanded to 1 bar producing electric power (in EXP-RE), the resulting stream H₂CO₂E is, then, sent to a post-combustion chamber, simulated through a Gibbs reactor (POST-COM), in which it is combusted adding a portion of the cathodic exhausts of the SOFC (CAT-EXH3, $\dot{n}_{\text{cat-exh3}} = 70 \frac{\text{kmol}}{\text{hr}}$). This is shown in [Figure 58](#). The resulting stream H₂OCO₂₋₁ is firstly cooled in a heat recovery steam generator (SRG3) and then separated in a flash unit (SEP-RE) at T=15°C and P=1 bar. The obtained water at the bottom of the reactor is used to produce steam in counter-flow with the post-combustion exhausts in the previously mentioned SRG3, while the gaseous stream feeds the following biomethane reforming reactor (METH-REF) after being mixed (in MIX-CO_{2R}) with the streams of CO₂ coming from the anodic exhausts of the SOFC (CO₂-RS-3) and from the first distillation column of the distillation unit (CO₂-D2). The biomethane reforming reactor is simulated through a Gibbs reactor (METH-REF) [72] and it is also fed by biomethane (METH-2) to make its partial oxidation take place to produce syngas (SYN1) with a molar ratio H₂/CO equal to 1. This syngas is cooled in the heat recovery steam generator (SRG5) and split (in SPL-SYN) to be partially recirculated to the DME synthesis reactor (SYN-RE3R) and partially sent to a syngas duct (SYN-DUCT).

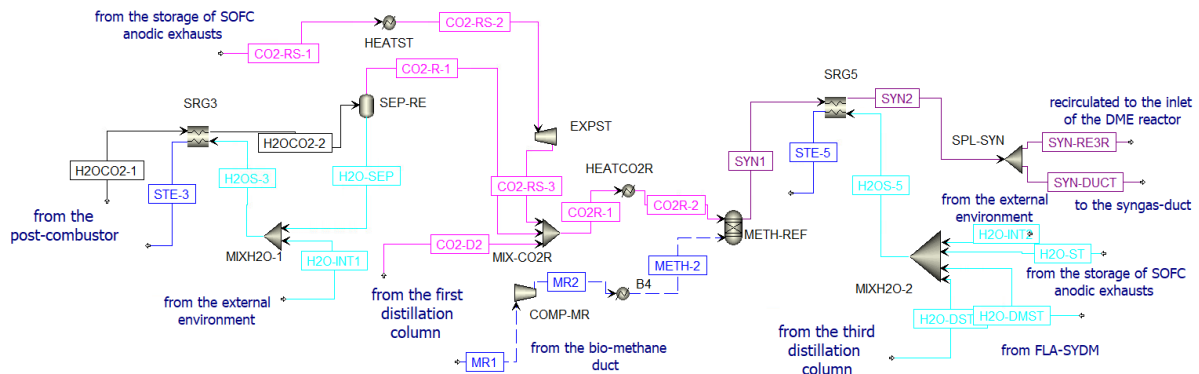


Figure 61: Treatment of the gaseous output of the DME reactor and reforming unit in Aspen Plus

INPUT FLOWS	PRESSURE [bar]	TEMPERATURE [°C]	MOLE FLOWS [kmol/s]	MOLAR FRACTIONS						
				CH ₄	H ₂ O	CO ₂	CO	H ₂	O ₂	N ₂
CO2R-2	1	500	0.7112	0.0612	0.0119	0.7693	0.0453	0.0748	0	0.0367
METH-2	1	700	0.4167	0.95	0	0.05	0	0	0	0
OUTPUT FLOW	PRESSURE [bar]	TEMPERATURE [°C]	MOLE FLOWS [kmol/s]	MOLAR FRACTIONS						
				CH ₄	H ₂ O	CO ₂	CO	H ₂	O ₂	N ₂
SYN1	1	800	1.9820	0.0065	0.0340	0.0415	0.4768	0.4281	0	0.0132

Table 17: Input and output flows of the reforming reactor

The properties of the two streams of syngas obtained after the splitting (in SPL-SYN) are listed in [Table 18](#):

FLOWS	PRESSURE [bar]	TEMPERATURE [°C]	MOLE FLOWS [kmol/s]	MOLAR FRACTIONS						
				CH ₄	H ₂ O	CO ₂	CO	H ₂	O ₂	N ₂
SYN-REC3	1	30	0.8333	0.0065	0.0340	0.0415	0.4768	0.4281	0	0.0132
SYN-DUCT	1	30	1.1486	0.0065	0.0340	0.0415	0.4768	0.4281	0	0.0132

Table 18: Recirculated syngas stream and syngas stream sent to the duct

2) a liquid stream mainly constituted of dissolved CO₂, DME and CH₃OH (LIQ1). The latter stream is treated in the three distillation columns (DIST-CO₂, DIST-DME, DIST-MET) simulated through the component RadFrac in Aspen Plus, as shown in [Figure 62](#).

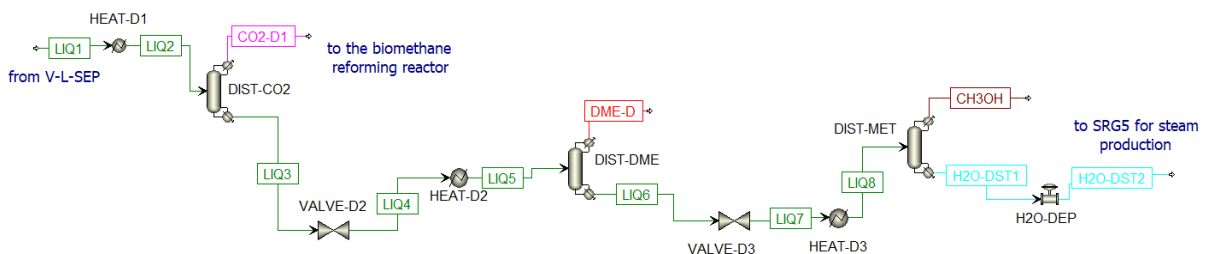


Figure 62: Distillation unit in Aspen Plus

A valve and a heat exchanger are placed before each column to adjust the pressure to the optimal value and to have 50% of vapour in the inlet stream of the column [67]. The number of stages used in the distillation columns is estimated by increasing them until a certain change in composition is

detected. In the following *Table 19*, the data inserted in the distillation columns for the modelling of the plant are listed.

	Pressure [bar]	T _{REB} [°C]	Q _{REB} [MW]	T _{COND} [°C]	Q _{COND} [MW]	Number of stages	Feed-in stage	Purity of the product
DIST-CO2	10	49.64	1.1	-40.58	-1.5	25	10	-
DIST-DME	9	140.73	2.7	45.18	-1.7	30	24	98%
DIST-MET	2	113.63	1	82.89	-0.8	24	18	99%

Table 19: Distillation columns of operation parameters

The streams obtained at the output of the distillation units are listed in *Table 20*. As written before:

- the CO₂ stream (CO₂-D1) obtained from the first distillation column (DIST-CO₂) is recirculated to the reforming reactor;
- the DME and methanol streams obtained respectively from the second (DIST-DME) and third (DIST-MET) columns are two of the material streams outputs of the plant;
- the water stream (H₂O-DST1) obtained from the third distillation column (DIST-MET) is depressurized (in H₂O-DEP) and mixed with other water streams (in MIXH₂O-2) to be used for steam production in the heat recovery steam generator SRG5.

FLOWS	PRES [bar]	TEMP [°C]	MOLE FLOWS [kmol/s]	MOLAR FRACTIONS								
				CH ₄	H ₂ O	CO ₂	CO	H ₂	O ₂	N ₂	DME	CH ₃ OH
CO ₂ -D1	10	-40.58	0.1416	0.0026	0	0.9833	0.0119	0.0005	0	0.0017	0	0
DME-D	9	45.18	0.1345	0	0	0.0099	0	0	0	0	0.9835	0.0065
CH ₃ OH	2	82.89	0.0222	0	0	0	0	0	0	0	0	0.9999
H ₂ O-DST1	2	113.63	0.0100	0	0.8959	0	0	0	0	0	0	0.1041

Table 20: Outlet streams from the distillation columns

6.1.2.5. Steam production

In the analysed plant, there are five heat recovery steam generators (SRG1, SRG2, SRG3, SRG4, SRG5). These generators have as a primary purpose the cooling of certain streams of the plant without losing their high-temperature heat, which is, instead, exploited to produce an additional useful product: steam. In certain generators (SRG1, SRG2), the water needs are completely satisfied through the recirculation of water produced in the system itself from different processes e.g. dehydration of a certain material stream and SOFC anodic exhausts; in others, there is the necessity to integrate water from the external environment to both cool material streams and produce additional steam. The amount of water which circulates in each generator is strictly dependent on the temperature drop that is necessary and should be fixed in the hot side of the exchanger itself:

HRSG	INLET STREAM		OUTLET STREAM	
	NAME	TEMPERATURE [°C]	NAME	TEMPERATURE [°C]
SRG1	SYN-SOF2	1546.05	SYN-SOF3	800
SRG2	SYN-DME1	900	SYN-DM11	40
SRG3	H2OCO2-1	400	H2OCO2-2	20

CASE STUDY: POLYGENERATION PLANT

SRG4	CAT-EXH4	511.22	CAT-EXH5	30
SRG5	SYN-REC1	800	SYN-REC2	30

Table 21: Hot side of the heat recovery steam generators

Considering an inlet water temperature equal to 15°C, the mole flows of water required to satisfy the needs of cooling in SRG1 and SRG2 are listed in Table 22:

HRSG	WATER REQUIREMENTS		
	MOLE FLOWS [$\frac{kmol}{min}$]	OUTLET TEMPERATURE [°C]	YEARLY MOLES [$\frac{kmol}{year}$]
SRG1	22.163	1326.50	2438103.82
SRG2	13.575	546.52	1493341.75

Table 22: Water requirements in SRG1 and SRG2

In Table 22, the yearly amount of water for each component is evaluated considering that SRG1 and SRG2 are in function only simultaneously with the chemical looping:

$$\begin{aligned} \text{yearly amount of} & \quad \text{mole flow of water for a} & \quad \text{yearly operating} \\ \text{water required in a} & = \text{certain temperature drop} & \cdot \text{minutes of the} \\ \text{certain SRG} & \quad \text{in the hot side} & \quad \text{CL} \\ & \quad \left[\frac{kmol}{min} \right] & \quad \left[110010 \frac{min}{year} \right] \end{aligned} \quad (95)$$

Considering the yearly amount of water separated from the anodic exhausts of the SOFC:

$$n_{H_2O,SOFC,yearly} = \dot{n}_{H_2O,SOFCanode} \cdot \begin{matrix} \text{yearly operating} \\ \text{minutes of the SOFC} \\ \left[525600 \frac{min}{year} \right] \end{matrix} = 5456691.60 \frac{kmol}{year} \quad (96)$$

and the yearly amount of water necessary to the oxidation reactor of the chemical looping to operate properly:

$$n_{H_2O,OXY,yearly} = \dot{n}_{H_2O,OXY} \cdot \begin{matrix} \text{yearly operating} \\ \text{minutes of the CL} \\ \left[110010 \frac{min}{year} \right] \end{matrix} = 1149459.20 \frac{kmol}{year} \quad (97)$$

The surplus of H₂O produced in the SOFC and not exploited in the oxidation reactor (ΔH_2O) is:

$$\Delta H_2O = n_{H_2O,SOFC,yearly} - n_{H_2O,OXY,yearly} = 4307232.41 \frac{kmol}{year} \quad (98)$$

a portion of this surplus $\Delta H_2O_{SRG1,SRG2}$ can be used for the steam production in SRG1 and SRG2 satisfying the entire flow rates required in the generators themselves:

$$\Delta H_2O_{SRG1,SRG2} = 3931445.57 \frac{kmol}{year} \quad (99)$$

while the remaining part (ΔH_2O_{SRG5}) can be used in to partially satisfy the needs of SRG5 (which is in function only when the CL operates) with a molar flow rate $\Delta \dot{H}_2O_{SRG5}$:

$$\Delta H_2O_{SRG5} = 375786.84 \frac{kmol}{year} \quad (100)$$

$$\Delta \dot{H}_2O_{SRG5} = 3.42 \frac{kmol}{min} \quad (101)$$

An additional amount of water can be recovered from the:

- 1) separation of the H₂O after the post-combustion unit (in SEP-RE): $\dot{n}_{H_2O-SEP} = 0.7994 \frac{kmol}{min}$. This water is sent to SRG3 in addition to the water injected from the external environment;
- 2) dehydration of the syngas produced in the oxidation reactor (in FLA-SYDM) prior to the production of DME: $\dot{n}_{H_2O-DMST} = 1.3480 \frac{kmol}{min}$. This water is sent to SRG5 in addition to the water injected from the external environment;
- 3) last column of distillation (in DIST-MET): $\dot{n}_{H_2O-DST1} = 0.5970 \frac{kmol}{min}$. This water is sent to SRG5 in addition to the water injected from the external environment.

However these streams of water recovered and recirculated in the plant cannot completely satisfy the needs of the heat recovery steam generators SRG3 and SRG5 (which only work when the CL is in function) and SRG4 (which always work because it is downstream the SOFC), so additional water has to be introduced from the external environment:

HRSG	WATER REQUIREMENTS			
	MOLE FLOWS $\left[\frac{kmol}{min}\right]$	OUTLET TEMPERATURE [°C]	YEARLY MOLES $\left[\frac{kmol}{year}\right]$	ADDITIONAL WATER FROM THE EXTERNAL ENVIRONMENT $\left[\frac{kmol}{min}\right]$
SRG3	4.3161	381.39	474810.86	3.5167
SRG4	41.5548	475.18 when CL does not work 463.875 when CL works	21841202.88	41.5548
SRG5	40.4044	748.24	4444888.04	35
TOTTAL ADDITIONAL WATER REQUIREMENT $\left[\frac{kmol}{min}\right]$				80.1149

Table 23: Additional water requirement from the external environment

6.1.2.6. Solar Tower and heliostats

As previously written, both the reduction reaction of the chemical looping and the bio-methane reforming reaction downstream the DME synthesis and distillation unit are supplied by concentrated

solar power. The two reactions could occur in two different receiver-reactors of a solar tower system, the structure of the CSP plant is described in [Chapter 4.5](#). The reduction reaction is executed at 900°C, while the biomethane reforming at 800°C. However, this last unit is in function only if syngas is produced in the oxidation reaction of the chemical looping and, consequently, only when the reduction reaction can unfold. This happens when the receiver-reactor of the reduction reaction of the CL is hit by a sufficient solar irradiance to reach the temperature of 900°C (as written in the introduction to this [Chapter 6](#)). The aim of this paragraph is to define the size of the heliostat field which is able to satisfy the thermal requirements of both the reduction and reforming reactions themselves. Different steps are executed.

Step 1: Definition of the daily hours in which the receiver-reactor of the CL can reach the required temperature of 900°C in a clear sky day in the different seasons of the year. This can be executed considering the seasonal daily average temperature curves of the receiver-reactor, shown in [Figure 53](#):

- 1) in Summer, the CL can work from 9:30 am to 6:30 pm;
- 2) in Autumn, the CL can work from 11 am to 14:50 pm;
- 3) in Spring, the CL can work from 9:30 am to 5:15 pm;
- 4) in Winter, never.

Step 2: Definition of the direct normal irradiance hitting the heliostats in the daily hours mentioned in the step 1. This can be realized taking into account the data of the daily values of the direct normal irradiance in the neighbourhood of the Energy Center, measured by the meteorological station of the Politecnico, relatively to the year 2019. These data provide the value of the DNI for the all year with a time step of 15 min. In this study, it is considered one representative clear sky day for each season and the average value of the direct normal irradiance in that day and in the time interval of the step 1 (which depends on the season) is calculated:

Season	Representative day	Average DNI $\left[\frac{W}{m^2}\right]$
Summer	July 30 th	833.36
Autumn	November 5 th	614.04
Spring	May 30 th	921.06

Table 24: Average DNI on the receiver-reactors in the different seasons when $T \geq 900^\circ\text{C}$

Step 3: Calculation of a weighted mean of the values of the irradiances in step 2 considering the effective operation time of the CL in the different seasons of the year:

- 47430 min/year in Summer;
- 42780 min/year in Spring;
- 19800 min/year in Autumn.

As a result, the yearly average DNI hitting the receiver-reactors and making the CL work properly is around $828 \frac{W}{m^2}$.

Step 4: Calculation of the extension area of the solar field and the number of heliostats. To satisfy the solar total thermal requirement of the plant, equal to 293.93 MW_t, with an optical efficiency of the solar field equal to 80%, the extension area of the solar field should be:

$$\text{Extension area of the solar field} = \frac{293.93 \text{ MW}_t}{0.8 \cdot 828 \frac{W}{m^2}} = 443743.5 \text{ m}^2 = 44.27 \text{ hectares} \quad (102)$$

Considering a heliostat aperture area of 140 m^2 , the total number of heliostats which should be installed is:

$$\text{Total number of heliostats} = \frac{\text{Extension area of the solar field}}{140 \text{ m}^2} = 3170 \text{ heliostats} \quad (103)$$

The total number of required heliostats for the Solar Tower plant is much lower than the number of Dish collectors which would be required. Considering the solar Dish panel installed on the roof of the Energy Center, it is able, at the given $828 \frac{\text{W}}{\text{m}^2}$ DNI, to concentrate power equal to 2.98 kW for an aperture surface of 4.5 m^2 ; the $W_{\text{th,tot}}$ of the present study would be satisfied with a total number of identical modules equal to 98610. That's why, for this thermal requirement, a Solar Tower system is preferred. The dimensions of the obtained solar field in the mid between the ones of the Khi Solar One system by Abengoa in Northern Cape (South Africa) [73] and the Spanish Gemasolar system [74]. In addition, considering only the solar thermal power required for the reduction reaction ($W_{\text{th,reduction}} \sim 141.51 \text{ MWt}$), the solar field extension satisfying this needs is 213634 m^2 , so 21.36 hectares with 1526 heliostats. If there was not the reforming unit, the solar field sufficient to make only the reduction reaction occur and, consequently, to feed the SOFC throughout all year is slightly lower than the one of the Spanish Gemasolar system [74]. This aspect is highlighted because the electricity production of the polygeneration plant analysed in this work is more or less equal to the electricity production of the Spanish system (24.19 MWe vs 20 MWe), underling the possible competitiveness of this plant with other CSP systems.



Figure 63: Solar field of the Spanish Gemasolar system



Figure 64: Central receiver tower of the Spanish Gemasolar system

6.1.3. Plant operating components in the absence of a sufficient irradiance

As specified in the introduction to this [Chapter 6](#), in the operating conditions in which there is not enough solar irradiance to make the chemical looping operate properly ($T_{\text{receiver-reactor}} < 900^{\circ}\text{C}$), the only units which still operate are the SOFC and the heat recovery steam generator fed by the cathodic exhausts (SRG4, downstream the SOFC), as shown in [Figure 57](#). The SOFC functioning is unvaried compared to the operating conditions in which also the chemical looping is able to work properly. The main difference stays in the fact that the anodic exhausts of the SOFC are not sent to the oxidation reaction of the chemical looping, but, after their splitting, they are stored:

- H_2O can be directly stored in an AISI 306 tank after the splitting at 15°C and 1 bar;
- CO_2 has to be pressurized and heated prior the storage because this stream is stored at 80°C and 25 bar in a stainless steel tank. At the outlet of the flash unit that separates the anodic exhausts (FLA-AN-E), CO_2 is at 15°C and 1 bar, so it is subjected to two-steps intercooled compression (in COMCO2-1, INTCO2-1, COMCO2-2, INTCO2-2) and brought to the storage conditions (CO2-ST4 is obtained).

In addition, in this situation, the cathodic exhausts do not need to be split because the post-combustor of the DME-distillation unit is not working, so the whole stream of air exiting the cathode of the SOFC can be used to produce steam in the heat recovery steam generator (SRG4).

6.2. Thermal balance of the plant

The thermal balance of the plant components is fundamental to evaluate the total expenditures and products of the system. In the present study, the plant is analysed at steady-state conditions. To meet the heat requirements of certain components, the recirculation of the above-mentioned produced steam and the redistribution of the hot loads is made. For the seek of simplicity, this regenerative heat transfer is not shown in the previous figures of the system. At the beginning, when the plant is made to operate for the first time, a transitory is present. During the transitory, those thermal loads that are not covered by solar energy should be provided from the external environment, reasonably through the use of electric heaters. Thus, the system starts to be efficient after a certain period, when the plant works in the regime and these thermal loads are internally satisfied. The same thought can be formulated for the mechanical power required by the compressors, so this is an issue that has to be taken into account for both thermal and workstreams. In this paragraph, the different sections of the plant and their thermal needs are evaluated.

6.2.1. Thermal analysis of the chemical looping

As specified in [Chapter 3](#), the chemical looping is characterized by a reduction reaction and an oxidation reaction. The reduction reaction is endothermic, the amount of heat necessary for this reaction is given by concentrated solar energy. Solar energy is necessary both to satisfy the heat duty of the reaction and to heat the streams of CeO_2 and biomethane entering in the reactor itself. The amount of CeO_2 recycled from the oxidation reaction is heated from 880°C to 900°C to take into account a possible thermal loss of 20°C between the oxidation and the reduction, while the CeO_2 that is re-integrated at each cycle has to be heated from the ambient temperature to 900°C (as for the biomethane entering in the reduction reactor). On the other hand, the oxidation reaction is exothermic, so a certain amount of heat can be recovered and used in other sections of the plant. In [Table 25](#) the heat duties of both the reduction and the oxidation reactions are shown with a positive sign in case of energy released by the component (oxidation reaction) and a negative sign in case of energy needed by the component (it is an expenditure, reduction reaction).

CASE STUDY: POLYGENERATION PLANT

COMPONENT	HEAT DUTY [MW]	
Reduction reactor	Reduction reaction	-114.0000
	Methane stream	-20.1168
	Total ceria stream	-7.3927
Oxidation reactor	32.9662	

Table 25: Thermal balance of the chemical looping

Additionally, the inlet flows in the oxidation reaction have to be brought to the temperature of 900°C. As written before, the CO₂ stream is constituted of two flows mixed prior the reactor: one of them directly comes from the anodic exhausts of the SOFC (CO₂), while the other comes from the storage of the CO₂ separated from the anodic exhausts of the SOFC when the CL is not able to operate (CO₂-INT1). This latter stream is taken from the storage at 80°C and 25 bar, so it is subjected to an inter-heated expansion; the heating is executed in HEA-CDS1 and HEA-CDS2 exploiting a portion of the steam produced in SRG2 (STE2-1) that previously cools in HEA-CDS2 (STE2-P1 is obtained) and then in HEA-CDS1 (STE2-PP1 is obtained) as shown in [Figure 65](#).

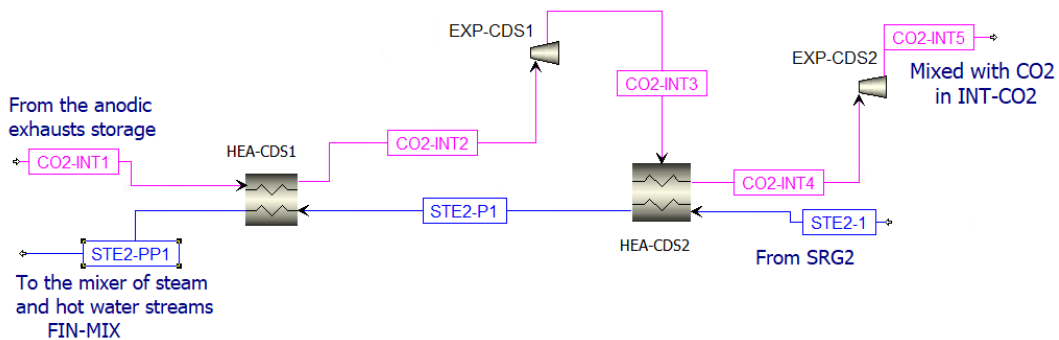


Figure 65: Thermal balance of HEA-CDS1 and HEA-CDS2 in Aspen Plus

	MOLE FLOW [$\frac{kmol}{hr}$]	INLET TEMPERATURE [°C]	OUTLET TEMPERATURE [°C]
HEA-CDS2			
HOT FLUID: STE2-1	388.559	546.53	398.15
COLD FLUID: CO2-INT3	292.16	280.12	450
HEA-CDS1			
HOT FLUID: STE2-P1	388.559	398.15	165.24
COLD FLUID: CO2-INT1	292.16	80	350

Table 26: Inlet and outlet streams of HEA-CDS1 and HEA-CDS2

After its heating and compression, this stream (CO₂-INT3) is mixed with the stream exiting from the anode of the SOFC (CO₂) in INT-CO₂ and this mixture is further heated to 800°C (in HEAT-CO₂) through a portion of the steam produced in SRG1:

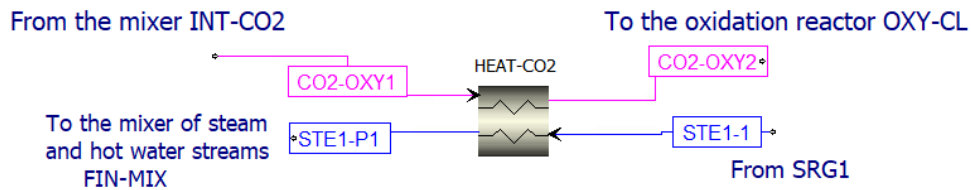


Figure 66: Thermal balance of HEAT-CO₂ in Aspen Plus

	MOLE FLOW [$\frac{kmol}{hr}$]	INLET TEMPERATURE [°C]	OUTLET TEMPERATURE [°C]
HOT FLUID: STE1-1	610.59	1326.50	316.85
COLD FLUID: CO2-OXY1	706.65	94.42	900

Table 27: Inlet and outlet streams of HEAT-CO₂

Concerning the stream of H₂O entering in the oxidation reactor, it directly comes from the anodic exhausts of the SOFC and it is heated by a portion of the steam produced in SRG1:

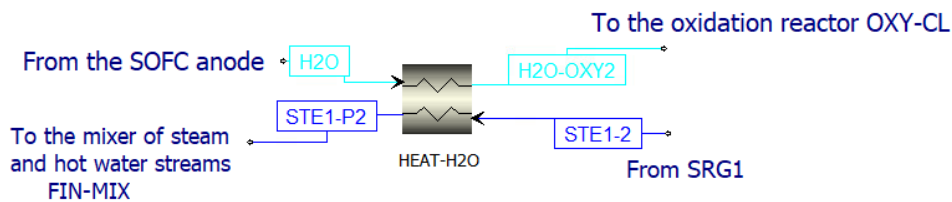


Figure 67: Thermal balance of HEAT-H₂O in Aspen Plus

	MOLE FLOW [$\frac{kmol}{hr}$]	INLET TEMPERATURE [°C]	OUTLET TEMPERATURE [°C]
HOT FLUID: STE1-2	610.59	1326.50	99.65
COLD FLUID: H2O	661.62	15	900

Table 28: Inlet and outlet streams of HEAT-H₂O in Aspen Plus

6.2.2. Thermal analysis of the SOFC

In the SOFC scheme, a large amount of heat is required to bring air to around 600°C prior the entrance in the cathode to avoid a possible thermal shock of the fuel cell itself. This thermal requirement (in HEAT-AIR) can be satisfied by the usage of two heat sources:

- 1) after the compression in COMP-AIR, air is heated in REG1 from around 200°C to 265°C through the steam produced in SRG4, the outlet temperature of the steam is 228.53°C;

- 2) after this pre-heating, the air stream can be further heated to 600°C in two different ways, depending on the functioning or not of the CL unit:
 - a) if the CL unit properly operates, air can be further heated through the heat produced in the oxidation reaction in REG2 for two reasons:
 - the oxidation reaction works at 900°C, which is a much higher temperature than the final temperature required for air;
 - the thermal power released by the oxidation reaction (32.966 MW) is comparable with the thermal power required to bring the stream of air, which is necessary in the SOFC, to the desired temperature (31.8939 MW) even considering possible thermal losses in the heat transfer, which could be executed through a thermovector fluid (eg. water);
 - b) if the CL does not operate, the further heating of air should be executed through the use of an electric heater in HEAT-EL. However, this drastically lowers the system efficiency and the electricity production of the plant.

6.2.3. Thermal analysis of the reforming unit

Different thermal flows are necessary for the section of the plant in which the reforming is executed:

- 1) after the vapour-liquid separation of the products of the DME reactor in V-L-SEP, the gaseous stream has to be heated prior to the expansion and the successive post-combustion. This heating is executed in HEAT-RE exploiting a portion of the steam produced in SRG5:

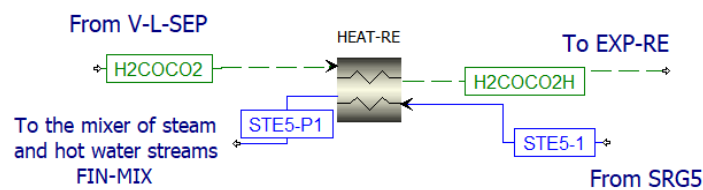


Figure 68: Thermal balance of HEAT-RE in Aspen Plus

	MOLE FLOW [$\frac{kmol}{hr}$]	INLET TEMPERATURE [°C]	OUTLET TEMPERATURE [°C]
HOT FLUID: STE5-2	1110.169	748.24	389.38
COLD FLUID: H2COCO2	989.442	-45	400

Table 29: Outlet and inlet streams of HEAT-RE

- 2) the stream of CO₂ coming from the storage of the anodic exhausts of the SOFC (CO2-RS-1), at 80°C and 25 bar, has to be heated and expanded. The heating is executed in HEATST through a portion of the steam produced in SRG5:

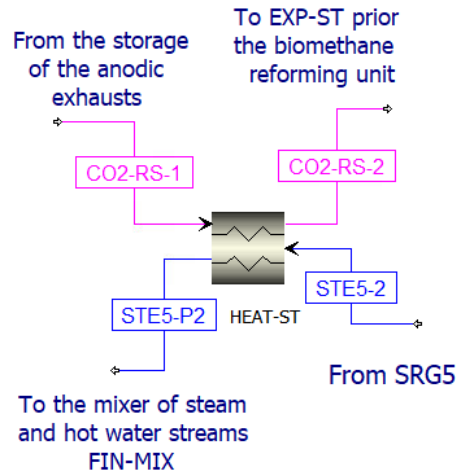


Figure 69: Thermal balance of HEAT-ST in Aspen Plus

	MOLE FLOW $\left[\frac{kmol}{hr}\right]$	INLET TEMPERATURE [°C]	OUTLET TEMPERATURE [°C]
HOT FLUID: STE5-2	1276.69	748.24	469.74
COLD FLUID: CO2-RS-1	1273.62	80	350

Table 30: Outlet and inlet streams of HEATST

- 3) the reforming of CH₄ is endothermic, so it requires heat, which is supplied by concentrated solar power. Since the reaction takes place simultaneously with the CL operation, the operating T is set equal to 800°C. The entering streams in the reactor should also be heated by the solar energy hitting the receiver:

COMPONENT	HEAT DUTY [MW]	
Reforming reactor	Reforming reaction	-126.74
	Methane stream	-11.53
	CO ₂ stream	-14.15

Table 31: Thermal balance of the reforming unit

6.2.4. Thermal analysis of the distillation unit

Prior the entrance in the different distillation columns, the liquid that has to be treated is heated to obtain a vapour fraction equal to 0.5 in HEAT-D2 and in HEAT-D3; the thermal energy requirements in these units can be satisfied by a portion of steam produced in SRG2:

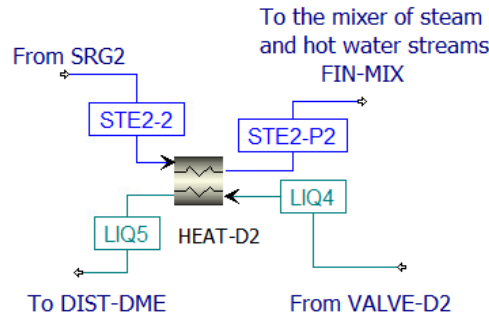


Figure 70: Thermal balance HEAT-D2 in Aspen Plus

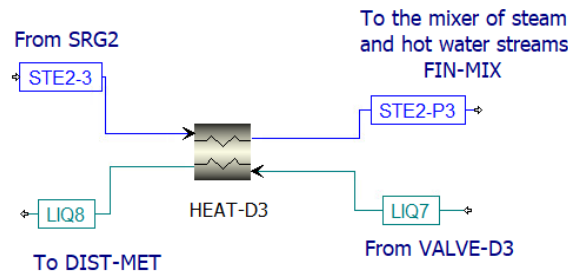


Figure 71: Thermal balance of HEAT-D3 in Aspen Plus

	MOLE FLOW $\left[\frac{kmol}{hr}\right]$	INLET TEMPERATURE [°C]	OUTLET TEMPERATURE [°C]
HEAT-D2			
HOT FLUID: STE2-2	138.77	546.53	99.65
COLD FLUID: LIQ4	599.70	46.14	57.67
HEAT-D3			
HOT FLUID: STE2-3	111.02	546.53	180.34
COLD FLUID: LIQ7	115.62	90.24	92.93

Table 32: Inlet and outlet streams of HEAT-D2 and HEAT-D3

In each distillation column, there is a reboiler. A reboiler is a heat exchanger used to furnish heat to the bottom of the column itself. This component produces the boiling of the liquid at the bottom of the column and vapours are generated. These vapours drive the distillation separation in the column. The heat supplied by the reboiler is then removed by the condenser, which is at the top of the column itself. A correct operation of the reboiler is very important for the distillation process because all vapours driving the separation action are produced in the reboiler itself. The heat required by the reboilers of the present plant can be supplied by the thermal load produced in the post-combustion Gibbs reactor, that can be removed from the reactor through a heat transfer fluid, because:

- post-combustion is executed at 400°C and the produced thermal power is of 8.05 MW;
- the reboilers' temperatures are much lower than 400°C (49.64°C, 140.73°C, 113.63°C) with a total thermal power requirement of 4.8 MW, that is much lower than 8.5 MW so the heat transfer is sufficient even with a not unitary efficiency.

6.3. Inputs and outputs of the plant

Once the distribution of the thermal loads of the plant is executed, a review of all the input and output streams is realized considering both those periods in which the chemical looping is in operation and those periods in which it is not. Two different streams can be defined:

- material streams;
- work streams.

The material streams in input and in output are listed in *Table 33*.

INPUT MATERIAL FLOWS	SECTION OF THE PLANT	OP OF THE CL	PRES [bar]	TEM [°C]	TOTAL MOLE FLOW $\left[\frac{kmol}{s}\right]$	MOLAR FRACTIONS						
						CeO ₂	CH ₄	CO ₂	O ₂	N ₂	H ₂ O	
Cerium oxide (CeO ₂)	Chemical looping (reduction reactor)	ON	1	15°C	1 st cycle	1	0	0	0	0	0	0
					0.5900 * 2 = 1.1800							
					from the 2 nd cycle							
					0.1010							
Biometh. (CH ₄)	Chemical looping (reduction reactor) & DME distillation unit (reforming reactor)	ON	0.08	15	0.8887	0	0.95	0.05	0	0	0	0
Air	SOFC (cathode)	ON and OFF	1	15	3.0441	0	0	0	0.21	0.79	0	0
Water	SRG3 and SRG5	ON	1	15	0.6427	0	0	0	0	0	0	1
	SRG4	ON and OFF	1	15	0.6926	0	0	0	0	0	0	1
OUTPUT MATERIAL FLOWS	SECTION OF THE PLANT	OP OF THE CL	PRES [bar]	TEM [°C]	TOTAL MOLE FLOW $\left[\frac{kmol}{s}\right]$	MOLAR FRACTIONS						
						CO ₂	DME	CH ₃ OH	CH ₄	CO	H ₂	H ₂ O
DME	DME synthesis and distillation units	ON	9	45.18	0.1345	0.0099	0.9835	0.0065	0	0	0	0
CH ₃ OH	DME synthesis and distillation units	ON	2	82.89	0.0222	0	0	0.9999	0	0	0	0
Syngas	DME synthesis and distillation units	ON	1	30	1.1486	0.0415	0	0	0.0065	0.4769	0.4281	0.0334

Steam	SRG1 → HEAT-CO2	ON	1	316.85	0.1696	0	0	0	0	0	0	1
	SRG1	ON	1	1326.50	0.0302	0	0	0	0	0	0	1
	SRG2 → HEAT-D3	ON	1	180.34	0.0308	0	0	0	0	0	0	1
	SRG2 → HEACDS1 /HEACDS2	ON	1	165.24	0.1079	0	0	0	0	0	0	1
	SRG2	ON	1	546.526	0.0489	0	0	0	0	0	0	1
	SRG3	ON	1	381.39	0.0719	0	0	0	0	0	0	1
	SRG4 → HEAT-AIR	ON and OFF	1	228.53	0.6926	0	0	0	0	0	0	1
	SRG5 → HEAT-RE	ON	1	389.38	0.3084	0	0	0	0	0	0	1
	SRG5 → HEAT-ST	ON	1	469.74	0.3546	0	0	0	0	0	0	1
	SRG5	ON	1	748.24	0.0104	0	0	0	0	0	0	1
Hot water	SRG1 → HEAT-H2O	ON	1	99.65	0.1696	0	0	0	0	0	0	1
	SRG2 → HEAT-D2	ON	1	99.65	0.0385	0	0	0	0	0	0	1

Table 33: Input and output material streams

The steam and hot water streams could be mixed in FIN-MIX and used in different ways, as shown in Figure 72:

- 1) self-consumption;
- 2) supply different users with domestic hot water;
- 3) supply heat in heat pumps for different users.

Consequently, the thermal power that could be obtained from these streams bringing them to their initial temperature (equal to 15°C) is another important output of the system. When the chemical looping is in on-state: $W_{th,tot,CL-ON} = 111.97$ MWt because all the heat recovery steam generators are in function.

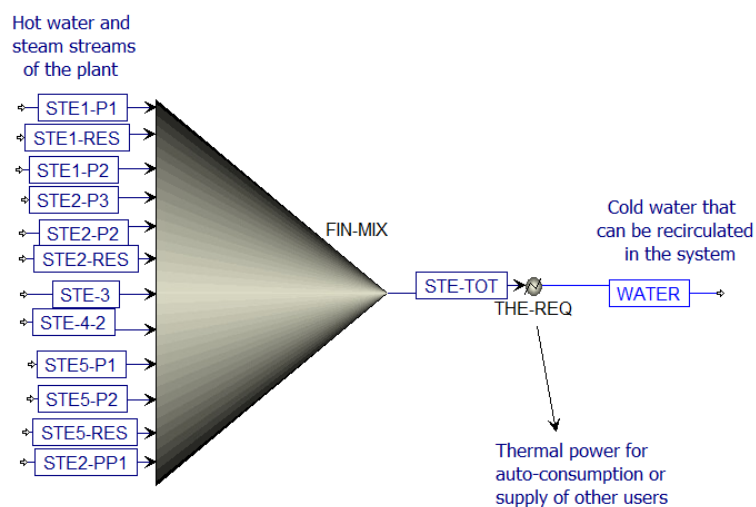


Figure 72: Mixer of the steam and hot water streams of the plant and simulation of the cooling of the output stream (STE-TOT) to obtain useful thermal power (THE-REQ) when CL is in ON-state

On the other hand, when the CL is in off-state only the heat recovery steam generator SRG4 is in function: $W_{th,tot,CL-OFF} = 35.82$ MWt.

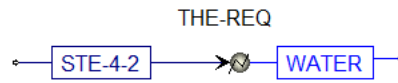


Figure 73: Simulation of the thermal recovery from steam when CL is in OFF-state

The cold water obtained after the cooling of these streams could be recirculated to the plant for satisfying its water needs from the external environment. The workstreams are listed in *Table 34* with a positive sign for those cases in which energy is supplied by the component and with a negative sign when energy has to be given to the component.

COMPONENT	OPERATION OF THE CL	WORK STREAM [kW]
TUR-AN-E	ON and OFF	3316.77
EXP-CAEX	ON and OFF	31559.87
COMP-AIR	ON and OFF	-16877.46
COMP-SYR	ON	-32134.07
COMPR-1	ON	-17396.62
COMPR-2	ON	-4006.55
EXP-RE	ON	2448.17
EXP-CDS1	ON	240.75
EXP-CDS2	ON	863.99
COMPRED1	ON	-4315.55
COMP-MR	ON	-3809.63
EXPST	ON	3840.05
COMCO2-1	OFF	-1056
COMCO2-2	OFF	-303
COMPONENT	OPERATION OF THE CL	ELECTRIC POWER STREAM [kW]
SOFC	ON and OFF	45823.74
AIR ELECTRIC HEATER	OFF	31893.9

Table 34: Input and output work streams

As a result, considering an electric efficiency of conversion of mechanical power to electric power equal to 97%, two different net electric power outputs can be defined depending on the operating conditions of the plant:

- when there is enough irradiance to make the chemical looping operate: $W_{EL,NET,CL-ON} = 6.17$ MWe;
- when the CL does not operate: $W_{EL,NET,CL-OFF} = 28.96$ MWe.

6.4. Plant efficiencies

In this chapter different plant efficiencies are evaluated considering the two possible yearly operating conditions of the system: chemical looping and DME synthesis and distillation unit in on state (high irradiance on the receiver-reactor) and off-state (low irradiance on the receiver-reactor).

6.4.1. Electric efficiency of the system

The electric efficiency of the system is evaluated through two different formulas considering respectively the operation (104) or not (105) of the chemical looping and of the DME synthesis and distillation units:

$$\eta_{electric,CL\ ON} = \frac{W_{EL,NET,CL-ON}}{Q_{RED-REACTOR} + m_{METH-1} \cdot LHV_{METHANE} + m_{METH-2} \cdot LHV_{METHANE} + Q_{REFORMING}} = 0.6\% \quad (104)$$

$$\eta_{electric,CL\ OFF} = \frac{W_{EL,NET,CL-OFF}}{m_{SYN-SOFC} \cdot LHV_{SYN-SOFC}} = 26.41\% \quad (105)$$

with:

$LHV_{METHANE}$ [MJ/kg]	47.10
$LHV_{SYN-SOFC}$ [MJ/kg]	23.14

Table 35: Data inserted in the formula (104) and (105)

The large difference between these two electric efficiencies is mainly related to the fact that $W_{EL,TOT,CL-OFF} \gg W_{EL,TOT,CL-ON}$. When the CL is in OFF-state, there is a much lower number of streams circulating in the system and, consequently, a lot of components of the plant (which during the CL operation are in ON-STATE and consume a lot of electricity e.g. COMP-SYR, COMPR-1 and COMPR-2) are in OFF-STATE. This difference in the electricity output of the system in its two operating conditions could be even higher if there was not the need to heat the air stream entering in the SOFC with an electric heater when the oxidation reaction does not occur. Additionally, when the CL is in OFF-STATE, only the SOFC operates, so the only fuel of the system is the syngas previously produced in the reduction reaction of the CL and stored in the AISI316L tank.

6.4.2. Thermal efficiency of the system

The thermal efficiency of the system is related to the thermal power which can be obtained cooling the hot water and steam streams produced in the plant. These streams are obtained from the waste heat fluxes of the plant and, after being recirculated in the plant itself to supply heat where it is necessary, they could be mixed. The single output stream could be cooled to the initial water temperature of 15°C to gain thermal power. This thermal power could be either auto-consumed either used to supply different users (for domestic hot water or the fed heat of heat pumps). Consequently, the thermal power released by this stream is an additional output of the plant. The cold water could be recirculated to the system itself to satisfy its water needs. Two different thermal efficiencies can be obtained considering respectively the operation (106) or not (107) of the chemical looping and of the DME synthesis and distillation units:

$$\eta_{thermal,CL-ON} = \frac{W_{th,tot,CL-ON}}{Q_{RED-REACTOR} + m_{METH-1} \cdot LHV_{METHANE} + m_{METH-2} \cdot LHV_{METHANE} + Q_{REFORMING}} = 10.94\% \quad (106)$$

$$\eta_{thermal,CL-OFF} = \frac{W_{th,tot,CL-OFF}}{m_{SYN-SOFC} \cdot LHV_{SYN-SOFC}} = 32.67\% \quad (107)$$

This large difference in the thermal efficiencies of the plant is mainly related to the different fuels required by the system during its two operating conditions. When the CL is in ON-state, the plant necessitates of both solar energy and biomethane; while when the CL is in OFF-STATE the only fuel requirement is the syngas stream entering in the SOFC. The larger amount of fuel supply of the first operating condition of the system reduces its thermal efficiency, evaluated as $\frac{\text{useful effect}}{\text{requirement for the useful effect}}$, even if the useful effect obtained when the CL is in ON-state is much higher than the one obtained when the CL is in OFF-state ($W_{th,tot,CL-ON} \gg W_{th,tot,CL-OFF}$).

6.4.3. Solar/biomethane-to-fuel efficiency of the system

The fuel production only occurs when the CL operates because the DME synthesis and distillation unit only functions when the oxidation reaction can take place and, consequently, when a high irradiance hits the solar receiver-reactor of the reduction reaction of the chemical looping.

$$\eta_{SOLAR/BIOMETHANE-TO-FUEL,CL ON} = \frac{m_{DME} \cdot LHV_{DME} + m_{METHANOL} \cdot LHV_{METHANOL} + m_{SYN-DUCT} \cdot LHV_{SYN-DUCT}}{Q_{RED-REACTOR} + m_{METH-1} \cdot LHV_{METHANE} + m_{METH-2} \cdot LHV_{METHANE} + Q_{REFORMING}} = 51\% \quad (108)$$

$$\eta_{SOLAR/BIOMETHANE-TO-FUEL,CL OFF} = \frac{0}{m_{SYN-SOFC} \cdot LHV_{SYN-SOFC}} = 0 \quad (109)$$

LHV_{DME} [MJ/kg]	28.82
$LHV_{METHANOL}$ [MJ/kg]	19.99
$LHV_{SYN-DUCT}$ [MJ/kg]	16.78

Table 36: Data inserted in equations (108) and (109)

From these results, it can be noted that the main production of the plant during the operation of the chemical looping is the production of the fuel.

6.4.4. Global efficiencies of the system

In this paragraph, the global efficiency of the plant considering its two different operating conditions is evaluated. This efficiency can be calculated as the sum of the previous mentioned efficiencies:

$$\eta_{global,CL-ON} = \eta_{electric,CL ON} + \eta_{thermal,CL-ON} + \eta_{SOLAR/BIOMETHANE-TO-FUEL,CL ON} = 62.56\% \quad (110)$$

$$\eta_{global,CL-OFF} = \eta_{electric,CL OFF} + \eta_{thermal,CL-OFF} + \eta_{SOLAR/BIOMETHANE-TO-FUEL,CL OFF} = 59.08\% \quad (111)$$

These results highlight the slight decrease of the global efficiency of the polygeneration plant in the absence of solar energy irradiating the receiver-reactor of the chemical looping. This happens because, even if the electric power production is higher and the fuel requirement is lower with the CL in OFF-state, when the chemical looping does not operate, the only outputs of the system are given

by electric and thermal power, but there is not the production of solar fuels. This happens because only the SOFC and the heat recovery steam generator downstream the SOFC (SRG4) can operate.

6.5. Evaluation of the plant results

To better evaluate the plant performance and its outputs, a comparison between the present study and a similar work by Farooqui et al. [4] is executed and exposed in this chapter. Additionally, attempts to improve the electricity production of the analysed polygeneration plant follows.

6.5.1. Results discussion

The examination of the electric/thermal power and the material streams produced in the polygeneration plant analysed in the present work is made taking into account the results obtained from a similar study by Farooqui et al. [4]. The two plants are characterized by some differences. The main ones are:

- 1) the unit chosen for the electric power production by Farooqui et al. [4] is a gas turbine. The thermal energy generated by the oxyfuel combustion chamber of the GT is used to make the chemical looping operate continuously during the year, therefore there is not the exploitation of solar energy;
- 2) the chemical looping executed by Farooqui et al. [4] is not isothermal, the two reactions take place at different temperatures. These temperatures are around 1312°C and 900°C respectively (much higher than the temperatures proposed in the present study);
- 3) a higher operating pressure of the chemical looping of Farooqui et al. [4], fixed to 2 bar.

The results of the plants in a steady-state condition are compared in the table below:

	Farooqui et al. [4]	Present study with the CL in ON state	Present study with the CL in off state
NG feed [ton/h]	25.20	55.80	0
$W_{el,net}$ [MWe]	102.90	6.17	28.96
W_{th} [MWt]	0	111.97	35.82
\dot{m}_{DME} [kg/s]	2.15	6.18	0
\dot{m}_{MeOH} [kg/s]	0.03	0.71	0
Syngas [kg/s]	0	19.68	0
Captured CO ₂ to be sequestered [kg/s]	8.62	0	0
η_{global} [%]	50.21	62.56	59.08

Table 37: Comparison between the present study and the Farooqui et al. one [4] considering the two different operations of the present polygeneration plant

Since the polygeneration plant analysed in the present study has different outputs depending on the operating conditions, a comparison between the average yearly outputs and inputs of the two plants has to be made:

	Farooqui et al. [4]	Present study
NG feed [kton/year]	220.75	102.30
$W_{el,net,average}$ [MWe]	102.90	24.19

$W_{th,average}$ [MWt]	0	51.76
\dot{m}_{DME} [kton/year]	67.80	40.79
\dot{m}_{MeOH} [ton/year]	946.08	4686.43
Captured CO ₂ to be sequestrated [kton/year]	271.84	0
Syngas [kton/year]	0	129.90
$\eta_{tot,ave}$ [%]	50.21	59.82

Table 38: Comparison between the yearly average outputs of the plants

As it can be seen in *Table 38*, the main lacks of the present plant stay in the lower power and DME production. This is strictly linked to the intermittence of solar energy which makes the chemical looping not working continuously throughout the year. Consequently, considering the same size of the chemical looping for both the present study and the study of Farooqui et al. [4], the chemical looping of this work can produce a lower average yearly amount of syngas in both the oxidation and the reduction reactor, as shown in *Table 39* and *Table 40*.

	Farooqui et al. [4]	Present study when the CL is on
CeO ₂ feed in the reduction reactor [kmol/s]	0.59	0.59
Methane feed in the reduction reactor [kmol/s]	0.413	0.472
Syngas produced in the reduction reactor [kmol/s]	1	1.137
Ce ₂ O ₃ feed in the oxidation reactor [kmol/s]	0.29	0.266
Syngas produced in the oxidation reactor [kmol/s]	0.47	0.422

Table 39: Comparison between the present study and the Farooqui et al. one [4] considering the operation of the present polygeneration plant with the CL in ON state

	Farooqui et al. [4]	Present study
Syngas produced in the reduction reactor [Gmol/year]	31.536	7.505
Syngas produced in the oxidation reactor [Gmol/year]	14.820	2.785

Table 40: Comparison between the yearly average syngas produced by the chemical loopings of the plants

The lower yearly amount of syngas produced in the reduction reactor has to be spread over the entire

year and used to continuously feed the SOFC, a storage system could be implemented. As a result, the molar flow of syngas entering in the SOFC is much lower than that one entering in the gas turbine of Farooqui et al. [4], thus a much lower electric power production of the SOFC compared to the GT is obtained. However, the electricity production of the present polygeneration plant is comparable to the electric power produced by the Spanish GemaSolar system. This latter system uses concentrated solar power as the main fuel to produce electricity in a Rankine cycle and it is characterized by a heliostat field extension which is very similar to the one required for the reduction reaction of this work [75].

	$W_{el,net\ average}$ [MWe]
GemaSolar (Spain) [75]	20
Present work	24.19

Table 41: Comparison between the electricity output of the present plant and the GemaSolar system

This aspect is highlighted to underline the possible competitiveness of this plant with others using CSP systems. Concerning the DME unit, in the present study, it only operates simultaneously with the CL. Therefore, the intermittence of solar energy makes the yearly average production of DME slightly lower than what is obtained by Farooqui et al. [4]. However, it is also important to highlight the higher amounts of thermal power, methanol and syngas at the output of the studied plant, the much lower yearly average methane consumption and the slightly higher efficiency. In addition, among its outputs, there is no carbon dioxide to be sequestered because the plant can completely reuse the produced CO₂ and execute the CCU. On the other hand, in Farooqui et al. [4], there is the issue of CCS coupled with the necessity to find a proper storage for the CO₂. An attempt to increase the electric power production of the present plant could be made trying to decouple the syngas production of the chemical looping from the intermittence of solar energy. This could be done eliminating the CSP systems of the reforming unit and the chemical looping, as follows in [Chapter 6.5.2](#).

6.5.2. Improvement in the electricity production of the plant

In the attempt to increase the electricity production of the plant, it is thought to supply the reduction reactor of the chemical looping through the thermal energy released by the exothermic SOFC. With this trick, all the polygeneration plant's components operate continuously during the year and the operating conditions of the system are always the same despite the presence or not of irradiance (this plant no more uses irradiance as main fuel). To do this, it is necessary to lower the reduction reaction temperature at 800°C (the SOFC operates at 850°C) and, consequently, for the complete ceria reduction, it is necessary to increase the amount of biomethane, sent to the reduction reactor at 900°C. The new operating conditions of both the reduction and the oxidation reactors are 800°C and 1.2 bar, the molar ratio biomethane/ceria is set at 1, so the molar ratio CH₄/CeO₂ is equal to 0.95. At this temperature, for molar ratios biomethane/ceria lower than 0.96, the incomplete thermal reduction of ceria is obtained, as shown in [Table 42](#). Therefore, a molar ratio biomethane/ceria equal to 1 is considered to be sure to predictably obtain a complete thermal reaction also in real operating conditions. In fact, in the Aspen Plus simulation, the reduction reactor is simulated through a Gibbs reactor, which is an ideal reactor, while, in reality, losses (e.g. thermal losses, too long time for the equilibrium to be reached) will be present.

Biomethane/CeO ₂ molar ratio	Molar ratios of the solid portion of the outlet stream of the reduction reactor at P=1.2 bar and T=800°C	
	CeO ₂	Ce ₂ O ₃

0.8	0.2760	0.7240
0.9	0.1045	0.8955
0.95	0.0052	0.9948
0.96	0	1

Table 42: Effect of the biomethane/CeO₂ molar ratio on the completion of the reduction of ceria

In this plant, the storage system of the SOFC is eliminated and the whole amount of syngas produced in the reduction reaction is sent to the anode of the SOFC itself. The SOFC can operate continuously thanks to the decoupling of the CL from the intermittence of solar energy: the reduction reaction is now supplied by the thermal energy produced in the SOFC stacks. In the oxidation reaction side, beyond the variation of the operating temperature, everything is unchanged, therefore this reaction is supplied by the reduced ceria and by the CO₂ and H₂O, coming from the anodic exhausts of the SOFC. In this case, there is no need of the integration of additional CO₂ to the CO₂ produced by the SOFC during its operation because the amount of produced anodic exhausts are much higher than the previous plant evaluated in this study (this is because a much higher amount of syngas feeds the SOFC). The quantities of CO₂ and H₂O in the anodic exhausts are too high to be directly sent to the oxidation reactor of the CL. Thus, after the separation of the carbon dioxide and water in a flash unit at 15°C and 1 bar, the two output streams of CO₂ and H₂O are further split into four streams (two of CO₂ and two of H₂O). One stream of H₂O is sent to the oxidation reactor, the other is used for steam production in the plant; one stream of CO₂ is sent to the oxidation reactor, the other is sent to the post-combustion unit (in addition to the CO₂ produced in the DME distillation unit). The input and output streams of the CL are listed in the table below:

REDUCTION REACTOR	INPUT/OUTPUT	PRES [bar]	TEMP [°C]	TOT MOLE FLOW [kmol/s]	MOLAR FRACTION							
					CeO ₂	Ce ₂ O ₃	CH ₄	CO ₂	H ₂ O	H ₂	CO	
OXIDATED CERIA	INPUT	1	800	0.5900	1	0	0	0	0	0	0	0
BIOMETHANE	INPUT	1	900	0.5900	0	0	0.9500	0.0500	0	0	0	0
PROD-1	SOLID PHASE	OUTPUT	1.19	800	0.2655	0	1	0	0	0	0	0
	GAS PHASE	OUTPUT It feeds the SOFC unit	1.19	800	1.2617	0	0.0234	0.1900	0.0010	0.0017	0.5073	0.2769
OXIDATION REACTOR	INPUT/OUTPUT	PRES [bar]	TEMP [°C]	TOT MOLE FLOW [kmol/s]	MOLAR FRACTION							
					CeO ₂	Ce ₂ O ₃	CH ₄	CO ₂	H ₂ O	H ₂	CO	
REDUCED CERIA	INPUT	1.19	800	0.2655	0	1	0	0	0	0	0	0
H ₂ O	INPUT	1	800	0.1838	0.0647	0	0	0	0.9353	0	0	0
CO ₂	INPUT	1	800	0.3533	0	0	0	0.5209	0.0137	0.2984	0.1669	0
PROD-2	SOLID PHASE	OUTPUT	1.19	800	0.4886	1	0	0	0	0	0	0
	GAS PHASE	OUTPUT It feeds the DME unit	1.19	800	0.5766	0.0941	0	0.0025	0.0868	0.3381	0.3976	0.3381

Table 43: Input and output streams of the chemical looping in the new plant

In this case, the SOFC stacks are able to continuously produce: $W_{EL,SOFC} = 243.48$ MW. The main problem of this system is that it requires the integration of thermal loads externally from the plant:

- 1) the produced SOFC thermal energy is sufficient to feed the reduction reactor and to accomplish the reaction, but it is not sufficient to heat the inlet streams of the system. These streams could be heated through an oxyfuel combustion of biomethane: $\dot{m}_{BIO-METH-1} = 0.7698$ kg/s ($LHV_{bio-meth} = 47.1$ MJ/kg);

- 2) the air stream entering the cathode of the SOFC has to be heated to 600°C to avoid the thermal shock of the SOFC itself, a portion of this thermal requirement is covered by the heat released from the oxidation reactor and by hot steam produced in the plant, while the other portion has to be supplied by an oxyfuel combustion of biomethane: $\dot{m}_{\text{BIO-METH-2}} = 1.9247 \text{ kg/s}$ ($\text{LHV}_{\text{bio-meth}} = 47.1 \text{ MJ/kg}$) ;
- 3) the reforming reactor thermal requirement should be completely satisfied through the oxyfuel combustion of biomethane: $\dot{m}_{\text{BIO-METH-3}} = 2.88 \text{ kg/s}$ ($\text{LHV}_{\text{bio-meth}} = 47.1 \text{ MJ/kg}$), while the inlet streams are heated by the recirculation of the plant's thermal loads.

The total biomethane requirement for thermal purposes is: $\dot{m}_{\text{BIO-METH-THERMAL-TOT}} = 5.5749 \text{ kg/s} = 0.3204 \text{ kmol/s}$ ($\text{LHV}_{\text{bio-meth}} = 47.1 \text{ MJ/kg}$) . This biomethane (95% CH₄ and 5% CO₂) is supposed to be burnt in an oxyfuel combustion, according to the following reaction:



For each 0.95 moles of CH₄, 1.9 moles of O₂ are necessary. The total amount of O₂ required to burn $\dot{m}_{\text{BIO-METH-TOT}}$ is equal to 0.6088 kmol/s, therefore $\dot{m}_{\text{O}_2\text{-required}} = 19.4803 \text{ kg/s}$. The oxyfuel combustion of biomethane is executed to apply the Carbon Capture and sequestration, as shown in [Chapter 3.2](#). The reaction of biomethane with pure O₂ leads to combustion exhausts mainly constituted of H₂O and CO₂. Therefore, the CO₂ can be easily captured by condensing water and then it can be sequestered. However, to obtain pure O₂ an Air Separation Unit is necessary. The energy expenditure of the Air Separation Unit to produce an O₂ stream with 98% of purity equal to 925 kJ/kg_{O₂} [76] can be assumed as shown in [Figure 74](#).

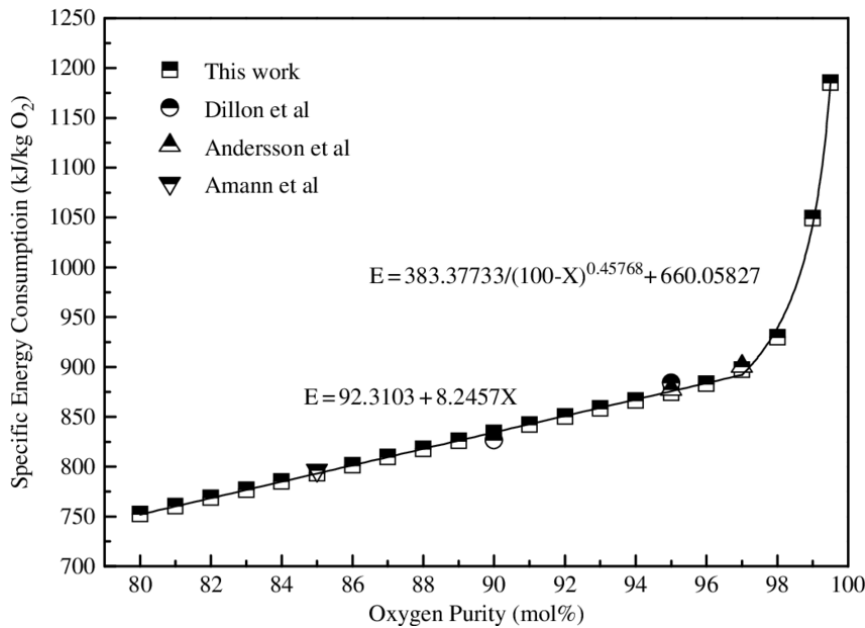


Figure 74: ASU specific energy consumption [76]

As a result, the total power expenditure of the ASU is:

$$W_{\text{el,ASU}} = \dot{m}_{\text{O}_2\text{-required}} \cdot 925 \frac{\text{kJ}}{\text{kg}_{\text{O}_2}} = 18.019 \text{ MW} \quad (113)$$

The results of the simulation of the plant are shown in the table below:

	Equations	New Plant without solar energy
NG feed [ton/h]	$\dot{m}_{\text{BIO-METH-TOT}} = \dot{m}_{\text{BIO-METH-THERMAL-TOT}} + \dot{m}_{\text{BIO-METH-REDUCTION}} + \dot{m}_{\text{BIO-METH-REFORMING}}$	83.276
$W_{\text{el,net}}$ [MWe]	$W_{\text{net}} = W_{\text{el,SOFC}} + \sum_{\text{PLANT COMPONENTS}} W_{\text{EL}} - W_{\text{el,ASU}}$	119.72
\dot{m}_{DME} [kg/s]	-	6.0029
\dot{m}_{MeOH} [kg/s]	-	1.3163
Syngas [kg/s]	-	23.4340
Captured CO ₂ from the oxyfuel combustion of biomethane to be sequestered [kg/s]	$\dot{m}_{\text{CO}_2} = \dot{n}_{\text{BIO-METH-THERMAL-TOT}} \cdot \text{PM}_{\text{CO}_2}$	14.10
η_{tot} [%]	$\eta_{\text{tot}} = \frac{W_{\text{EL,TOT,CL-ON}} + \dot{m}_{\text{DME}} \cdot \text{LHV}_{\text{DME}} + \dot{m}_{\text{METHANOL}} \cdot \text{LHV}_{\text{METHANOL}} + \dot{m}_{\text{SYN-DUCT}} \cdot \text{LHV}_{\text{SYN-DUCT}}}{\dot{m}_{\text{bio-meth,tot}} \cdot \text{LHV}_{\text{METHANE}}}$	66.13

Table 44: Results of the simulation of the new plant

A comparison between the solar energy supplied polygeneration plant, the new plant and the plant of Farooqui et al. [4] at steady state conditions is made in Table 45:

	New Plant without solar energy integration	Farooqui et al. [4]	Plant with CSP and the CL in ON state	Plant with CSP and the CL in off state
NG feed [ton/h]	83.276	25.20	55.80	0
$W_{\text{el,net}}$ [MWe]	119.720	102.90	6.17	28.96
W_{th} [MWt]	0	0	111.97	35.82
\dot{m}_{DME} [kg/s]	6.0029	2.15	6.18	0
\dot{m}_{MeOH} [kg/s]	1.3163	0.03	0.71	0
Syngas [kg/s]	23.4340	0	19.68	0
Captured CO ₂ to be sequestered [kg/s]	14.10	8.62	0	0
η_{tot} [%]	66.13	50.21	62.56	59.08

Table 45: Comparison between the solar fed plant, the new plant and the plant of Farooqui et al. [4] at steady state conditions

The following table shows the comparison between the same plants on yearly basis, which is necessary to better take into account the inputs and outputs of the solar-aided polygeneration plant:

	New Plant without solar energy integration	Farooqui et al. [4]	Present study
NG feed [kton/year]	729.497	220.75	102.30
$W_{el,net,average}$ [MWe]	119.72	102.90	24.19
$W_{th,average}$ [MWt]	0	0	51.76
\dot{m}_{DME} [kton/year]	189.307	67.80	40.79
\dot{m}_{MeOH} [ton/year]	41510.84	946.08	4686.43
Captured CO₂ to be sequestered [kton/year]	444.658	271.84	0
Syngas [kton/year]	739.014	0	129.90
$\eta_{tot,ave}$ [%]	66.13	50.21	59.82

Table 46: Comparison of the yearly average outputs of the three plants

Comparing the three plants, the new one is the best from the point of view of electricity, DME, methanol and syngas production. However, there is a much higher amount of biomethane consumption. A portion of this biomethane is subjected to the oxyfuel combustion for heat production and, at the output of this unit, there is sequestered CO₂ (after its separation from water) to be stored properly. This is an important point to highlight because both Farooqui et al.'s plant and the new studied plant have the not negligible issue of CO₂ sequestration, which has to be done carefully not to contribute to the greenhouse effect. Additionally, there is not the bulk of the gas turbine as in Farooqui et al. [4], but there is the presence of an Air Separation Unit and additional oxyfuel combustion units. This plant is much more complex than the previous presented and studied. The biomethane requirement of the new plant could be reduced eliminating the reforming unit, but, in this way, the CO₂ produced by the plant increases. This happens because, beyond the CO₂ production from the biomethane oxyfuel combustion, there also are the portions of CO₂ from the distillation unit and the SOFC, which are not converted into syngas. The lack of syngas as an additional plant output and the necessity to sequester this amount of CO₂ produces a large decrease of the plant efficiency (even if the produced electric power is the highest). The results of the simulation of the new plant without the reforming unit are shown in the following table:

	Equations	New Plant without solar energy and reforming unit
NG feed [ton/h]	$\dot{m}_{BIO-METH-TOT} = \dot{m}_{BIO-METH-THERMAL-TOT} + \dot{m}_{BIO-METH-REDUCTION}$	48.54
W_{net} [MW]	$W_{net} = W_{el,SOFC} + \sum_{PLANT\ COMPONENTS} W_{EL} - W_{el,ASU}$	144.38
\dot{m}_{DME} [kg/s]	-	2.6229
\dot{m}_{MeOH} [kg/s]	-	0.3077
Syngas [kg/s]	-	0

Captured CO ₂ to be sequestered [kg/s]	$\dot{m}_{CO_2} = \dot{m}_{BIO-METH-THERMAL-TOT} \cdot PM_{CO_2} + \dot{m}_{CO_2, \text{distillation unit and SOFC}}$	25.29
η_{tot} [%]	$\eta_{tot} = \frac{W_{EL,TOT,CL-ON} + m_{DME} \cdot LHV_{DME} + m_{METHANOL} \cdot LHV_{METHANOL}}{m_{bio-meth,tot} \cdot LHV_{METHANE}}$	35.6

Table 47: New plant without reforming unit at steady-state

From a purely planning point of view, there is not an optimal plant solution, the choice depends on the main objective of the plant. In the project and installation of a polygeneration plant, it is important to fix:

- 1) initial capital availability;
- 2) net electricity/thermal power requirement, DME, methanol and syngas requirement;
- 3) availability of biomethane. To avoid to contribute to the carbon depletion problem, the methane streams entering in the plant should have a biological origin;
- 4) possibility to execute a sure and permanent carbon capture and sequestration or storage for further uses (e.g. in an electrolyzer or chemicals production);
- 5) space availability (the solar field of the first polygeneration system is very bulky, a wide extension of land is required);
- 6) location of the plant (a gas turbine has moving parts that make noise, the solar field could be a problem for the landscape).

Once the purposes of the system are fixed, the plant can be projected and installed. Considering the three plants analysed in this work, different requirements can be defined:

- 1) if there is the necessity of a medium-size plant ($W_{el, \text{average requirement}} < 50$ MW) to be installed in a location with a high solar energy and space availability, the best choice would be the first analysed polygeneration system with CSP integration and without CO₂ production;
- 2) if a large-size plant ($W_{el, \text{average requirement}} > 100$ MW) is required and a high amount of biomethane is available to feed the system, the best system is the new analysed plant with the integration of the reforming unit as long as a proper sequestration of the produced CO₂ can be executed;
- 3) if a large-size plant ($W_{el, \text{average requirement}} > 100$ MW) is still required, but there is not the availability of a so large amount of biomethane to feed the system, the best solution is the new analysed system without the integration of the reforming unit. However, in this last case, it is important to have a proper and much larger storage system for the captured and sequestered CO₂.

From the point of view of the production of the fuel, the optimal plant is the new system without solar energy integration but with the reforming unit; the other two systems are more or less comparable.

6.6. Applications of the useful outputs of the plant

The analysed polygeneration plant produces different relevant useful outputs:

- electric power;
- steam;
- dimethyl ether (DME);
- syngas;
- methanol.

Electric power can be directly used by the user to satisfy his needs without an intermediate process, while the syngas applications are already listed in [Chapter 2](#). In the following paragraphs, a more detailed evaluation of the applications of steam, methanol and DME is executed.

6.6.1. Steam applications

Steam is widely used in the industry. Its main application is the production of electricity in a Rankine cycle as shown in *Figure 75*:

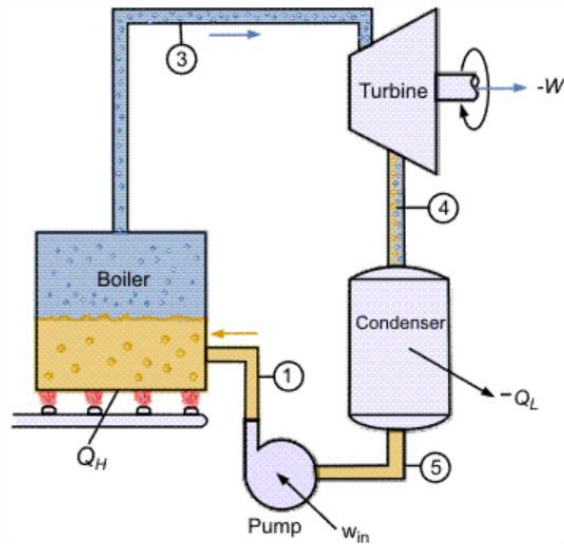


Figure 75: Rankine cycle

However, there also are uses of steam in the industry which extend far beyond the electricity production, such as [77]:

- 1) heating/sterilization;
- 2) propulsion/drive;
- 3) motive;
- 4) atomization;
- 5) cleaning;
- 6) moisturization;
- 7) humidification.

6.6.2. Methanol: properties and applications

Methanol (CH_3OH) is the simplest alcohol consisting of a methyl group (CH_3) linked to a hydroxy group (OH). At the beginning, its production took place through the distillation of wood, while the modern method to produce it is based on the direct combination of carbon monoxide and hydrogen (syngas) in the presence of a catalyst. Pure methanol can be used in the synthesis of chemicals: synthetic dyestuffs, resins, pharmaceuticals and perfumes. Methanol is also used in automotive antifreeze, in rocket fuels and as a general solvent. Methanol also is a high-octane, clean-burning fuel that is a potentially important substitute for gasoline in automotive vehicles. It is a colourless liquid that boils at $64.96\text{ }^\circ\text{C}$ and solidifies at $-93.90\text{ }^\circ\text{C}$; it forms explosive mixtures with air and burns with a nonluminous flame. Methanol is completely miscible in water and it has an odour that is similar to ethyl alcohol, but it is a dangerous poison; many cases of blindness or death have been caused by drinking mixtures containing it [78].

6.6.3. Dimethyl ether: properties and applications

Due to the continuous increasing problems of environmental pollution, energy security and future oil supplies, the global community is looking for nonpetroleum based alternative fuels. One possible solution is the use of fuels derived by natural gas, biomass and coal. Different possible fuel candidates are considered (i.e. methane, methanol, ethanol and Fischer–Tropsch fuels), but dimethyl-ether seems to have the largest potential impact on society, so it should be considered as the fuel that could eliminate the dependency on petroleum. DME has the chemical formula CH_3OCH_3 and its physical properties are very similar to those of liquefied petroleum gases (LPG, i.e. propane and butane).

	Methane	Methanol	Dimethyl ether	Ethanol	Gasoline	Diesel
Formula	CH_4	CH_3OH	CH_3OCH_3	$\text{CH}_3\text{CH}_2\text{OH}$	C_7H_{16}	$\text{C}_{14}\text{H}_{30}$
Molecular weight (g mol^{-1})	16.04	32.04	46.07	46.07	100.2	198.4
Density (g cm^{-3})	0.00072 ^a	0.792	0.661 ^b	0.785	0.737	0.856
Normal boiling point ^c ($^{\circ}\text{C}$)	-162	64	-24.9	78	38–204	125–400
LHV ^d (kJ cm^{-3})	0.0346 ^a	15.82	18.92	21.09	32.05	35.66
LHV (kJ g^{-1})	47.79	19.99	28.62	26.87	43.47	41.66
Exergy ^e (MJ L^{-1})	0.037	17.8	20.63	23.1	32.84	33.32
Exergy ^e (MJ kg^{-1})	51.76	22.36	30.75	29.4	47.46	46.94
Carbon Content ^d (wt.%)	74	37.5	52.2	52.2	85.5	87
Sulfur content ^d (ppm^f)	~7–25	0	0	0	~200	~250

^a Values per cm^3 of vapor at standard temperature and pressure.

^b Density at $P = 1 \text{ atm}$ and $T = -25^{\circ}\text{C}$.

^c Data reproduced from reference [2].

^d Data reproduced from reference [1].

^e Data reproduced from reference [3].

^f Mass basis.

Figure 76: Comparison of dimethyl ether's physical and thermo-physical properties to commonly used fuels [79]

As regards the environmental and health impacts, DME is a volatile organic compound but it is:

- non-carcinogenic;
- non-teratogenic;
- non-mutagenic;
- non-toxic.

In addition, in *Table 48*, global warming potentials of carbon dioxide, methane and dinitrogen oxide are listed and it can be seen that dimethyl ether is environmentally benign.

	Time horizon		
	20 years	100 years	500 years
DME ^a	1.2	0.3	0.1
CO_2 ^b	1	1	1
CH_4 ^b	56	21	6.5
N_2O ^b	280	310	170

^a Data reproduced from reference [80]

^b Data reproduced from reference [81]

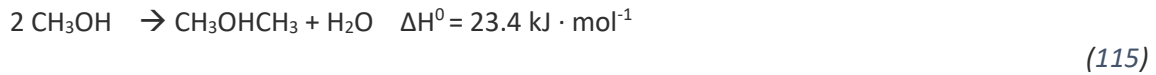
Table 48: Global Warming Potentials

Generally, DME is produced through a two-step process in which syngas is converted in methanol (reaction generally catalysed by Co) and then methanol is dehydrated (reaction generally catalysed by ZnO) to obtain dimethyl ether, as follows:

METHANOL SYNTHESIS)



METHANOL DEHYDRATATION)



WATER GAS SHIFT, SIDE REACTION)



NET REACTION)



As a result, methanol and, consequently, DME are not natural resources, so their prices depend on the price of the feedstock from which the syngas is produced (generally natural gas). As per long term future predictions, both diesel and natural gas prices have been projected to rise at an equal steady rate ([82], [83]), so relative economic competitiveness of DME and methanol concerning with diesel will be present. Another important issue is the supply of DME to the user. To distribute an alternative fuel to the user, an infrastructure for the ocean transport, land transport and refuelling stations may be needed. Based on the considered fuel, existing infrastructures can be used after some modifications or as they are or new infrastructures have to be built. Building a new infrastructure requires time and large amounts of capital. Since DME has properties which are similar to those ones of LPG fuels, it can be transported and distributed through the existing land-based and ocean-based LPG infrastructures with minor modifications to the pumps, seals, and gaskets. Worldwide, there are numerous refilling stations for LPG, so a transitioning to dimethyl ether could be less costly than building a completely new infrastructure as for hydrogen; additional refuelling stations could be built as the demand for dimethyl ether increases. As previously written, dimethyl ether can be used as a diesel substitute, even though DME has a lower LHV than conventional diesel and its use requires pressurization to maintain it in a liquid state at ambient conditions. The advantages of dimethyl ether over conventional diesel include decreased emissions of NO_x, SO_x, particulate, hydrocarbons and carbon monoxide and its combustion does not produce soot. However, the use of DME in a CIDI engine requires a new storage system and a new fuel delivery system, while the engine itself does not need modification. These variations have to be executed to achieve an equivalent driving range as that of a diesel-fed CIDI engine because, due to the lower energy density of DME compared with diesel fuel, a DME fuel storage tank has to be twice the size of a conventional diesel fuel tank. In addition, the most challenging aspects of a DME engine are related to its physical properties and not to its combustion characteristics. The viscosity of DME is lower than that of diesel by a factor of about 20; causing an increased amount of leakage in pumps and fuel injectors. There also are lubrication issues with DME; resulting in premature wear and eventual failure of pumps and fuel injectors, so additives have been used to increase the lubricity of DME. Another solution to avoid these variations on the existing systems and to make DME utilization more suitable for conventional engines (and, accordingly, for a short term applicability and economic viability of DME) could be the mixture of DME with conventional automotive fuels. Other applications of dimethyl ether are:

CASE STUDY: POLYGENERATION PLANT

- 1) residential fuel. Liquefied petroleum gases are mainly used as residential fuels for heating and cooking. Since DME has methods of storage and handling which are similar to those of LPG fuels, DME itself can replace LPG fuels;
- 2) power generation via DME-fired turbines with high efficiency and low emissions of NO_x and CO compared to methane and liquid naphtha;
- 3) production of hydrogen-rich fuel-cell feeds with hydrogen yields equivalent to those of methanol at comparable operating temperature;
- 4) raw material for the synthesis of aromatics, gasoline, olefins and other chemicals.

7. FOCUS ON THE CHEMICAL LOOPING MODEL

The present study simulates the $\text{CeO}_2/\text{Ce}_2\text{O}_3$ chemical looping through the use of two Gibbs reactors, which can be considered as ideal fluidized bed reactors. Setting the temperature, pressure and mass balance, RGIBBS reactors evaluate the most stable phase combination of the reactants/products, obtained through chemical reactions, where the Gibbs free energy of the reaction itself reaches its minimum value. As a result, a thermodynamic study of the cycle is executed, without considering all those factors which could be noticed in real reactions. These factors concern the kinetics of the reaction itself and they could be related to the effects of:

- 1) particle size;
- 2) mass flow rates and concentration of the reactants;
- 3) porosity of the particles;
- 4) presence of a catalyst;
- 5) temperature (a higher temperature determines a higher probability of energetic collisions between molecules);

on the reaction yields and evolution. For these reasons, it is not possible to obtain a strict validation of the CL model of the present study executing real chemical reactions because the results obtained from the model itself cannot be reached in real systems due to the limitations imposed by the kinetics of the reactions.

7.1. Thermodynamic vs kinetics

This discrepancy between the thermodynamic simulation and real chemical reactions can be highlighted through the comparison between the results obtained from the present model and the experimental results on the combined ceria reduction and methane reforming in a solar-driven particle-transport reactor by Welte, Warren and Scheffe [84]. Since the CL of this study is simulated in reactors which could be assimilated to ideal fluidized bed, the study of Welte et al. [84] is chosen because it is an example of what could happen in a real fluidized bed, shown in [Figure 77](#). However, the experiment is executed by Welte, Warren and Scheffe at a temperature equal to 1302°C , which is different from the temperatures chosen in this study. Thus, this new temperature is considered for the comparison of the model results and the experimental studies in the literature.

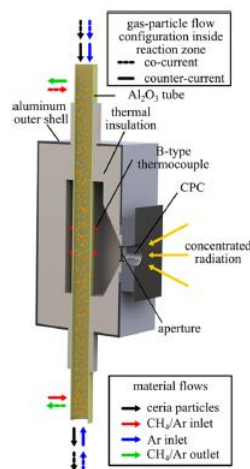


Figure 77: Schematic of the solar particle-transport reactor of the study of Welte, Warren and Scheffe [84]. Material flows are indicated by the coloured arrows for either co-current (dashed) or counter-current (solid) flow configuration.

Reduction reaction set up		
Temperature (°C)	1303° C	
$n_{\dot{C}eO_2} \left[\frac{mmol}{min} \right]$	44.2	
$n_{\dot{C}H_{4,0}} \left[\frac{mmol}{min} \right]$	9	
Products composition at the steady-state		
Component	Present study	Welte, Warren and Scheffe [84]
$n_{\dot{H}_2} \left[\frac{mmol}{min} \right]$	10.85	14
$n_{\dot{C}O} \left[\frac{mmol}{min} \right]$	7.49	6
$n_{\dot{C}O_2} \left[\frac{mmol}{min} \right]$	1.51	0.24
$n_{\dot{H}_2O} \left[\frac{mmol}{min} \right]$	6.25	0.75
$n_{\dot{C}H_4} \left[\frac{mmol}{min} \right]$	0	1.4
$n_{\dot{C}} \left[\frac{mmol}{min} \right]$	0	1.2
Methane conversion		
$x_{CH_4} = 1 - \frac{n_{\dot{C}H_4}}{n_{\dot{C}H_{4,0}}}$	1	0.85

The main differences between the thermodynamic simulation and real experiments stay in:

- 1) absence of the carbon deposition phenomenon in the model of the present study. Thermodynamically, for carbon deposition, it is necessary to have methane to ceria feed ratios above 1 and a temperature above 900 °C [48]. Subsequently, this phenomenon increases with higher molar flows of methane and temperature. This is important in prevision of the further oxidation of the just reduced ceria. In this second step, steam and carbon dioxide preferentially react with solid carbon and this causes the metal oxide to remain at a reduced state, as shown in [Chapter 3.3.2.2.4](#);
- 2) much higher methane conversion in the ideal model of this study. Consequently, it is chosen to execute a comparison of the Aspen Plus model of the CeO₂/Ce₂O₃ chemical looping, coupled with bio-methane reforming, with data of other similar thermodynamic models in the literature to better evaluate the performances of the present study model.

7.2. Comparison between the model of this study and other models in the literature

7.2.1. Reduction reaction

The operating conditions of the solar aided chemical looping which works in the polygeneration plant analysed in the present study are selected mainly considering the thermodynamic simulation studies on this ceria cycle of Farooqui et al. [48]. In [Table 49](#), a comparison between the syngas composition obtained from the reduction reactor of the CL of the present study, at the chosen operating conditions of the system, and the results of Farooqui et al. [48] is executed and agreement between the data is obtained.

Reduction reaction, P= 1 bar		Farooqui et al. [48]	Present study
Operating conditions	Temperature	900-950 °C	900 °C
	CH ₄ /CeO ₂	0.7-0.8	0.8
Produced syngas	H ₂	63%	55%
	CO	31%	31%

Table 49: Comparison of the thermodynamic results of the model of this study with the results reported by Farooqui et al. [48] for the reduction of ceria with methane at the chosen operating conditions of the solar aided CL

The obtained thermodynamics results from the present model are further compared to the results of ceria reduction with methane as presented by Warren et al. [85]. The following *Table 50* shows the thermodynamic results of the production of syngas and other gaseous components at the temperatures of 900 and 1000 °C and 0.25 mol of CH₄/ mol CeO₂ and agreement between the results of the model of the present study and those obtained in literature is shown:

Reduction reaction, CH ₄ /CeO ₂ = 0.25 P= 1 bar					
Temperature (°C)	Mole fraction of exit gas				
	H ₂	CO	CH ₄	H ₂ O	CO ₂
900 °C					
Warren et al. [85]	0.718	0.273	0.004	0.004	0
Farooqui et al. [48]	0.655	0.329	0.006	0.009	0.001
Present study	0.585	0.400	0.007	0.009	0.004
1000°C					
Warren et al. [85]	0.699	0.301	0	0	0
Farooqui et al. [48]	0.639	0.325	0	0.028	0.008
Present study	0.572	0.400	0	0.028	0.010

Table 50: Comparison of the thermodynamic results of the model of this study with the results reported by Warren et al. [85] and by Farooqui et al. [48] for the reduction of ceria with methane at different operating conditions

7.2.2. Oxidation reaction

For the oxidation reaction, less data are available to validate the model of the present study. Farooqui et al. [48] realized a model of the chemical looping of ceria coupled with methane reforming in which the same operating conditions (900°C) of the solar aided chemical looping analysed in the present study were considered. In *Table 51* the comparison between the obtained syngas composition at the outlet of the oxidation reactor of the present study and of Farooqui et al. [48] analysis is shown considering:

- 1) two different working temperatures of the oxidation reaction: 900°C and 1000°C;
- 2) different waste gas (equimolar mixture of CO₂ and H₂O) flows 0.5, 0.75 and 1.

Agreement between the data is obtained.

Oxidation reaction, $\dot{n}_{\text{CeO}_2} = 0.5 \frac{\text{kmol}}{\text{h}}$, P= 1 bar					
Temperature (°C)	Waste gas flow $\left[\frac{\text{kmol}}{\text{h}}\right]$	Mole fraction of exit gas			
			H ₂	CO	Other gases + CeO ₂ residuals
900°C	0.5	Farooqui et al. [48]	0.440	0.450	0.110
		Present study	0.406	0.411	0.183
	0.75	Farooqui et al. [48]	0.280	0.320	0.400
		Present study	0.280	0.303	0.417
	1	Farooqui et al. [48]	0.210	0.240	0.550
		Present study	0.212	0.238	0.550
1000°C	0.5	Farooqui et al. [48]	0.435	0.455	0.110
		Present study	0.400	0.407	0.193
	0.75	Farooqui et al. [48]	0.270	0.330	0.400
		Present study	0.267	0.316	0.417
	1	Farooqui et al. [48]	0.198	0.251	0.551
		Present study	0.197	0.253	0.550

Table 51: Comparison of the thermodynamic results of the model of this study with the results reported by Farooqui et al. [48] for the oxidation of ceria with H₂O and CO₂ at the chosen operating conditions of the solar aided CL

8. EXPERIMENTS AT THE ENVIRONMENT PARK

The initial idea was to practically test the solar aided chemical looping, studied in this work, in the receiver-reactor of the Dish system installed on the roof of the Energy Center. This could be done because, as shown in *Figure 53* [51], the measured operating temperatures of this Dish system reveal that, in certain periods of the year, in clear sky conditions and without considering effects of cloudiness and rainfall, the receiver-reactor can reach temperatures widely above 900°C (operating T of the isothermal CL in the present study). However, for these on-site tests, a very large amount of material is necessary, so they could not be realized due to the unavailability of a sufficient amount of cerium oxide. As a result, preliminary experiments on the chemical looping are realized in the test bench at the Environment Park, for which a much lower quantity of ceria is necessary. However, the microreactor in this test bench is a fixed bed reactor, thus it is not possible to directly compare the obtained experimental results with the chemical looping model of this study (realized in two ideal fluidized bed reactors).

8.1. Description of the test bench

The experimental tests are executed in a microreactor installed in the laboratory of Environment Park. A microreactor is a microstructured/microchannel reactor in which chemical reactions occur in a confined zone, in general with the shape of a microchannel. The microreactor used in the present study, shown in *Figure 78*, is from Carbolite Gero [86] and it could work in the range of temperatures between 30°C-1700°C at atmospheric pressure.



Figure 78: Carbolite Gero microreactor

It is a continuous flow reactor, this means that chemical reactions take place in a continuously flowing stream in the microchannel of the microreactor rather than in batch production. The microchannels are tubes in alumina (Al_2O_3), shown in *Figure 79*:



Figure 79: Microchannels in alumina

These tubes are installed in another concentric tube with a much higher diameter (tube-in-tube structure) and they are supported by a refractory material.

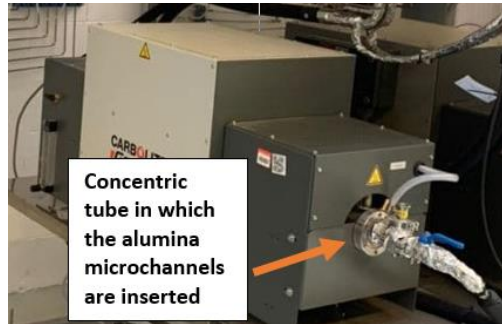


Figure 80: Location of the Alumina microchannels

In the middle of the tubes, particles of CeO_2 are inserted and maintained in place through the presence of quartz wool, to avoid the entrainment of these particles in the continuous flow of reactants.

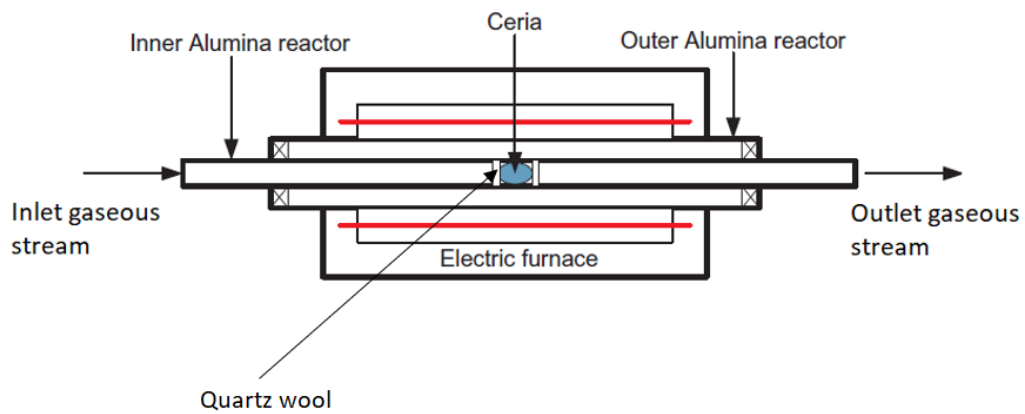


Figure 81: Scheme of the microreactor

These particles are placed in the microchannels in a granulated state, their mass is measured in the weight scale in [Figure 82](#) and the fulfilling of the tubes is executed in the case in [Figure 83](#) for security reasons.



Figure 82: Weight scale of the ceria particles



Figure 83: Case for the fulfilling of the tubes

Ceria particles must remain in place to guarantee:

- 1) the correct execution of the chemical looping;
- 2) the complete reduction/re-oxidation of the particles;
- 3) the production of a “pure gas” stream.

During the cycle, in the real microreactor, there are two main operations:

- 1) reduction of the CeO_2 particles. They are reduced when they are invested by the continuous flow of the CH_4 stream for a prolonged time interval. At the beginning of this interval, at the output of the microreactor, a gaseous flow mainly constituted of CH_4 should be obtained. Then, as the reduction of the particles of ceria proceeds, the output stream should be characterized by a decreasing fraction of CH_4 and an increasing fraction of syngas. At a certain point, the fraction of syngas should reach its highest value (peak when the complete reduction of ceria is reached). Continuing to send CH_4 to the micro-reactor, since the ceria particles are already reduced, at the output of the microreactor it could be re-obtained a large amount of CH_4 . At this point, a flow of N_2 for the cleaning of the reaction zone to avoid the formation of hot spots and explosive mixtures is sent. Thus, the oxidation reaction of Ce_2O_3 particles can occur;
- 2) the reduced particles should remain in place to be invested by the steam and carbon dioxide flux for another prolonged time interval that allows the production of another amount of syngas and the re-oxidation of the particles. As in the previous step, at the beginning, the output stream should be mainly constituted of vapour and CO_2 , then, as the oxidation proceeds, the amount of syngas in the outlet stream should increase until the complete oxidation of the particles is obtained.

Then, the cycle can restart. The composition of the streams exiting from the microreactor is analysed in the Emerson Gas Analyzer, shown in [Figure 84](#).



Figure 84: Emerson Gas Analyzer

The function of this component is based on the comparison of the physical properties of the entering stream with the properties of a reference material. Through this comparison, it is able to evaluate the molar fractions of the different components present in the stream. This composition is shown in the interface of the machine, which is the software “XStream”; in this software also the number and type of components of the inlet stream have to be set through the calibration process. The heating of the microreactor is executed through resistances in which current is made circulate. The regulation of the current is executed through a “power supply”, which is external than the microreactor and it is shown in *Figure 85*.



Figure 85: Power supply of the microreactor

The command of the power supply is executed through a software called “Euroterm iTools”. In this software:

- ramps;
- step of the ramp (speed at which the temperature should be increased/decreased);
- set point temperatures of the ramp;
- duration of the steady-state condition;

are defined. On the basis of these data, the value of the current that should circulate in the resistances is evaluated to establish a certain thermal energy production to supply the chemical reaction which takes place in the microreactor. The values inserted in this software should be identical to the values that are introduced in the software API M-IoT, which regulates the mass flow controllers of both the gaseous and liquid streams circulating in the microreactor. It is very important to have the coordination between these two softwares both in terms of time and reactions for the yield of the chemical looping e.g. methane has to be sent by the mass flow controller in the microreactor exactly when the power supply reaches the temperature of the reaction at the end of the ramp. As written before, the software API M-IoT commands the mass flow controllers of the streams (which regulate and measure the gaseous mass flows) entering in the microreactor. In addition, it also controls the switching-on and switching-off of the two three-ways valves included in the pipeline of the streams entering and exiting the microreactor.

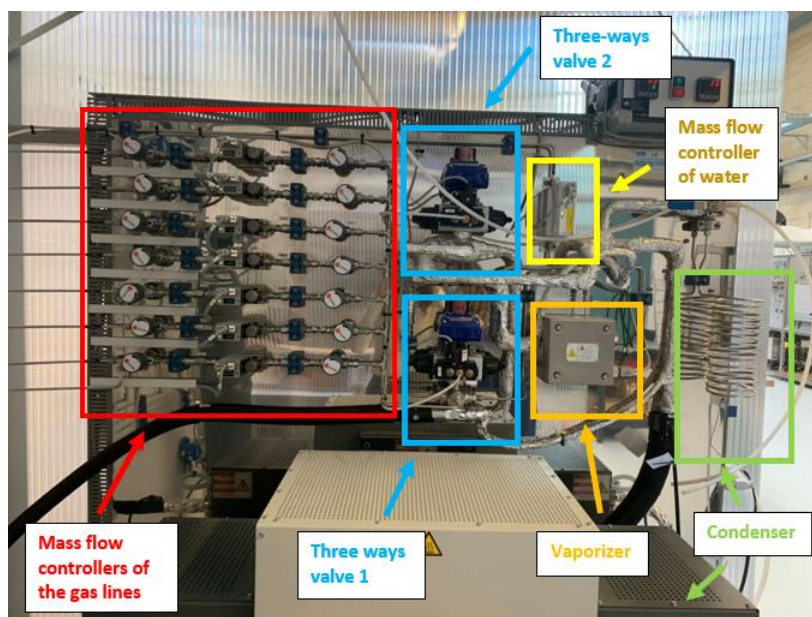


Figure 86: Pipeline of the streams entering/exiting the microreactor

The pipeline is characterized by a system for the production of vapour starting from demineralized water contained in a tank and 7 gas lines:

- 1) 5 lines directly connected to the laboratory gas lines (N_2 , CH_4 , CO , CO_2 , H_2). This connection is executed through pressure reducers installed on the wall (*Figure 87*), downstream the reducers there are the mass flow controllers of the bench;
- 2) 2 connected to cylinders under the hood. These gases are constituted by argon and gaseous mixtures and their pressure reducers are directly installed on the cylinder.

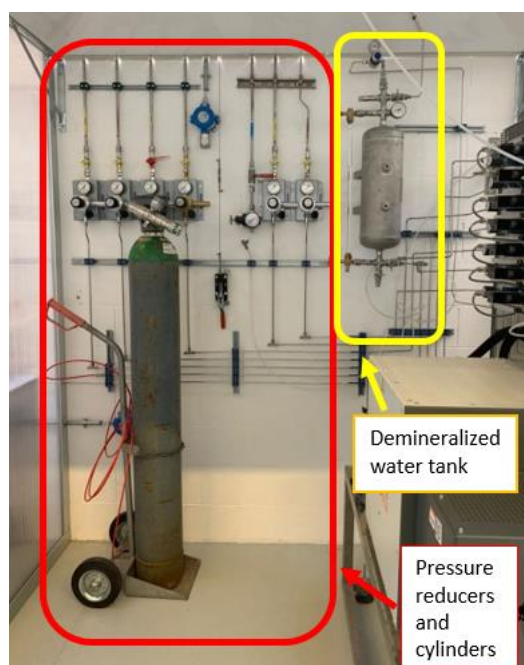


Figure 87: Pressure reducers, cylinders and demineralized water tank

The pressure of the gas lines is 2.5 bar, despite the line of N_2 which is at 5 bar because this gas is also connected to the water tank to maintain it under-pressure. Downstream the mass flow controllers, the 7 gas lines converge towards only one line, which is the line of the dry mixture. The pressure of this line is more or less the atmospheric pressure. This line of the 7 gases dry mixture is connected to the first three-ways valve (see *Figure 86*). This valve is an on-off type and allows to choose to:

- 1) feed the micro-reactor directly with the dry mixture;
- 2) humidify the mixture. In this case, the mixture is sent to the demineralized water evaporator where the gaseous mixture itself is mixed with steam, produced from the demineralized water. At the outlet of the evaporator, there is a heated pipe (it is heated to avoid the condensation of water) which is connected to the cold line of the first section of the three-ways valve. Downstream the junction between the two lines, there is the feeding of the second three-ways valve which allows to choose between two heated lines:
 - a) direct feeding of the microreactor;
 - b) by-pass of the microreactor.
 These two lines converge at the outlet of the microreactor in a heated line. A manual valve allows to choose to direct the mixture to the condenser or to the outlet line. Both these two lines can be connected to:
 - discharge line in the hood;
 - gas analyser. It is important to highlight that it can analyse only dry mixtures and its outlet is connected to the discharge line of the hood.

A more schematic representation of this architecture is given in *Figure 88*:

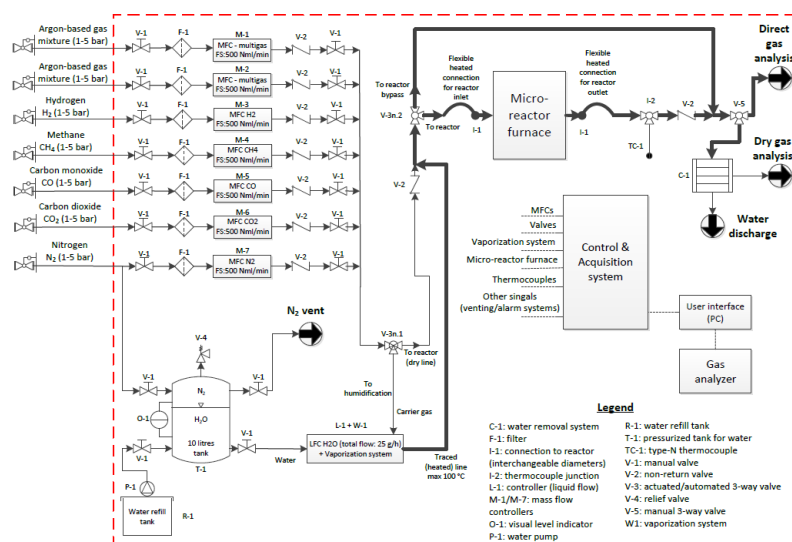


Figure 88: Scheme of the test bench

8.2. Experiments parameters and results

The microreactor of the Environment park is a fixed bed reactor, while the reactors used in this study for the modelling of the chemical looping are Gibbs reactors. These reactors could be assimilated to ideal fluidized bed reactors, thus it is not possible to recreate the reactions of the CL of the study in the real test bench. The main considered parameters are listed in the following table:

Temperature step ramp <i>(in Euroterm iTools)</i> $\left[\frac{^{\circ}\text{C}}{\text{min}}\right]$	20
GHSV $\left[\frac{\text{dm}^3}{\text{h}\cdot\text{g}}\right]$	28.8
Ceria mass [g]	0.5
$\frac{\text{CH}_4}{\text{CeO}_2}$	0.76
Total volume flow diluted in N₂ <i>(both in the reduction and the oxidation)</i> $\left[\frac{\text{ml}}{\text{min}}\right]$	320
Temperature <i>(both in the reduction and in the oxidation)</i> $[^{\circ}\text{C}]$	900
Pressure <i>(both in the reduction and in the oxidation)</i> $[\text{bar}]$	1

Table 52: Main parameters of the experiments in Environment Park

One steady-state cycle is constituted of different steps, as shown in *Figure 89*:

- 1) stabilization (10 min): N₂ is made circulate in the reactor to create inert zones and avoid the presence of hot spots or explosive mixtures;
- 2) stabilization of the reduction (5 min): a molar flow equal to the molar flow of the reactants used in the reduction reaction is made circulate in the gas analyser to calibrate this component. This flow by-passes the microreactor;
- 3) reduction reaction (30 min): CH₄ circulates in the microchannel to reduce the particles of ceria. Reduction takes place after a very small-time interval. However, at the output of the reactor, it is not detected the presence of CO. This could be due to different reasons:
 - in the “competition” between CDS and WS, water shift prevails;
 - carbon deposition;
 - CO remains involved in other reactions in the system (as it can be read in [Chapter 3.3.2.2.4](#));
 - the gas analyser is set at a too high scale concerning the CO;
- 4) stabilization with the switching on of the evaporator (10 min): N₂ is sent to the reactor, but it also passes through the evaporator, which is switched on at 120°C;
- 5) stabilization of the oxidation (5 min): a molar flow equal to the molar flow of reactants used in the oxidation reaction (but in the dry form) is made circulate in the gas analyser to calibrate this component. This flow by-passes the microreactor but passes through the evaporator;

- 6) oxidation (15 min): the flow of steam and carbon dioxide circulates in the reactor and oxidizes ceria particles. Even in this case, the reaction occurs very fast but CO is not detected at the output of the reactor itself, probably for the same reasons of the reduction reaction.

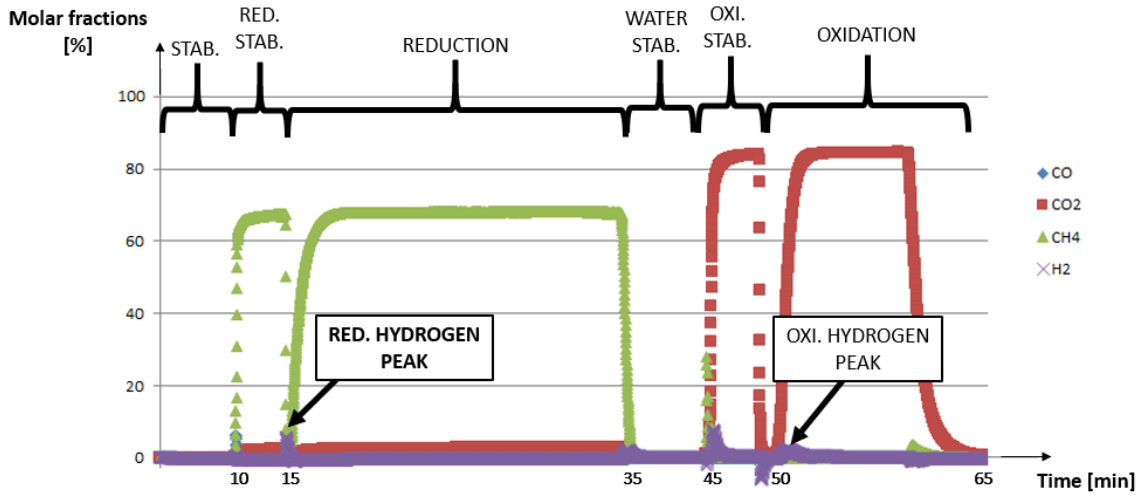


Figure 89: Example of one cycle of the experiment

The peak of H_2 in the reduction, reaction is shown in Figure 90.

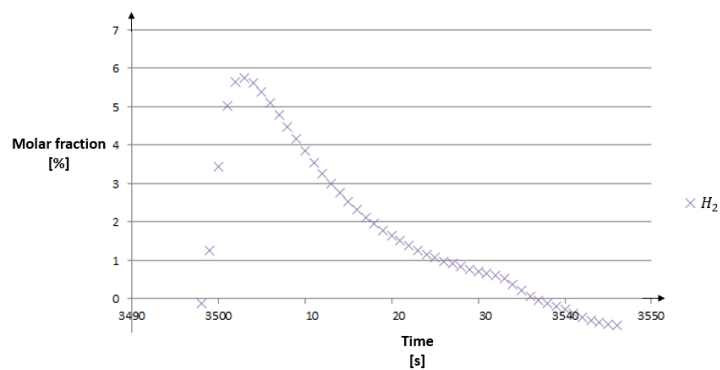


Figure 90: Peak of H_2 in the reduction

Hydrogen production in the reduction reaction	
H_2 [mol]	0.00029
$\frac{H_2}{CeO_2} \left[\frac{mol}{g} \right]$	0.00058
$\frac{H_2}{CeO_2} \left[\frac{g}{g} \right]$	0.00116

Table 53: Hydrogen in the reduction reaction

The peak of H_2 in the oxidation reaction is shown in Figure 91:

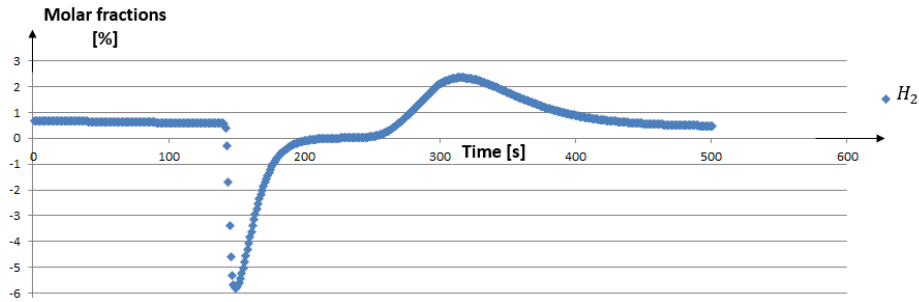


Figure 91: Peak of H_2 in the oxidation reaction

Hydrogen production in the oxidation reaction	
H_2 [mol]	0.00067
$\frac{H_2}{CeO_2} \left[\frac{mol}{g} \right]$	0.00134
$\frac{H_2}{CeO_2} \left[\frac{g}{g} \right]$	0.0027

Table 54: Hydrogen in the oxidation reaction

These results could also be affected by the moving of the particles in the microchannel because, during the experiment, the quartz wool was not able to correctly maintain in place the particles themselves. However, it is important to highlight that the peaks of production of H_2 are pretty evident, so the reactions at these temperature and pressure occur even in this reactor. These experiments could be considered as preliminary studies, which could be elaborated in the future.

9. CONCLUSIONS

The aim of this study is to evaluate the performance of a polygeneration plant for the production of electricity, heat, DME, methanol and syngas with the integration of a solar energy fed $\text{CeO}_2/\text{Ce}_2\text{O}_3$ chemical looping coupled with the partial oxidation of biomethane. Different advantages of this system can be defined:

- 1) sustainability and green fuels and electric/thermal power production. The plant only uses renewable energy sources (solar energy and biomethane), so it contributes to the decarbonization of the industrial sector and the solution of the carbon depletion problem;
- 2) no CO_2 emissions. The whole amount of produced CO_2 in the plant is exploited in the different sections of the system. Carbon Capture and Utilization is applied both in the oxidation reactor of the chemical looping and in the reforming unit. This characteristic makes this system very versatile also while still relying upon power production from fossil fuels. In fact, the SOFC unit of the system could be substituted by an existing fossil fuel power plant, whose exhausts can be sent to the oxidation reaction of the CL and the reforming unit. In this way, the CO_2 produced by these existing systems is utilized to produce useful outputs, thus contributing to the reduction of the CO_2 emissions and the greenhouse effect;
- 3) production of innovative and green fuels (DME and methanol) that can contribute to the reduction of the dependence on liquid petroleum gases. Particularly, DME has physical properties which are very similar to LPGs and it also has low environmental and health impacts;
- 4) use of SOFC stacks for power production. SOFCs have much higher efficiencies than thermal machines, they also are less bulky and, due to the absence of moving parts, they are not noisy;
- 5) production of syngas as an energy vector to store solar energy. The solar energy fed chemical looping shows a way to solve the problem of intermittence of solar energy. The syngas stream is produced during those periods of the year in which there is a sufficiently high irradiance, then it can be stored and used on-demand. In this study, the syngas is stored in an AISI315L tank to be used in the SOFC stacks continuously during the year.

However, as it can be seen in [Chapter 6.5](#), the coupling of the chemical looping with solar energy produces the intermittence in the operation of the CL itself. Consequently, the solar fed CL produces a much lower amount of syngas compared to the same chemical looping supplied by a continuous energy source. In this regard, other two plants in which the chemical looping is supplied by the thermal energy produced by the SOFC stacks are evaluated in [Chapter 6.5.2](#). Because of the continuous operation of the CL throughout the year, these two other plants revealed to produce much higher amounts of electric power and green fuels. However, they also demonstrated to be more complex because the absence of solar energy has to be covered by the introduction of heat from the external environment. This heat can be supplied by an oxyfuel combustion of biomethane. Two consequences of the introduction of the oxyfuel combustion units have to be considered:

- 1) higher biomethane consumption of these two systems compared to the solar energy fed plant;
- 2) CO_2 production in the oxyfuel combustion units. This leads to the issue of the sequestration of the produced and properly captured CO_2 permanently or for further uses (e.g. electrolyzer, chemicals production).

From a planning point of view, there is not the best plant solution. The choice of the plant to be installed is strictly linked to the purpose of the plant itself, in terms of electrical and thermal energy production, fuel production, investment costs.... However, in the view of decarbonization, energy transition and reduction of greenhouse emissions, the best system to be installed would be the polygeneration plant with the integration of a solar fed chemical looping because it is a sustainable and green solution without any issue of sequestration of CO_2 to be evaluated. In the case in which a higher amount of electricity is required, it could be thought to:

- 1) increase the size of the chemical looping and, consequently to increase the CSP system in which the CL takes place, to produce a higher amount of syngas to continuously feed the SOFC;
- 2) realize a solar thermal energy storage system to supply heat to the air entering in the SOFC when the CL does not operate.

Additional studies could be made on this system such as:

- evaluation of a kinetic model for the chemical looping;
- an exergetic and economic analysis to evaluate its Net Present Value and the Pay Back Time;
- a more detailed evaluation of its environmental impact;
- further experiments and applications of the chemical looping.

REFERENCES

- [1] "www.ipcc.ch/2014/," [Online].
- [2] "www.lifegate.it/cambiamenti-climatici-cause-conseguenze/," [Online].
- [3] https://ec.europa.eu/clima/policies/international/negotiations/paris_it.
- [4] A. Farooquia, F. Di Tomaso, A. Bosec, D. Ferrero, J. Llorca, M. Santarelli, "Techno-economic and exergy analysis of polygeneration plant for power and DME production with the integration of chemical looping CO₂/H₂O splitting," *Energy Conversion and Management*, vol. 186, p. 200–219, 2019 .
- [5] "fuergy.com/en/blog/the-duck-curve-why-renewables-still-rely-on-fossil-fuel-backups/," [Online].
- [6] M. R. S. C. Agrafiotis, "A review on solar thermal syngas production via redox pair-based water/carbon dioxide splitting thermochemical cycles," *Renewable and Sustainable Energy Reviews*, vol. 42, pp. 254-285, 2015.
- [7] C. Agrafiotis, M. Roeb, C. Sattler, "A review on solar thermal syngas production via redox pair-based water/carbon dioxide splitting thermochemical cycles," *Renewable and Sustainable Energy Reviews*, vol. 42, p. 254–285, 2015.
- [8] M. Enjavi-Arsanjania, K. Hirbodnia, M. Yaghoubi, "Solar Energy Potential and Performance Assessment of CSP Plants in Different Areas of Iran," *Energy Procedia*, vol. 69, pp. 2039-2048, 2015.
- [9] "<https://ingvambiente.com/2020/01/14/come-fatto-il-sole/>," [Online].
- [10] "<https://solarsystem.nasa.gov/solar-system/sun/by-the-numbers/>," [Online].
- [11] "<https://energyeducation.ca/encyclopedia/Sun/>," [Online].
- [12] M. Günther, *Advanced CSP Teaching Materials*, vol. 2, 2011.
- [13] "<https://www.ifp.cnr.it/la-fusione-nucleare/>," [Online].
- [14] "https://www.nasa.gov/mission_pages/sunearth/science/solar-anatomy.html," [Online].
- [15] "<http://www.instesre.org/Solar/PyranometerProtocol/PyranometerProtocol.htm>," [Online].
- [16] "<https://www.enea.it/it/seguici/le-parole-dellenergia/radiazione-solare/quanta-energia-solare-arriva-sulla-terra/>," [Online].
- [17] J. Pye, "Dispense del corso di "Technology for renewable energy sources"," Politecnico di Torino, 2019.
- [18] M. Perino e G. Fracastoro, "Dispense del corso di "Technology for renewable energy sources"," Politecnico di Torino.
- [19] "<https://www.enea.it/it/seguici/le-parole-dellenergia/radiazione-solare/qualcosa-da-sapere-sul-sole-1/spettro-elettromagnetico-solare-e-assorbimento-in-atmosfera/>," [Online].
- [20] "<https://www.e-education.psu.edu/eme812/node/8>," [Online].
- [21] T. Crescenzi, M. Falchetta, A. Fontanella, E. Metelli, A. Miliozzi, F. Spinelli, L. Sipione, *Opportunità di applicazione delle tecnologie solari termodinamiche in Italia*, Frascati: ENEA, 2016.
- [22] A. Lanzini, T.G. Kreutz, E. Martelli, M. Santarelli, "Energy and economic performance of novel integrated gasifier fuel cell (IGFC) cycles with carbon capture," *International Journal of Greenhouse Gas Control*, vol. 26, pp. 169-184, 2014.
- [23] Y. An, T. Lin, F. Yu, Y. Yang, L. Zhong, M. Wu & Y. Sun , "Advances in direct production of value-added chemicals via syngas conversion," *Science China Chemistry*, vol. 60, pp. 887-903, 2017.
- [24] "<https://www.energy.gov/eere/fuelcells/hydrogen-production-photobiological/>," [Online].

- [25] H.I. Villafán-Vidales, C.A. Arancibia-Bulnes, D. Riveros-Rosas, H. Romero-Paredes, C.A. Estrada, "An overview of the solar thermochemical processes for hydrogen and syngas production: Reactord and facilities," *Renewable and Sustainable Energy Reviews*, vol. 75, pp. 894-908, 2017.
- [26] C. Graves, S.D. Ebbesen, M. Mogensen, K. S.Lackner, "Sustainable hydrocarbon fuels by recycling CO₂ and H₂O with renewable or nuclear energy," *Renewable and Sustainable Energy Reviews*, vol. 15, no. 1, pp. 1-23, 2011.
- [27] "<https://www.isprambiente.gov.it/it/servizi/registro-italiano-emissiontrading/contesto/protocollo-di-kyoto>," [Online].
- [28] A. Lanzini, "Dispense del corso "Polygeneration and Avanced Energy Systems"," Politecnico di Torino , 2019/2020.
- [29] R. J. Carrillo, J. R. Scheffe, "Advances and trends in redox materials for solar thermochemical fuel production," *Solar Energy* , vol. 156, p. 3–20 , 2017.
- [30] A. Meier, "The Zn-based Thermochemical Cycle based Thermochemical Cycle for Splitting H₂O and CO₂," Solar Technology Laboratory, Paul Scherrer Institute, 5232 Villigen PSI, Switzerland.
- [31] L. Xiao, S.Y. Wu, Y.R. Li, "Advances in solar hydrogen production via two-step water-splitting thermochemical cycles based on metal redox reactions," *Renewable Energy* , vol. 41, pp. 1-12 , 2012.
- [32] L. O. Schunk,P. Haeberling, S. Wepf, D. Wuillemin, A. Meier, A. Steinfeld, "A Receiver-Reactor for the Solar Thermal Dissociation of Zinc Oxide," *Solar Energy Engineering* , vol. 130, pp. 021009-1 , 2008.
- [33] S. Abanades, " CO₂ and H₂O reduction by solar thermochemical looping using SnO₂/SnO redox reactions: Thermogravimetric analysis," *International Journal of Hydrogen Energy* , vol. 37, pp. 8223-8231 , 2012.
- [34] M. Chambon, S. Abanades, G. Flamant, "Kinetic investigation of hydrogen generation from hydrolysis of SnO and Zn solar nanopowders," *International Journal of Hydrogen Energy* , vol. 34, pp. 5326-5336 , 2009.
- [35] T. Nakamura, "Hydrogen production from water utilizing solar heat at high temperatures," *Solar Energy*, vol. 19, no. 5, pp. 467-475, 1977.
- [36] F. Fresno, R. Fernández-Saavedra, M. B. Gómez-Mancebo, A. Vidal, M. Sánchez, M. I. Rucandio et al., "Solar hydrogen production by two-step thermochemical cycles: Evaluation of the activity of commercial ferrites," *International Journal of Hydrogen Energy* , vol. 34, no. 7, pp. 2918-24, 2009.
- [37] C. Agrafiotis, M. Roeb, C. Sattler, "A review on solar thermal syngas production via redox pair-based water/carbon dioxide splitting thermochemical cycles," *Renewable and Sustainable Energy Reviews*, vol. 42, pp. 254-285, 2015.
- [38] K. Otsuka, M. Hatano, A. Morikawa, "Hydrogen from water by reduced cerium oxide," *Journal of Catalysis*, vol. 79, pp. 493-496, 1983.
- [39] S. Abanades, G. Flamant, "Thermochemical hydrogen production from a two-step solar-driven water-splitting cycle based on cerium oxides," *Solar Energy* , vol. 80 , no. 12, pp. 1611-1623 , 2006.
- [40] E.A. Kümmerle, G. Heger, "The Structures of C-Ce₂O₃+ δ , Ce₇O₁₂, and Ce₁₁O₂₀," *Journal of Solid State Chemistry*, vol. 147, no. 2, pp. 485-500, 1999.
- [41] W. C. Chueh, Christoph Falter, M. bbott, D. Scipio, P. Furler, S. M. Haile, A. Steinfeld, "High-Flux Solar-Driven Thermochemical Dissociation of CO₂and H₂O Using Nonstoichiometric Ceria," *Science*, vol. 330, pp. 1797-1801 , 2010.

- [42] H.Kaneko, T.Miura, H.Ishihara, S.Taku, T.Yokoyama, H.Nakajima, Y.Tamaura , “ Reactive ceramics of CeO₂–MO_x (M=Mn, Fe, Ni, Cu) for H₂ generation by two-step water splitting using concentrated solar thermal energy,” *Energy*, vol. 32, no. 5, pp. 656-663 , 2007.
- [43] J. E. Miller, M. D. Allendorf, R. B. Diver, L. R. Evans, N. P. Siegel & J. N. Stuecker, “Metal oxide composites and structures for ultra-high temperature solar thermochemical cycles,” *Journal of Materials Science* , vol. 43, p. 4714–4728 , 2008.
- [44] S. Abanades, A. Legal, A. Cordier, G. Peraudeau, G. Flamant & A. Julbe, “Investigation of reactive cerium-based oxides for H₂ production by thermochemical two-step water-splitting,” *Journal of Materials Science*, vol. 45, p. 4163–4173 , 2010.
- [45] A. Le Gal A, S. Abanades, “Catalytic investigation of ceria zirconia solid solutions for solar hydrogen production,” *International Journal of Hydrogen Energy* , vol. 36, pp. 4739-4748, 2011.
- [46] Q. Meng, C. Lee, T. Ishihara, H. Kaneko, Y. Tamaura, “Reactivity of CeO₂-based ceramics for solar hydrogen production via a two-step water-splitting cycle with concentrated solar energy,” *International Journal of Hydrogen Energy* , vol. 36, pp. 13435-13441 , 2011.
- [47] Xxx Azharuddin; J. Llorca; A Bose; M. Santarelli, “System analysis of natural gas combined cycle (NGCC) integrated with kinetics-based chemical looping syngas production,” Faouzi Hidoussi, 2019.
- [48] A. Bose, A. Farooqui, D. Ferrero, M Santarelli, J. Llorca, “Thermodynamic assessment of non-catalytic Ceria for syngas production by methane reduction and CO₂+H₂O oxidation,” *Materials for Renewable and Sustainable Energy* , vol. 8, no. 5, 2019.
- [49] R. Bader, L. J. Venstrom, J. H. Davidson and W. Lipiński, “Thermodynamic Analysis of Isothermal Redox Cycling of Ceria for Solar Fuel Production,” *Energy Fuels*, vol. 27, no. 9, p. 5533–5544, 2013.
- [50] A. Bose, A. Farooqui, D. Ferrero, M. Santarelli & J. Llorca , “Thermodynamic assessment of non-catalytic Ceria for syngas production by methane reduction and CO₂ + H₂O oxidation,” *Materials for Renewable and Sustainable Energy* , vol. 8, no. 5, 2019.
- [51] Edoardo Montà, Davide Papurello, Massimo Santarelli, “Tesi di Edoardo Montà,” Politecnico di Torino , Marzo 2020.
- [52] “<https://elcogen.com/for-investors/how-sofc-can-change-the-world/>,” [Online].
- [53] M. Santarelli, “Dispense del corso "Polygeneration and Avanced Energy Systems",” 2019/2020.
- [54] Geert H. Graaf and Jozef G. M. Winkelman, “Chemical Equilibria in Methanol Synthesis Including the Water–Gas Shift Reaction: A Critical Reassessment,” *Industrial & Engineering Chemistry Research*, vol. 55, no. 20, p. 5854–5864, 2016.
- [55] Hyun Min Shim, Seung Jong Lee, Young Don Yoo, Yong Seung Yun & Hyung Taek Kim , “Simulation of DME synthesis from coal syngas by kinetics model,” *Korean Journal of Chemical Engineering*, vol. 26, no. 2009, pp. 641-648, 2009.
- [56] Fanxing Li Liang Zeng Luis G. Velazquez-Vargas Zachary Yoscovits Liang-Shih Fan, “Syngas chemical looping gasification process: Bench-scale studies and reactor simulations,” *AIChE*, vol. 56, no. 8, pp. 2186-2199, 2009.
- [57] D-Y Peng, DB Robinson, “ A new two-constant equation of state,” *Industrial & Engineering Chemistry Fundamentals*, vol. 15, pp. 59-64, 1976.
- [58] Amira M. Eltony, Hyesung G. Park, Shannon X. Wang, Jing Kong and Isaac L. Chuang, “Motional Heating in a Graphene-Coated Ion Trap,” *Nano Letters*, vol. 14, p. 5712–5716, 2014.
- [59] “<http://www.energymed.it/>,” [Online].
- [60] “arpae.it,” [Online].
- [61] May Issa, Corinne Petit, Alain Brillard, Jean-Franc,ois Brillhac, “Oxidation of carbon by CeO₂: Effect of the contact between carbon and catalyst particles,” vol. 87, p. 740–750, 2008.

- [62] aspentech, "Aspen Plus: Getting Started Modeling Processes with Solids".
- [63] "<https://www.thoughtco.com/type-316-and-316l-stainless-steel-2340262/>," [Online].
- [64] "<https://www.bloomenergy.com/datasheets/energy-server-es5-200kw/>," [Online].
- [65] D. C. B. T. K.L. Ng, "Kinetics and modelling of dimethyl ether synthesis from synthesis gas," *Chemical Engineering Science*, vol. 54, pp. 3587-3592, 1999.
- [66] R. S. Treptow, "Le Châtelier's principle: A reexamination and method of graphic illustration," *Journal of chemical education*, vol. 57, no. 6, pp. 417-420, 1980.
- [67] M. Pozzo, A. Lanzini, M. Santarelli, "Enhanced biomass-to-liquid (BTL) conversion process through high temperature co-electrolysis in a solid oxide electrolysis cell (SOEC)," *Fuel*, vol. 145, pp. 39-49, 2015.
- [68] K.L.Ng, D.Chadwick, B.A.Toseland, "Kinetics and modelling of dimethyl ether synthesis from synthesis gas," *Chemical Engineering Science*, vol. 54, no. 15-16, pp. 3587-3592, 1999.
- [69] K.M.Vanden Bussche, G.F.Froment, "A Steady-State Kinetic Model for Methanol Synthesis and the Water Gas Shift Reaction on a Commercial Cu/ZnO/Al₂O₃ Catalyst," *Journal of Catalysis*, vol. 161, no. 1, pp. 1-10, 1996.
- [70] Gorazd Bercic and Janez Levec, "Catalytic dehydration of methanol to dimethyl ether. Kinetic investigation and reactor simulation," *Industrial & Engineering Chemistry Research*, vol. 32, no. 11, p. 2478-2484, 1993.
- [71] Wei-Hsin Chen, "CO₂ conversion for syngas production in methane catalytic partial oxidation," *Journal of CO₂ Utilization*, vol. 5, pp. 1-9, 2014.
- [72] González-Vargas, M. J. Meléndez-Zaragoza, V. Collins-Martínez, A. López-Ortiz, "Thermodynamic Analysis and Process Simulation of Syngas Production from Methane using CoWO₄ as Oxygen Carrier," in *XVI International Congress of the Mexican Hydrogen Society*, 2017.
- [73] "solarpaces.nrel.gov/khi-solar-one/," [Online].
- [74] Juan Ignacio Burgaleta, Santiago Arias, Diego Ramirez, "Gemaspolar, the first tower thermosolar commercial plant with molten salt storage".
- [75] "www.energy.sener/projects/gemasolar/," [Online].
- [76] Y. Hu, H. Li, J. Yan, "Integration of evaporative gas turbine with oxy-fuel combustion for carbon dioxide capture," *International Journal of Green Energy*, vol. 7, p. 615-631, 2010.
- [77] "<https://www.tlv.com/global/ME/steam-theory/principal-applications-for-steam.html/>," [Online].
- [78] "www.britannica.com/science/methanol/," [Online].
- [79] T. A. Semelsberger, R. L. Borup, H. L. Greene, "Dimethyl ether (DME) as an alternative fuel," *Journal of Power Sources*, vol. 156, p. 497-511, 2006.
- [80] D.A. Good, J.S. Francisco, A.K. Jain, D.J. Wuebbles, "Lifetimes and global warming potentials for dimethyl ether and for fluorinated ethers: CH₃OCHF₃ (E143a), CHF₂OCHF₂ (E134), CHF₂OCHF₃ (E125)," *JOURNAL OF GEOPHYSICAL RESEARCH*, vol. 103, pp. 28,181-28,186, , 1998.
- [81] M.Q. Wang, H.S. Huang, "A full fuel-cycle analysis of energy and emission impacts of transportation fuels produced from natural gas," ANL/ESD-40, 1999.
- [82] D. o. E. a. C. Change, "DECC fossil fuel price projections.," London, 2013.
- [83] W. Group, "Commodity markets outlook," Washington, DC, 2018.
- [84] Welte, Warren, Scheffe, Steinfeld, "Combined Ceria Reduction and Methane Reforming in a Solar-Driven Particle-Transport reactor," *Industrial and Engineering Chemistry Research*, vol. 56, no. 37, pp. 10300-10308, 2017.

- [85] Kent J. Warren Julie Reim Kelvin Randhir Benjamin Greek Richard Carrillo Prof. David W. Hahn Prof. Jonathan R. Scheffe, "Theoretical and Experimental Investigation of Solar Methane Reforming through the Nonstoichiometric Ceria Redox Cycle," *Wiley Online Library*, vol. 5, no. 11, pp. 2318-2149, 2017.
- [86] "www.carbolite-gero.com/?gclid=CjwKCAiAqJn9BRB0EiwAJ1SztSGcWROvldrTxVdrWRjr2iQ5RcscH6W2edjs7-1gt76FjCGMJHfAexoCg4QQAvD_BwE," [Online].
- [87] "https://convion.fi/products/," [Online].